Carbon Dioxide Capture Using Aqueous MEA Solutions in a Countercurrent Adiabatic Packed-bed Absorber

by

Sudesna Banerjee

B.S in Chemical Engineering, West Bengal University of Technology (WBUT), India

Submitted to the Graduate Faculty of

The Swanson School of Engineering in partial fulfillment

of the requirements for the Dual degree of

Master of Science in Chemical and Petroleum Engineering

University of Pittsburgh

2020

UNIVERSITY OF PITTSBURGH

SWANSON SCHOOL OF ENGINEERING

This thesis was presented

by

Sudesna Banerjee

It was defended on

April 6, 2020

and approved by

George E. Klinzing, Ph.D., Instructor
Department of Chemical and Petroleum Engineering

Hseen Baled, Ph.D., Assistant Professor
Department of Chemical and Petroleum Engineering

Thesis Advisor: Badie I. Morsi, Ph.D., Professor
Department of Chemical and Petroleum Engineering

Carbon Dioxide Capture Using Aqueous MEA Solutions in a Countercurrent Adiabatic Packed-bed Absorber

Sudesna Banerjee, MS

University of Pittsburgh, 2020

A 5-components mathematical model was developed in Matlab (R2016a) for CO_2 absorption from a gas mixture using aqueous MEA solutions in a countercurrent adiabatic packed-bed absorber based on the gas absorption with chemical reaction method developed by Pandya [1]. The absorber was operated under conditions similar to CO_2 capture in post-combustion applications. The model equations were derived, and their parameters were obtained from the literature. The Henry's Law constant (He) and CO_2 diffusivity in the aqueous MEA solutions were calculated using the N_2O analogy. Also, a rate-based model for the system in the same absorber was developed in Aspen Plus (v.8.8). Both models were used to predict the experimental results of CO_2 capture from a gas mixture using aqueous MEA solutions in a 0.10 m ID, 6.55 m height packed-bed absorber with 12.7 mm Berl Saddles reported by Tontiwachwuthikul et al. [2]. The experimental results include CO_2 mole fraction, CO_2 loading and liquid-phase temperature profiles for four different runs.

The Matlab model predictions indicated that under all operating conditions used, the reactions between CO_2 and aqueous MEA were fast as enhancement factors greater than 10 were calculated, and consequently the overall mass transfer rates were dependent on the specific wetted gas-liquid interfacial areas (a_w) and independent of the liquid-side mass transfer coefficients (k_L). In the Matlab model, the correlations by Cho [3] were used to calculate the specific wetted area (a_w) and the liquid-side mass transfer coefficient (k_L); and the model predictions were in a good

agreement with the experimental data. In the Aspen Plus model, the correlations by Billet and Schultes [4] were used to calculate (a_w) and the liquid-side mass transfer coefficient (k_L); and the model could not satisfactorily predict the experimental data. The reason for this behavior was attributed to the small a_w values calculated using the correlations by these authors when compared with those using the correlations by Cho [3]. Therefore, an interfacial area correction factor was introduced into the Aspen Plus model; and as a result, a good agreement was possible between the corrected model predictions and the experimental data.

Table of Contents

List of Tables

List of Figures

Acknowledgment

I would like to express my deepest appreciation and gratitude to my committee chair, Professor Badie I. Morsi for allowing me to be part of his research team and the continuous support and guidance through my graduate education of Master of Science program. His unwavering enthusiasm for the Process Engineering and tremendous encouragement kept me constantly engage with the research. I would also like to thank Professors George E. Klinzing and Hseen O. Baled for serving at my defense committee.

My appreciation also extends to the Reactor and Process Engineering Laboratory (RAPEL) research group members (Mr. Rui Wang and Mr. Husain Ashkanani) for helping, supporting and sharing their research experiences with me. I also would like to thank all the professors who taught me and guided me to overcome academic challenges. I also want to thank all the staff members of the Department of Chemical and Petroleum Engineering who helped me and made my time at the University of Pittsburgh easier and more enjoyable.

Above ground, I am indebted to my family whose value to me only grows with age. I am extremely grateful to my parents for their love, prayers, care, support and sacrifices for the growth of my career. I also want to thank my husband, Arnab, and my little girl, Aahana for all the love, support, and persistent encouragement. They all kept me going and this would not be have been possible without them.

Nomenclature

a	Specific packing area	(m^{-1})
a_w	Specific wetted packing area	(m^{-1})
C	Concentration	$mol\ m^{-3}$
C_P	Heat Capacity	$(J\ mol^{-1}\ K^{-1})$
D	Diffusivity	$(m^2\ s^{-1})$
D_c	Column diameter	(m)
d_{eq}	Equivalent diameter of the packing	(m)
d_p	Diameter of packing Particle	(m)
E	Enhancement factor	(-)
E_1	First-order enhancement factor	(-)
E_i	Instantaneous enhancement factor	(-)
g	Gravitational acceleration	$(m\ s^{-2})$
G	Superficial gas molar velocity	$(mol\ m^{-2}\ s^{-1})$
G_B	Superficial gas molar velocity of inert gas	$(mol\ m^{-2}\ s^{-1})$
h	Heat transfer coefficient	$(W\ m^{-2}\ K^{-1})$
He	Henry’s law constant	$(Pa\ m^{-3}\ mol^{-1})$
k_L	Liquid-side mass transfer coefficient	$(m\ s^{-1})$
k_G	Gas side mass transfer coefficient	$(mol\ Pa^{-1}\ m^{-2}\ s^{-1})$
$\dot{k}_G$	Gas side mass transfer coefficient	$(m\ s^{-1})$
k_2	Reaction rate constant	$(m^3\ kmol^{-1} s^{-1})$

k_{ij}	Binary interaction parameter for PR-EOS	(-)
L	Superficial liquid molar velocity	($mol\ m^{-2}\ s^{-1}$)
$\dot{m}$	Mass flow rate	($kg.s^{-1}$)
Mw	Molecular weight	($g.mol^{-1}$)
M	Superficial mass velocity	($kg.m^{-2}.s^{-1}$)
N_A	Molar flux of component A (CO_2)	($mol.m^{-2}.s^{-1}$)
N_G	Superficial gas molar velocity	($mol.m^{-2}.s^{-1}$)
N_B	Superficial gas molar velocity of inert gas	($mol.m^{-2}.s^{-1}$)
P	Pressure	(Pa)
P_C	Critical pressure	(Pa)
Pr	Prandtl number	
R	Gas constant	($m^3\ Pa\ K^{-1}\ mol^{-1}$)
S	Surface renewal rate	(s^{-1})
Sc	Schmidt number	
St	Stanton number	
St_H	Stanton number for heat transfer	
T	Temperature	(K)
T_B	Boiling Temperature	(K)
T_C	Critical Temperature	(K)
u	Velocity	($m\ sec^{-1}$)
V	Molar volume of the solution	($ml.mol^{-1}$)
v_R	Molar volume of reactant R at its boiling point	($cm^2.mol^{-1}$)
$\sum_{A} v_i$	Summation of diffusion volume of each atom of A	(-)

w	Mass fraction of MEA	(-)
x_i	Mole fraction of species i in solution	(-)
X_2	Mole fraction of absorbents in solution	(-)
y	Mole fraction of gas component	(-)
Y	Molar ratio between a single gas and the inert gas	(-)
ΔH_r	Heat of reaction	$(J.mol^{-1})$
ΔH_{LV}	Latent heat of vaporization	$(J.mol^{-1})$
$\Delta H_{CO2\ in\ Solution}$	Enthalpy of physical absorption and chemical reaction	$(J.mol^{-1})$

<u>GREEK LETTERS</u>

α	Loading, mole CO_2/initial Amine	(-)
β_L	Liquid hold up	(-)
φ	Association Factor	(-)
γ	Stoichiometric number	(-)
ω	Acentric factor	(-)
ρ	Density	$(kg\ m^{-3})$
ν	Kinetic viscosity	$(m^2\ s^{-1})$
μ	Dynamic viscosity	(Pa. s)
λ	Thermal conductivity	$(W\ m^{-1}\ K^{-1})$
σ	Surface tension	$(N\ m^{-1})$
ε	Packing porosity	(-)

SUBSCRIPT

A	Solute gas (i.e. CO_2)
B	Inert Gas (i.e. Air)
P	Product
R	Reactant (i.e. MEA)
S	Solvent (H_2O)
L	Liquid
G	Gas

ABBREVIATION

AMP	2-amino-2-methyl-1-propanol
CCS	Carbon Capture and Storage
DEA	Diethanolamine
GISS	Goddard Institute for Space Studies
GHG	Green House Gases
IEA	International Energy Agency
IEO	International Energy Outlook
LCOE	Levelized Cost of Energy
MEA	Monoethanolamine
MDEA	Methyl diethanolamine
NASA	National Aeronautics and Space Administration
PZ	Piperazine
TEA	Triethanolamine

1.0 Introduction and Background

Over the past years, there has been growing concern about the rise of the global temperatures [5]. Figure 1-1 shows that the global annual-mean air temperature increases by about 0.8^{o}C in the period from 1880 to 2019 [6].

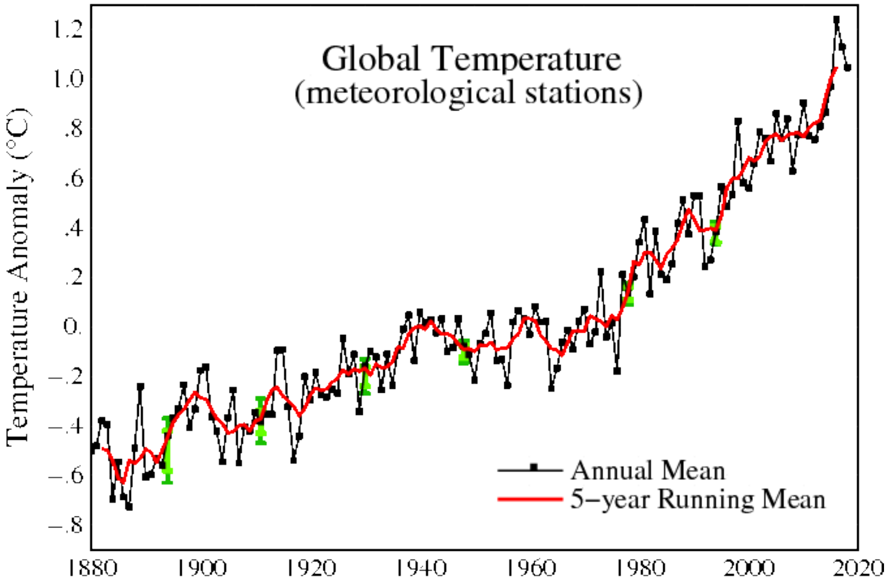

Figure 1-1: Global Temperature Anomaly vs. Time [6]

According to the National Aeronautics and Space Administration (NASA) [7], increasing emissions of greenhouse gases (GHGs), including CO_2, CH_4, and NO_X, into the atmosphere block the heat escaping from earth surface, leading to the global temperature rise. It was reported that the atmospheric concentration of the GHGs has increased by more than one third since the Industrial Revolution [8]. The CO_2 emissions are due mainly to anthropogenic human activities, such as respiration, deforestation, and burning fossil fuels [7]. CO_2 emitted from burning fossil fuels, such as coal and natural gas has a major effect because of its abundance, while CH_4 is a more potent GHG than CO_2 [9].

Figure 1-2, taken from the Intergovernmental Panel on Climate Change (IPCC) 2014 report, shows that CO_2 emission from combusting fossil fuel and other industrial processes is 65%, and that from forestry and other land issues is 11% [10]. The figure also shows that the emissions of CH_4, NO_X and fluorinated gases (F-gases) are 16%, 6% and 2%, respectively [10].

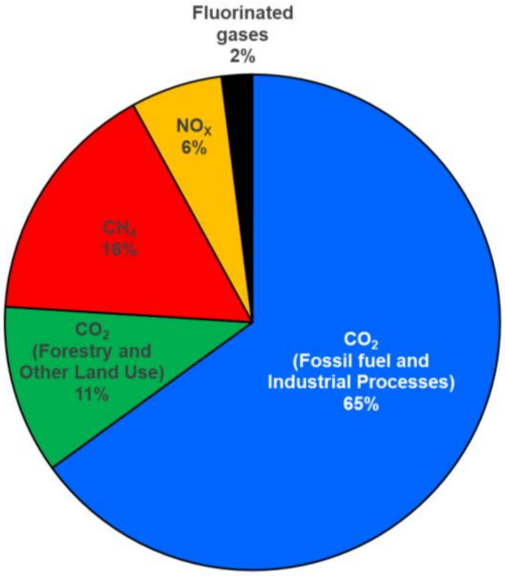

Figure 1-2: Greenhouse Gas Emission Sources [10]

In 2009, Meinshausen et al. [11] reported that if the CO_2 emission is not limited to 50 Gt/year, the global temperature will very likely to increase by 2 °C. The US is heavily relying on fossil energy for its power generation and approximately 1,925 million metric tons per year of carbon dioxide (CO_2) were emitted from the energy sector, of which 71% was from coal-fired power plant and 28% was from natural gas-fired power plants [12]. This implies that burning coal releases approximately 2.5 times as much CO_2 as natural gas does for each unit of electricity or power generated. Other industrial applications, such as cement industries, are also a huge source of CO_2 emissions. The US-Energy Information Administration (US-EIA) predicts that in 2030, the

US will produce around 6.4 billion metric ton of CO_2 from burning coal and natural gas, which will be almost 48% of the world energy-related CO_2 emission [13]. Therefore, CO_2 mitigation is an urgent need.

In 2015, the US government planned to cut by 2025 more than 1,300 metric tons of carbon emission [14] by implementing the carbon capture and sequestration (CCS) program. In this program, the US government aims at capturing 90% of CO_2 from power plants and industrial processes without substantially increasing the cost of electricity (COE). This CCS approach is attractive, since it would allow coal to be used without radically contributing to the GHG effects [15, 16].

1.1 CO_2 Capture Processes

The main CO_2 capture processes include chemical methods; physical methods; solid sorbents; membranes; and cryogenics [17, 18]. Physical methods, solid sorbents, membranes and cryogenics are not the subjects of this study and therefore they will not be discussed. Only chemical methods are briefly described in the following.

In conventional power generation facilities, pulverized coal is combusted in the presence of air in a boiler at 1600 ~ 1800 °C. The boiler generates steam which derives turbines to generate electricity. As a result, flue gas containing mainly CO_2, water vapor, remaining unreacted oxygen and other combustion side products is produced. Nitrogen oxides (NO_x), can be also produced in the boiler due the presence of N_2 at high temperature. A schematic of a coal-based power plant with post-combustion CO_2 capture is shown in Figure 1-3, which includes two main units, namely power generation unit and post-combustion CO_2 capture unit. In the power generation unit, coal is combusted in the boiler. The resulting flue gas is then deashed and the nitrogen-containing and sulfur-containing compounds are removed. The partially cleaned flue gas enter the post-combustion CO_2 capture unit, in which acid gases (CO_2 and H_2S) are removed in the acid gas removal (AGR) unit. The “treated” flue gas is then released into the atmosphere through the stacks of the power plant.

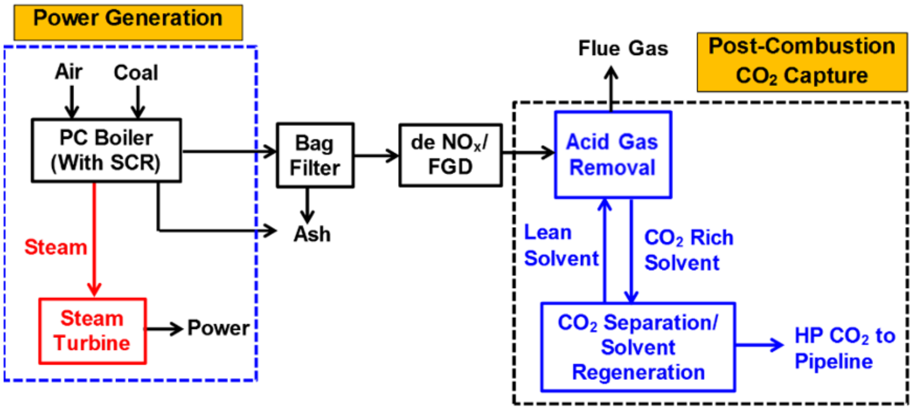

Figure 1-3: Power Generation Plant with Post-combustion CO_2 Capture [19]

A typical untreated flue gas composition from burning a low-sulfur eastern bituminous coal in a power plant is shown in Table 1-1 [20].

Table 1-1: A Typical Untreated Flue gas Composition [20]

Species	Concentration
H_2O	5~7 mol%
O_2	3~4 mol%
CO_2	15~16 mol%
CO	20 ppm
HCl	100 ppm
SO_2	800 ppm
SO_3	10 ppm
NO_x	500 ppm
Hydrocarbons	10 ppm
Total Hg	1 ppb
N_2	balance

This flue gas needs further preconditioning, including, desulfurization, dehydration and deoxygenation, to prevent degradation of the chemical absorbents used for CO_2 capture. NO_X can be removed from the flue gas using a selective catalytic reduction (SCR) process [21] and chemical methods are used to capture CO_2 from flue gas [22].

1.1.1 Chemical Methods

Chemical methods depend on direct reactions between CO_2 and a reactive solvent often in a countercurrent packed-bed absorber. The absorber contains solid packings to increase the mass transfer between CO_2 and the solvent. The flue gas enters from the bottom the absorber, while the chemical solvent enters from the top. Upon reaction, the CO_2-rich solvent is sent to a regenerator (stripper) where it is heated to release most CO_2 absorbed and the CO_2-lean solvent is recycled back into the absorber. Figure 1-4 presents a schematic of a post-combustion CO_2 capture process using amine [23].

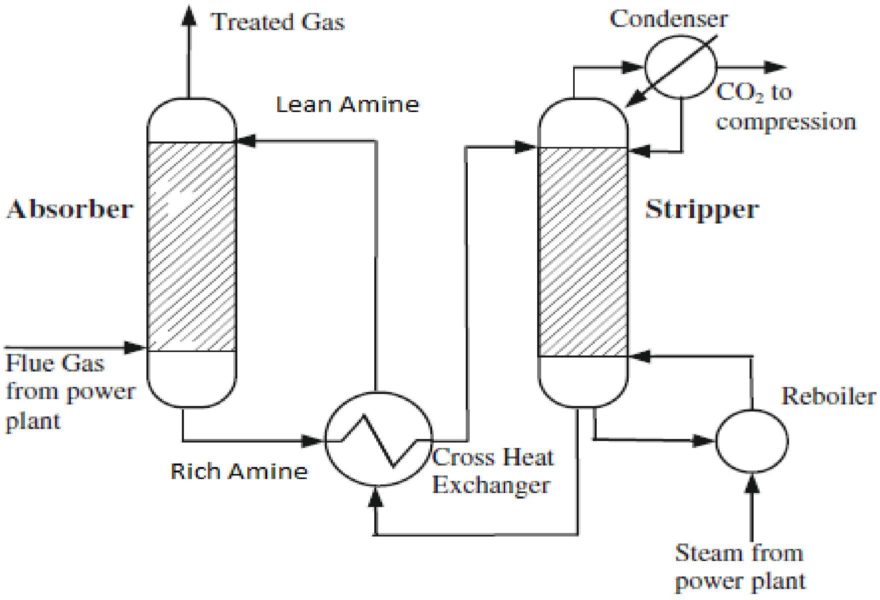

Figure 1-4: Schematic of a Post-combustion CO_2 Capture Process using Amine [23]

1.1.2 Chemical Solvents and Processes Used

Ammonium hydroxide (NH_4OH), sodium hydroxide (NaOH), potassium carbonates (K_2CO_3), monoethanolamine (MEA) [24-31], 2-amino-2-methyl-1-propanol (AMP) [32-44] and sodium glycinate [45-53] and others have been used for CO_2 capture from post-combustion applications.

The Aqua-Ammonia process uses aqueous ammonium hydroxide to capture CO_2 from the post-combustion flue gas. The advantages of this process reside in the fact that ammonia does not cause equipment corrosion and does not suffer from degradation due to the presence of SO_x and O_2 in the flue gas [54]. In addition, the major products of this process are useful fertilizers, including ammonium sulfate and ammonium nitrate [25]. The drawback of this process, however, is the volatility of ammonia, leading to its loss in the treated flue gas stream [29, 55]. In 2009, Kozak et al. [56] proposed a chilled ammonia process and constructed a field pilot plant to capture 15,000 ton of CO_2 per year. The plant included absorber vessels, pressure vessels, circulation pumps, regenerator feed pumps, heat exchangers, chillers, process instruments and control valves, gas sampling system, and Programmable Logic Controller (PLC) for process control.

The Benfield process [57], employing potassium carbonate (K_2CO_3) as a solvent, was used to capture CO_2 from flue gas. The overall reaction between CO_2 and potassium carbonate is shown in Equation (1-1) [58, 59].

$$\mathrm{CO_2 + H_2O + K_2CO_3 \rightarrow 2KHCO_3} \qquad (1\text{-}1)$$

In 2008, Ahmadi et al. [60] developed a model following the procedure by Aboudheir et al. [61] to simulate CO_2 capture from a simulated flue gas using a potassium-based solvent in a packed-bed absorber operating under a high pressure of 20.4 atm. The solvent contained 3.09 mol% K_2CO_3, 2.85 mol% $KHCO_3$, 91.28 mol% water, 1.25 mol% KBO_2 and 0.28 mol% KVO_3; and the simulated flue gas consisted of 10.32 mol% CO_2, 63 mol% N_2, 15.09 mol% C_2H_4, 6.27 mol% Ar and 3 mol% H_2O. The solvent and flue gas flow rates were 5,196.89 and 833.14 kmol/h, respectively. The temperature of the solvent and gas phases were 377.1 K and 321.2 K, respectively. The packed-bed dimensions were 1.219 m ID and 18.29 m height and it was packed with 50 mm steel Hy-pac. Under these conditions, the authors reported that the CO_2 capture efficiency reached 94.9% and their model was able to predict the experimental data with a good accuracy.

In 2009, Yi et al. [62] carried out experiments and modeled CO_2 capture by the Benfield solution in a rotating packed-bed. They reported a 10% deviation between their model predictions and the experimental data. They further used their model to study the effects of liquid flow rate, gas flow rate, rotating speed, temperature and end effects on the gas-phase volumetric mass transfer coefficients.

In 2012, Mumford et al. [63] described the performance of a pilot-plant absorber for CO_2 capture using 30 wt% potassium carbonate (K_2CO_3) solution at a temperature of 240 ºC and pressure of 1 kPag. The absorber dimensions were 1.5 m ID and 7 m height and it was packed with steel Sulzer Nutter rings. Although only 20% ~ 25% of CO_2 from the flue gas were captured under these conditions, the authors claimed that valuable operating data were obtained, which enabled a process simulation using Aspen Plus and a direct comparison with actual pilot plant data. They reported that the Aspen Plus model predictions were within 5% of the pilot plant data and therefore they claimed their model can contribute to the development of potassium carbonate processes in large-scale CO_2 capture in postcombustion applications.

In 1989, Tontiwachwuthikul et al. [64] conducted experiments for CO_2 absorption from CO_2-air mixture using AMP, NaOH and MEA solutions, in a packed-bed with 0.1 m ID and 7.2 m height containing 0.5 inch ceramic Berl Saddle packing. In 1992, Tontiwachwuthikul et al. [2] reported the liquid temperature, CO_2 loading and CO_2 mole fraction in the gas-phase at each section. These authors developed a Fortran program using Pandya's approach [1] to model two runs (T16, T22) of the experimental results. In 1993, Pintola et al. [65] developed a model using Pandya's approach [1] and reported that their model predictions were in agreement with the experimental results of T22 run. Aboudheir et al. [61] and Krishnamoorthy et al. [66] developed models for MEA system using run (T22) and Pandya's approach [1] and reported that their model predictions were in agreement with the experimental results. In 2017, Oko et al. [22] mentioned that MEA solution (30 wt% MEA or less) is generally considered as a benchmark solvent for post-combustion CO_2 capture. Rao et al. [67], however, reported that the oldest commercial post-combustion CO_2 capture processes, Kerr-McGee/ABB Lummus Crest process and the Fluor Daniel's Econamine FG process use 20 wt% and 30 wt% MEA solutions as solvents, respectively. Table 1-2 shows a summary of different processes used for CO_2 removal in post-combustion applications [68].

Table 1-2: Chemical Processes used for Post-combustion CO_2 Capture [68]

Process name	Reactant/Solvent + Additives	CO_2 in Treated Gas (ppm)
MEA	MEA (20%)/Water	< 50
Promoted MEA	MEA (25–30%)/Water + amine guard	< 50
Benfield	K_2CO_3 (25–30%)/Water + DEA	500–1000
Vetrocoke	K_2CO_3/Water + As_2O_3 + glycine	500–1000
Catacarb	K_2CO_3 (25–30%)/Water + additives	500–1000
Lurgi	K_2CO_3 (25–30%)/Water + additives	500–1000
Carsol	K_2CO_3/Water + additives	500–1000
Flexsorb HP	K_2CO_3 amine promoted/Water	500–1000
Alkazid	K_2-methylaminopropionate/Water	Suitable range of 50-3000
MDEA	MDEA (40%)/Water + additives	100–500

Even though MEA has been used in numerous applications, it inherits the following limitations: (1) it has rapid kinetics and requires high solvent regeneration energy (in the range of 3.2-4.2 GJ/ton CO_2) [22], (2) the CO_2-loaded MEA solution is very corrosive and degrades rapidly, (3) the MEA solution require high solvent circulation rate, which leads to large equipment sizes and high energy consumption [22], and (4) the manufacture of MEA by ammonia and ethylene oxide reaction raises concern due to CO_2 emission [69]. This is because the production of ammonia using the Haber–Bosch process releases CO_2 and the production of ethylene oxide produces CO_2. Considering the above limitations of using MEA, new chemical solvents are being considered, which include mixed amines (MEA and MDEA, AMP and PZ) [70] and biphasic solvents [71], which have shown high potential for CO_2 capture. For example the biphasic solvents appeared to require about 50% less regeneration energy and have about four times cyclic loading capacity compared to MEA [72]. The existing commercial post-combustion CO_2 Capture processes using new solvents are given in Table 1-3.

Table 1-3: Commercial Chemical Processes for Post-Combustion CO_2 Capture

Process	Developer	Solvent	Demonstration	Commercial project
CanSolv® (Shaw 2009) [73]	Shell	Amine-based	TCM Norway	Boundary Dam Canada (Operational)
PostCap™ (Siemens 2015) [74]	Siemens	Amino acid salt	TCM Norway Big Bend post-combustion CO_2 capture, Florida	ROAD Netherlands (Planning) Masdar Abu Dhabi (Planning)
Advanced Amine Process (Chopin 2014) [75]	Alstom Power/ Dow Chemical	DOW UCARSOL™ FGC 3000	EDF PCC Le Havre, France Charleston post-combustion CO_2 capture, West Virginia	Elektownia Belchatow, Poland (Planning) GETICA Romania (on-hold)
KM-CDR™ (MIT 2016b) [71]	MHI/KEPCO	KS-1 (Hindered amine)	Plant Barry, Alabama Plant Yates, Georgia	Petro-Nova CCS, Texas (On-going)
HTC (HTC Purenergy 2016) [22]	HTC Purenergy/ Doosan Babcock	Amine-based	International Test Centre, Canada	Antelope Valley CCS, North Dakota
CO_2 Solution (MIT 2016) [76]	CO_2 Solutions Ltd.	Enzyme-based solvent	Pikes Peak South post-combustion CO_2 capture, Saskatchewan, Canada	
DMX™ (Raynal et al. 2013) [71]	IFPEN/ PROSERNA	Biphasic solvent	ENEL's Brindisi Pilot post-combustion CO_2 capture, Italy	

1.2 Potential Benefits and Utilizations of the CO_2 captured

CO_2 has significant financial benefit, such as "carbon trading," which is a market-based system aimed at reducing GHGs responsible for global warming by burning fossil fuels [77]. CO_2 can be considered as a plentiful potential feedstock for many products, including commercial chemicals, plastics, and improved cement. CO_2 injection for enhanced oil recovery (EOR) has been widely accepted as an effective technique for oil production for over 40 years [78]. The economic benefits due to the oil produced are attractive and can offset the cost of CO_2 injection [79]. CO_2 can also be utilized as a food grade-quality in gaseous beverages or to produce high-value chemicals, such as sodium, ammonium or calcium carbonates or bicarbonates, which can be used or sold to offset some of the cost associated with the CO_2 capture process. Figure 1-5 shows various potential benefits and utilizations of the captured CO_2 [80].

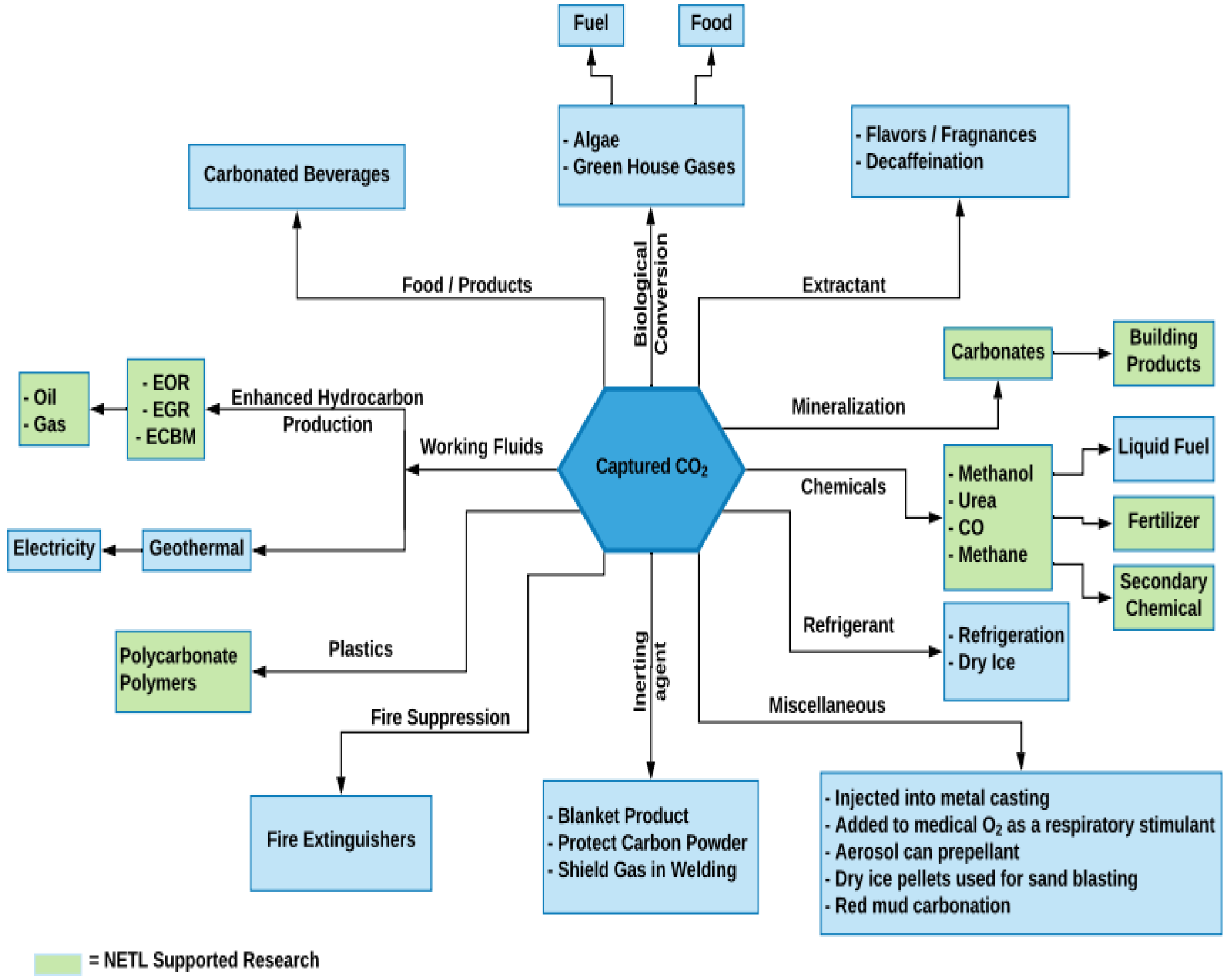

Figure 1-5:Potential Benefits and Utilizations of the Captured CO_2 [80]

2.0 Research Objectives

The objectives of this study are:

(1) To develop a five-components (CO_2, air, H_2O, MEA, Carbamates) comprehensive mathematical model in Matlab (R2016a) to predict the behavior of CO_2 capture from a mixture with air using aqueous MEA solutions in a countercurrent adiabatic packed-bed absorber;

(2) To develop a model in Aspen Plus v8.8 to predict the behavior of the same absorber under identical operating conditions; and

(3) To validate the predictions of the two models with the experimental data reported by Tontiwachwuthikul et. al. [2] for CO_2 capture from a gaseous mixture in air with aqueous MEA solutions.

In order to achieve these objectives, the following tasks are proposed:

Task 1: Develop a comprehensive mathematical model in Matlab 2016a following Pandya's [1] approach for CO_2 capture from a CO_2/air mixture using aqueous MEA solutions in an adiabatic packed-bed absorber.

Task 2: Conduct extensive literature search to obtain and correlate the required equation parameters in the equations of the reactor model.

Task 3: Validate the Matlab model predictions against the adequate experimental data (with accurate CO_2 material balance) reported by Tontiwachwuthikul et al. [2].

Task 4: Develop another model using a Rate Base model in Aspen Plus v8.8 for CO_2 capture from a CO_2/air mixture using aqueous MEA solutions.

Task 5: Validate the Aspen Plus model predictions against the adequate experimental data (with accurate CO_2 material balance) reported by Tontiwachwuthikul et al. [2].

Task 6: Compare the predictions of the Matlab and Aspen Plus models. The predictions include CO_2 mole fraction, CO_2 loading, CO_2 capture efficiency, gas-phase temperature, and liquid-phase temperature.

2.1 Chemistry of CO_2 - MEA System

The CO_2 - MEA reaction mechanism is highly complex and has not been well understood, even though, it has been theoretically and experimentally studied [65]. The MEA molecule is bifunctional with a primary alcohol and a primary amine, with a formula of $OH\text{-}CH_2\text{-}CH_2\text{-}NH_2$, denoted as RNH_2. In 1967, Astarita [81], represented the overall reaction mechanism, which includes the 4 main reactions represented by Equation (2-1) through (2-5).

1. Carbamate formation:

$$\mathrm{CO_2 + 2\,RNH_2 \rightarrow RNHCOO^- + RNH_3^+} \qquad (2\text{-}1)$$

2. Bicarbonate formation:

$$\mathrm{CO_2 + RNH_2 + H_2O \rightarrow HCO_3^- + RNH_3^+} \qquad (2\text{-}2)$$

3. Carbamate hydrolysis:

$$\mathrm{RNHCOO^- + H_2O \rightarrow HCO_3^- + RNH_2} \quad (2\text{-}3)$$

4. Carbonic acid formation and dissociation [82]:

$$\mathrm{CO_2 + H_2O \leftrightarrow H_2CO_3} \quad (2\text{-}4)$$

$$\mathrm{H_2CO_3 \leftrightarrow H^+ + HCO_3^-} \quad (2\text{-}5)$$

It should be noted that the reaction of CO_2 with H_2O followed by dissociation of the carbonic acid also occurs, but the reaction rate is negligible, except at low pH.

Astarita et al. [81] suggested that for CO_2/MEA loading of less than 0.5 mol/mol, the rate of bicarbonate formation is insignificant and the overall reaction is irreversible and can be expressed as Equation (2-1). Therefore, the reaction rate is first order with respect to CO_2 and first order with respect to MEA, i.e., the overall reaction is a second-order. Thus, for a CO_2/MEA loading of less than 0.5 moles of CO_2 per mole of amine, the rate of chemical reaction can be expressed as Equation (2-6) [65]:

$$\mathrm{Reaction\ Rate} = \mathrm{k_2[CO_2][RNH_2]} \quad (2\text{-}6)$$

In 1968, Caplow et al. [83] proposed a zwitterion formation mechanism for MEA-CO_2 system. This mechanism reintroduced in 1979 by Danckwerts et al. [31, 35] was generally accepted. Amino acids such as MEA, AMP and SG could form a zwitterion due to the presence of the basic amine group and the acidic carboxylic acid group in the same structure, as shown in Figure 2-1 (a). If an internal transfer of a hydrogen ion from the carboxylic acid group to the basic amine group, this will lead to an ion with both negative and positive charges, as shown in Figure 2-1 (b). This is called a “zwitterion,” which is the form of amino acids, that even exists in a solid state. As a whole, a zwitterion is neutral, but it may contain separate groups which are positively or negatively charged.

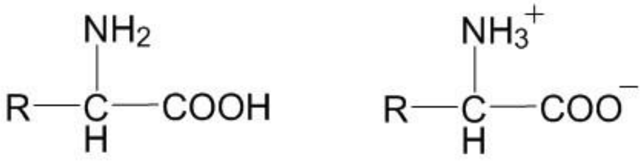

(a) (b)

Figure 2-1: Amino Acid (a) and Zwitterion Structure (b)

For a zwitterion, if a hydroxide ion (OH^-) is added, such as NaOH, the hydrogen ion is removed from – NH_3^+ group as in Equation (2-7). If an acid ion (H^+) is added, such as (HCl), the –COO^- group of a zwitterion will pick up a hydrogen ion as in Equation (2-8).

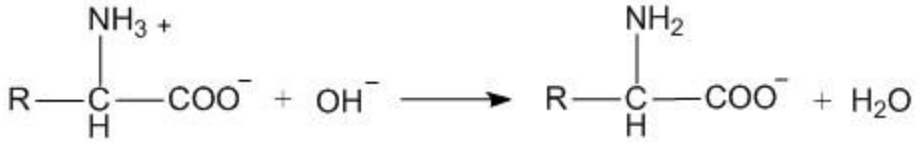

$$R\text{—}\underset{H}{\overset{NH_3^+}{C}}\text{—}COO^- + OH^- \longrightarrow R\text{—}\underset{H}{\overset{NH_2}{C}}\text{—}COO^- + H_2O \qquad (2\text{-}7)$$

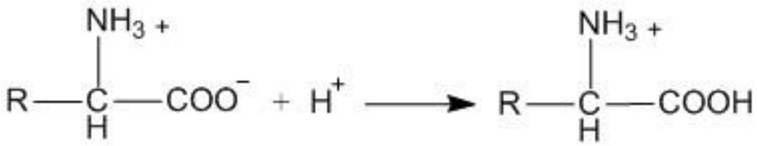

$$R-\underset{H}{\overset{NH_3^+}{C}}-COO^- + H^+ \longrightarrow R-\underset{H}{\overset{NH_3^+}{C}}-COOH \quad (2\text{-}8)$$

As discussed earlier, the theoretical loading is 0.5 mole of CO_2/mole of amine, however, it was noticed as the loading approaches 0.5 mole CO_2/mole of amine, the hydrolysis reaction starts [81]. It should be emphasized that in Pandya's [1] approach, the absorber model was developed considering no bicarbonate formation. This assumption is valid for most of the cases and the model will not predict reliable results when the loading becomes ≥ 0.5 mole of CO_2/mole of amine [1, 2].

2.2 Reaction Mechanism of CO_2 - MEA System

In 2015, Lv et al. [84] evaluated the reaction mechanism of CO_2-MEA system using nuclear magnetic resonance (NMR). They found that (1) the CO_2-MEA reaction takes place in two stages, in the first stage, the pH decreases from 12.54 to 9.0 and the temperature gradually increases from 291 to 305 K; and in the second stage, the pH decrease from 9.0 to 7.83, the carbamate hydrolysis take place and the temperature decreases until it reaches room temperature [84]; (2) the reaction in the first stage is faster than that of the second stage and the CO_2 loading in the first stage was up to 0.40 mole CO_2/mole MEA, contributing to nearly 80% of the total loading (around 0.53 mole CO_2/ mole MEA).

Therefore, for our model development under steady-state conditions, the assumption of irreversible reaction proposed by Astarita [81] is valid in the first stage of reaction. Also, the hydrolysis of carbamate in the second stage can be modeled based on the knowledge of the charge of the solution pH. This phenomenon is included in the Rate Base model developed in Aspen Plus. However, the model developed based on Pandya's [1] method does not include these two stages, which can be considered as a limitation of this method.

2.3 Packed-Bed Absorbers

Packed-bed absorbers have been used for CO_2 absorption in the chemical and petroleum industries. The absorber is a long vertical pipe filled with structured or random packing. The gas mixture enters from the bottom of the absorber and the solvent (absorbent) is introduced from the top. The chemical reaction takes place in the packing whose main function is to increase the surface contact area between the gas and the solvent. The components of a typical packed-bed absorber are shown in Figure 2-2. These components are:

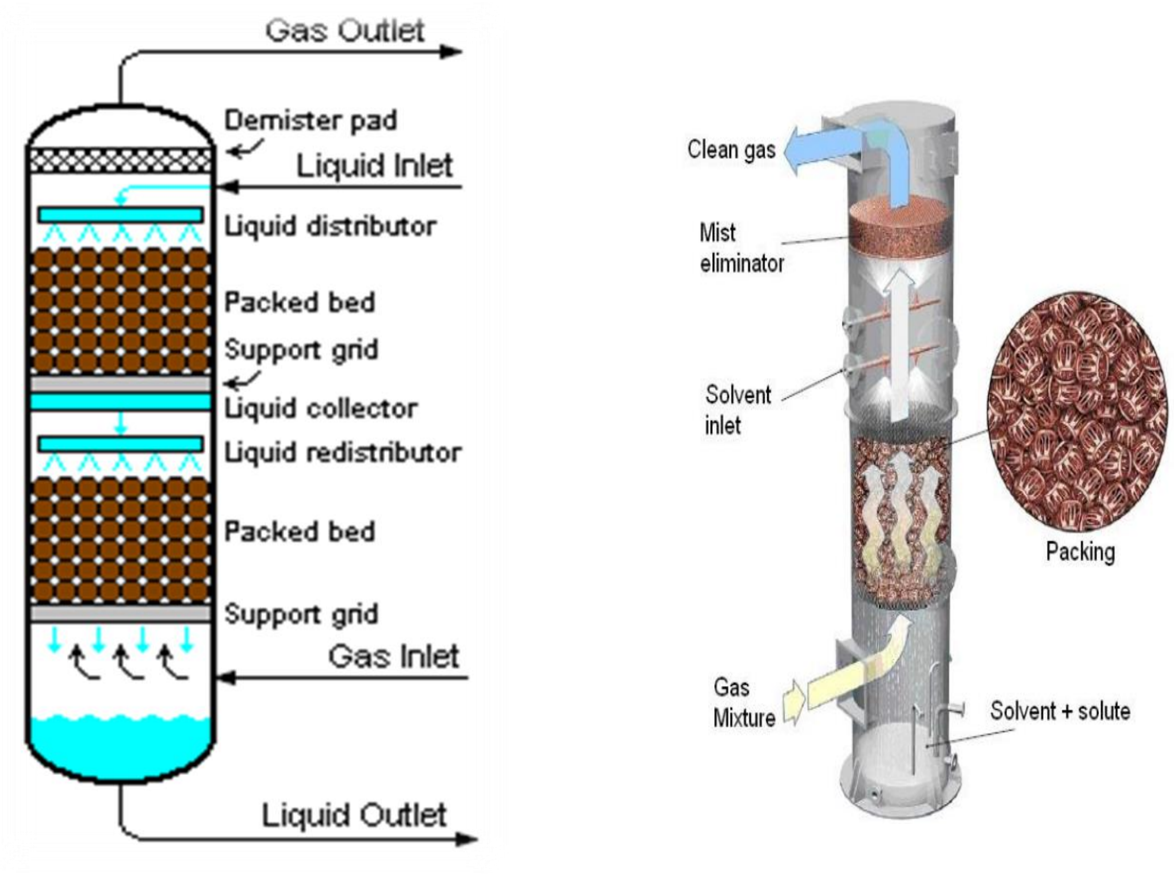

Figure 2-2: Components of a Typical Packed-bed [85], [86]

(1) Demister pad or mist eliminator is to remove the entrained mist from the gas stream leaving the absorber.

(2) Liquid and gas inlets is to deliver the solvent and flue gas into the absorber.

(3) Liquid distributor is to distribute the liquid evenly over the packing to ensure an appropriate gas-liquid mass transfer. Maldistribution of the liquid-phase leads to poor mass transfer and absorption efficiency. Liquid redistributors are required in tall packed-beds to maximize the gas-liquid interactions.

(4) Packing hold-down is to keep the packing from moving up due to the high gas throughput.

(5) Packing support is to support the packing from falling or moving downward with the liquid.

(6) Gas inlet is to ensure that the gas is well distributed at the bottom of the absorber to eliminate channeling in the absorber.

(7) Gas and liquid outlets are to ensure no gas nor liquid nor products would accumulate inside the absorber to maintain a continuous process.

2.4 Hydraulics of Countercurrent Packed-Bed Absorbers

2.4.1 Flooding in Countercurrent Packed-bed Absorbers

In two-phase countercurrent packed-beds, if the force exerted by the gas flowing upward ($\dot{m}_G u_G$) is greater than the force exerted by the liquid flowing downward ($\dot{m}_L u_L$), the liquid flow will be restricted, which is known as flooding. In a packed-bed containing certain type and size of packing and is operating at a given liquid flow rate, there is an upper limit of the gas velocity, known as flooding velocity ($u_{G,Fl}$) [87]. Similarly, at a given gas flow rate, there is a definite liquid velocity above which the column will be flooded [88]. Piché et al. [89] summarized several correlations available in the literature for flooding predictions in countercurrent packed-beds as listed in Table 2-1. If the flow pattern is close to the flooding point, adjusting the liquid and/or gas flow rate is an option to avoid flow instability in the packed-bed.

Table 2-1: Flooding Correlations in Countercurrent Packed-bed Absorbers [89]

References	Packing	System	Correlation	Constraints
Leva [90]	Ceramic Intalox Saddles Ceramic Raschig Rings Metal Raschig Rings Metal Pall Rings Metal Pall Rings	4% solution of NaOH/air + CO_2 Water/air $CaCI_2$ solution/air Methanol/ethanol	$d_p > 1\ in$ $\log[f(\mu_L)] = 0.1839\log(\mu_L) - 0.011$ $d_p < 1\ in$ $\log[f(\mu_L)] = 0.0591\cdot\log^3(\mu_L) + 0.0226\cdot\log^2(\mu_L) + 0.1701\cdot\log(\mu_L) - 0.0135$ $f(\rho_L) = 1.5052\cdot\ln\left(\frac{\rho_w}{\rho_L}\right) + 1.1883$ $X = \frac{u_L}{u_{G,Fl}}\cdot\sqrt{\frac{\rho_L}{\rho_G}}$ $Y = 0.016(\frac{\rho_G {u_G}^2}{g})F_p\cdot f(\mu_L)\cdot f(\rho_L)$ $\log(Yo) = -0.29\log^2(X) - 1.075\log(X) - 1.636$ (Yo represents the flooding line) & (F_P is packing factor)	$0.01 < X < 10$ $700 < \rho_L < 1400$ $[kg/m^3]$ $0.2 \le \mu_L \le 20$ $[cP]$ All English Units except for viscosity
Billet and Schultes [91]	Pall ring Raschig ring Berl saddle		$u_{G,Fl} = \frac{(\varepsilon - \beta_{L,Fl})^{1.5}}{\varepsilon^{0.5}}\cdot\sqrt{\frac{2g}{\psi_L}}\cdot\sqrt{\frac{\beta_{L,Fl}}{a_T}}\cdot\sqrt{\frac{\rho_L}{\rho_G}}$ $3{\beta_{L,Fl}}^4 - \varepsilon{\beta_{L,Fl}}^3 = \frac{6}{g}(\frac{{a_T}^2\mu_L\varepsilon u_L}{\rho_L})$ $\frac{1}{\psi_L} = \frac{{C_F}^2}{g}[\frac{u_L}{u_{G,Fl}}\sqrt{\frac{\rho_L}{\rho_G}}(\frac{\mu_L}{\mu_G})^{0.2}]^{2N_{Fl}}$ $if\ \frac{u_L}{u_{G,Fl}}\cdot\sqrt{\frac{\rho_L}{\rho_G}} \le 0.4, C_F = C_{Fl}, N_{Fl} = -0.194$ $if\ \frac{u_L}{u_{G,Fl}}\cdot\sqrt{\frac{\rho_L}{\rho_G}} \le 0.4, C_F = 0.6244\cdot C_{Fl}(\frac{\mu_L}{\mu_G})^{0.1028}$ $N_F = -0.708$	C_{Fl} is Packing Constant in reference $758 < \rho_L < 1237$ $0.07 < \rho_G < 4.93$ $[kg/m^3]$ $0.3 \le \nu_L \le 1.66$ $2.2 \le \nu_g \le 126$ ν is kinetic viscosity $[10^{-6}m^2/s]$ $17.2 \le \sigma_L \le 74$ σ is surface tension $[10^{-3}kg/s^2]$

As a standard procedure, flooding is checked using the Generalized Pressure Drop Correlation (GPDC) proposed in 1938 by Sherwood et al. [92], modified later in 1992 by Leva [93], and presented in Figure 2-3. This figure can also be used to interpolate for the two-phase (irrigated) pressure drop in packed-beds. This is how to use this figure under given operating conditions, the coordinates X and Y are calculated using Equations (2-9) and (2-10), respectively. The point (X, Y) is then plotted in Figure 2-3 and if it lies within the figure, no flooding occurs, otherwise alterations of the liquid and/or gas flow rates are required to avoid flooding. It should be noted that British units are used in Equations (2-9) and (2-10), except for viscosity (cP). Also, the pressure drops in Figure 2-3 are expressed in inches H_2O/ft of packing.

$$\mathrm{X} = \frac{u_\mathrm{L}}{u_\mathrm{G}} \cdot \sqrt{\frac{\rho_\mathrm{L}}{\rho_\mathrm{G}}} \tag{2-9}$$

$$\mathrm{Y} = 0.016\,\frac{\rho_\mathrm{G} {u_\mathrm{G}}^2}{\mathrm{g}}\,\mathrm{F_p} \cdot \mathrm{f}(\mu_\mathrm{L}) \cdot \mathrm{f}(\rho_\mathrm{L}) \tag{2-10}$$

Where $f(\mu)$ and $f(\rho_L)$ are given in Table 2-1 .

Figure 2-4 shows another GPDC graph found in the book by Towler and Sinnott [94]. The use of this figure is similar to Figure 2-3 as under a given operating condition, the coordinates F_{LV} and K_4 are calculated using Equation (2-11) and (2-12) and the point (F_{LV}, K_4) is plotted in Figure 2-4. Similar to the previous graph proposed by Leva [90], if the point lies within the figure (below flooding line) indicates no flooding occurs, otherwise alterations of the liquid and/or gas flow rates are required to avoid flooding.

It should be noted that the pressure drops in Figure 2-4 are expressed in mmH_2O/m of packing.

$$F_{LV} = \frac{M_L}{M_G} \cdot \sqrt{\frac{\rho_G}{\rho_L}} = \frac{u_L}{u_G} \cdot \sqrt{\frac{\rho_L}{\rho_G}} = X \qquad (2\text{-}11)$$

$$K_4 = \frac{13.1 M_G^2 F_p \left(\frac{\mu_L}{\rho_L}\right)^{0.1}}{\rho_G(\rho_L - \rho_G)} \qquad (2\text{-}12)$$

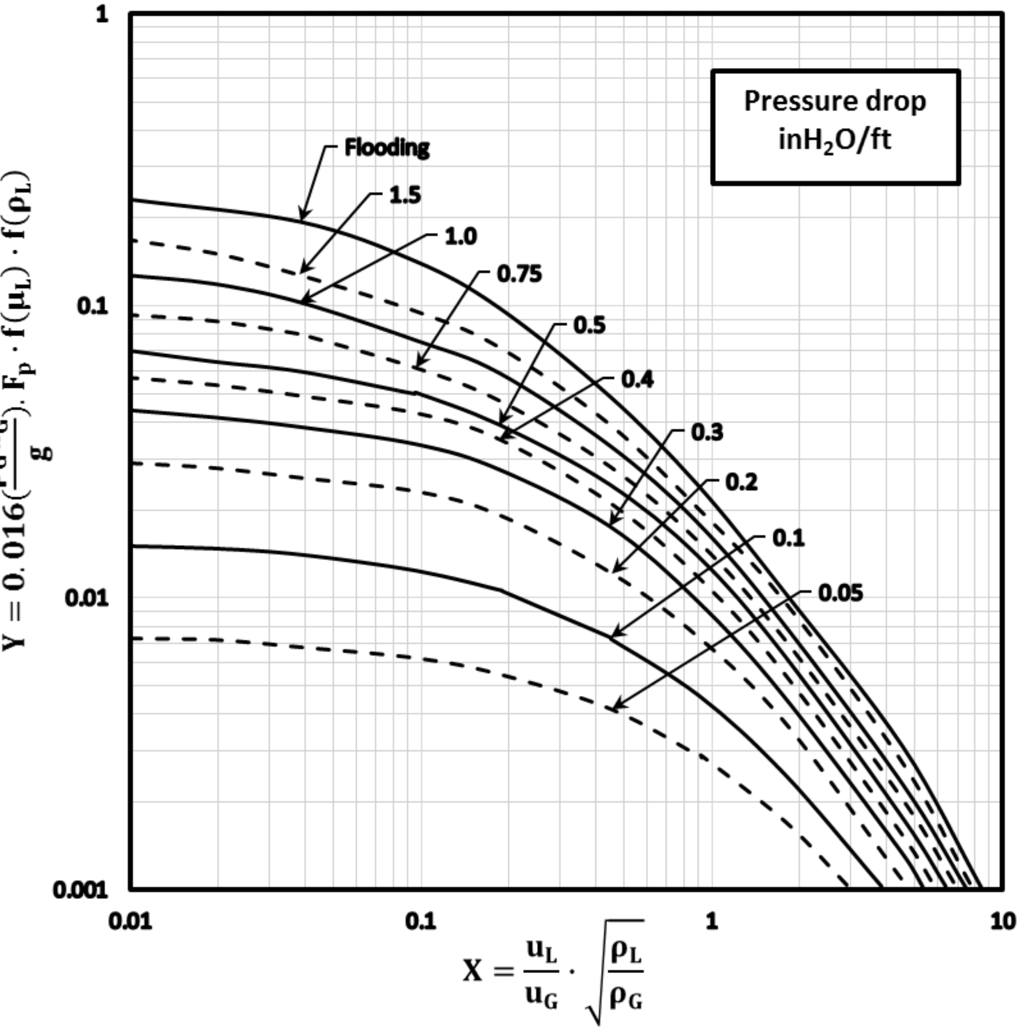

Figure 2-3: Leva’s Pressure Drop Correlation [90]

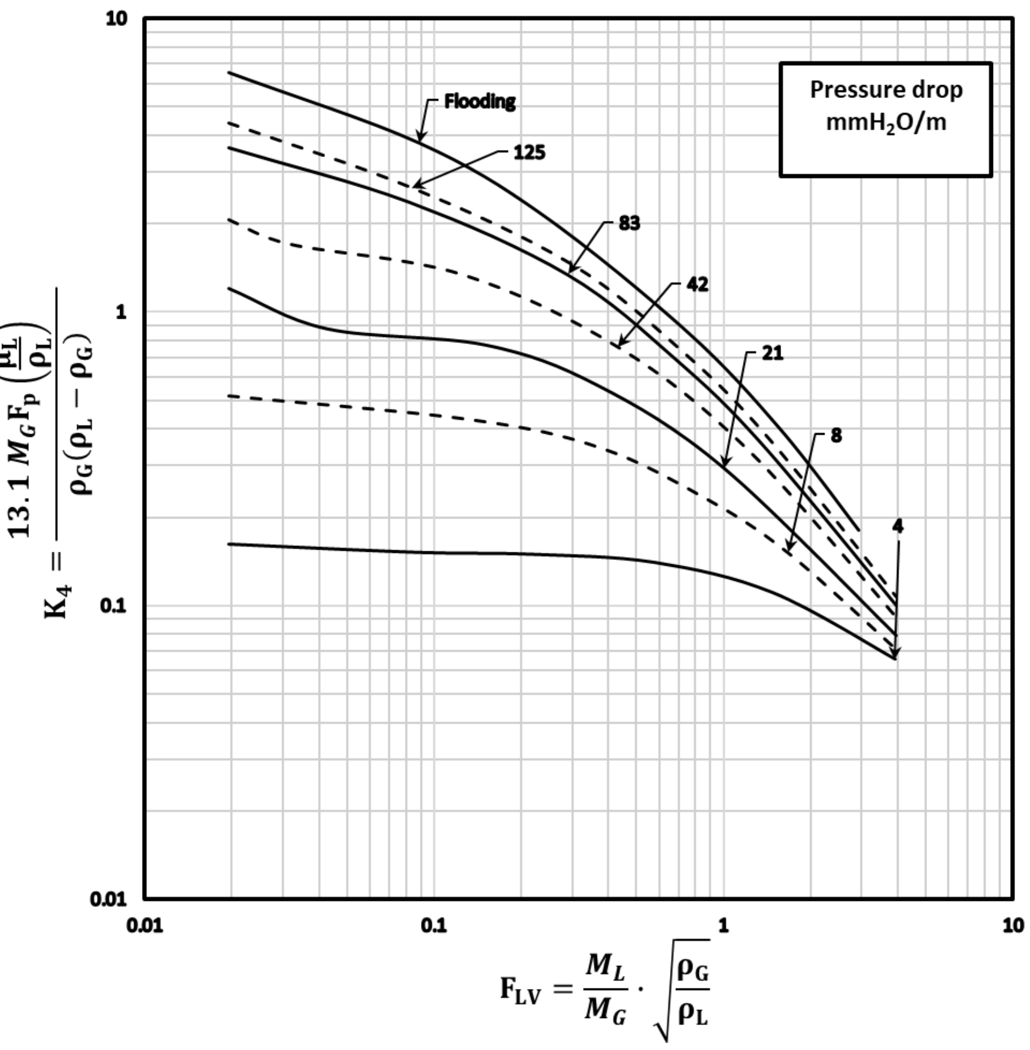

Figure 2-4: Generalized Pressure Drop Correlation (GPDC) [94]

2.4.2 Pressure Drop and Liquid Holdup

Pressure drop and liquid holdup are important parameters in packed-bed design. Systematic evaluations of different correlations available in the literature led to the recommendation of the correlations by Leva [90] and by Billet and Schultes [91, 95-97] to predict the pressure drop associated with two-phase flow in packed-beds [98].

To use Figure 2-3 by Leva [90] and obtain the two-phase pressure drop, testing for flooding should be conducted first as mentioned above, then the location of point (X, Y) on the figure would allow the interpolation of the pressure drop in the packed-bed under the prevailing conditions. The pressure drop in this figure is expressed in inches of water/ft of packing height.

In 1999, Billet and Schultes [96] proposed Equation (2-13) to directly calculate the irrigated two phase pressure drop based on over 3,500 measured data points, more than 50 test systems and over 70 types of random or structured packing including for Berl saddles.

$$\frac{\Delta \mathrm{P_{irr}}}{\mathrm{H}} = \psi_\mathrm{L} \frac{\mathrm{a}}{(\varepsilon - \beta_\mathrm{L})^3} \frac{\mathrm{F_G}^2}{2} (\frac{1}{\mathrm{K}}) \tag{2-13}$$

$$\frac{1}{\mathrm{K}} = 1 + (\frac{2}{3})(\frac{1}{1-\varepsilon}) \frac{\mathrm{d_p}}{\mathrm{D_C}} \tag{2-14}$$

$$\mathrm{Re_G} = \frac{u_\mathrm{G} \mathrm{d_p}}{(1-\varepsilon)\nu_\mathrm{G}} \mathrm{K} \tag{2-15}$$

$$\psi_\mathrm{L} = \mathrm{C_{p,0}} \left(\frac{64}{\mathrm{Re_G}} + \frac{1.8}{\mathrm{Re_G}^{0.08}} \right) \left(\frac{\varepsilon - \beta_L}{\varepsilon} \right)^{1.5} \left(\frac{a}{a_h} \right)^{0.2} \exp\left(\frac{13300}{a^{1.5}} \sqrt{u_L^2 \frac{a}{g}} \right) \tag{2-16}$$

$$\mathrm{F_G} = \mathrm{u_G} \sqrt{\rho_\mathrm{G}} \tag{2-17}$$

$$\mathrm{d_p} = \frac{6(1-\varepsilon)}{\mathrm{a}} \tag{2-18}$$

Where F_G is the gas capacity factor, D_C is the ID of the absorber; and the $C_{p,0}$ value appearing in Equation (2-16) was calculated in this study to be 0.9073 for Berl Saddle using a value predicted with Equation (2-27) by Stichlmair et al. [99] for the same packing.

It should be mentioned that Equation (2-13) is only valid under the following constraints:

$$361 \leq \rho_L \leq 1{,}115 \text{ kg/m}^3$$

$$0.61 \leq u_L \leq 60.1 \text{ m/h}$$

$$0.06 \leq \rho_G \leq 28 \text{ kg/m}^3$$

$$0.21 \leq F_G \leq 5.09 \text{ Pa}^{0.5}$$

$$1.4\text{e-}7 \leq \nu_L \leq 9.9\text{e-}5 \text{ m}^2/\text{s}$$

$$1.4\text{e-}7 \leq \nu_G \leq 1.06\text{e-}4 \text{ m}^2/\text{s}$$

The liquid holdup (β_L) in Equation (2-13) can be calculated using Equation (2-19) in two-phase flow. The liquid Reynolds number and Froude number are calculated using Equations (2-20)and (2-21), respectively.

$$\beta_L = \left(12 \cdot \frac{Fr_L}{Re_L}\right)^{1/3} \left(\frac{a_h}{a}\right)^{2/3} \qquad (2\text{-}19)$$

$$Re_L = \frac{u_L \rho_L}{a \mu_L} \qquad (2\text{-}20)$$

$$Fr_L = \frac{u_L{}^2 a}{g} \qquad (2\text{-}21)$$

$$\text{If } Re_L < 5, \qquad \frac{a_h}{a} = C_h Re_L{}^{0.15} Fr_L{}^{0.1} \qquad (2\text{-}22)$$

$$\text{If } Re_L \geq 5, \qquad \frac{a_h}{a} = 0.85 C_h Re_L{}^{0.25} Fr_L{}^{0.1} \qquad (2\text{-}23)$$

Where C_h is characteristic constant of the packing as given in Table 2-2.

Table 2-2: Values of Characteristic Parameters of Berl Saddle for Billet and Schulte's Equation [96]

Packing	Materials	Nominal Size, mm	Void Fraction, ε	Specific Area, m^{-1}	C_h
Berl Saddle	Ceramic	13	0.65	545	0.833
		25	0.68	260	0.62

It should be noted that Equation (2-19) is only valid under the following constraints:

$$800 \leq \rho_L \leq 1{,}810 \text{ kg/m}^3$$

$$7.4\text{e-}7 \leq \nu_L \leq 1.42\text{e-}4 \text{ m}^2/\text{s}$$

$$20.8 \leq \sigma_L \leq 86.3 \text{ mN/m}$$

$$1.33 \leq u_L \leq 82.8 \text{ m/h}$$

$$0.1 \leq F_G \leq 2.78 \text{ Pa}^{0.5}$$

Equations (2-24) and (2-27) proposed by Stichlmair et al. [99] to calculate the dry (single-phase) pressure drop and two-phase pressure drops, respectively. This correlation was developed to calculate pressure drop correlations in packed beds for both structured and dumped packings, including ceramic Berl Saddle. Equation (2-27) was used by applying an iterative method to calculate the irrigated pressure drop (ΔP_{irr}) based on the knowledge of the dry pressure drop (ΔP_{dry}), liquid holdup (β_L) and the specific surface area of the packing (a).

$$\frac{\Delta P_{dry}}{H} = \frac{3}{4} f_0 \left[\frac{1-\varepsilon}{\varepsilon^{4.65}}\right]\left(\frac{\rho_G {u_G}^2}{d_P}\right) \tag{2-24}$$

$$f_0 = \frac{C_1}{Re_G} + \frac{C_2}{{Re_G}^{\frac{1}{2}}} + C_3 \tag{2-25}$$

$$Re_G = \frac{u_G d_p \rho_G}{\mu_G} \tag{2-26}$$

$$\frac{\Delta P_{irr}}{\rho_L\, gH} = \left(\frac{\Delta P_{dry}}{\rho_L\, gH}\right)\left\{\frac{(1-\varepsilon)\left[1-\left(\frac{\beta_L}{\varepsilon}\right)\left[1+20\left(\frac{\Delta P_{irr}}{\rho_L\, gH}\right)^2\right]\right]}{1-\varepsilon}\right\}^{\frac{2+c}{3}}\left\{1-\left(\frac{\beta_L}{\varepsilon}\right)\left[1+20\left(\frac{\Delta P_{irr}}{\rho_L\, gH}\right)^2\right]\right\}^{-4.65} \quad (2\text{-}27)$$

$$c = -\left(\frac{C_1}{Re_G} + \frac{C_2}{2Re_G^{\frac{1}{2}}}\right)\frac{1}{f_0} \quad (2\text{-}28)$$

Liquid hold up was calculated using Equation (2-29):

$$\beta_L = 0.555(Fr_L)^{1/3} \quad (2\text{-}29)$$

$$Fr_L = \frac{u_L{}^2 a}{g\, \varepsilon^{4.65}} \quad (2\text{-}30)$$

Where, d_p was calculated using Equation (2-18), H is the packing height in m; and ΔP_{dry} and ΔP_{irr} are in Pa. and C_1, C_2 and C_3 are characteristic parameters of Berl Saddle are available in Table 2-3.

Table 2-3: Values of Characteristic Parameters of Berl Saddle for Stichlmair's Equation [99]

Packing	Materials	Size, mm	Void Fraction, ε	Specific Area, ft^{-1}	C_1	C_2	C_3
Berl Saddle	Ceramic	15	0.561	300	32	6	0.9
		35	0.75	133	33	14	1

2.5 Gas-Liquid Mass Transfer in Packed-Beds

In separation process, material must diffuse from one phase to another phase. In two film theory equilibrium is assumed at the interface as proposed by Whitman in 1923 and published by McCabe et al. [100]. A resistance to mass transfer in the two phases are encountered just as is done for heat transfer [100]. However, mass transfer between phases are more complex than heat transfer due to the discontinuity at the interface. The concentration of diffusing solute is never being the same as the opposite sides of the interface [100].

The two-film theory was used to describe gas absorption into liquid solvents whether in physical or chemical methods as shown in Figure 2-5. The absorption takes place as follows:

Step 1: Transport of gas species through gas-bulk to the gas-film (δ_G);

Step 2: Transport of gas species through the gas-film to gas-liquid interface;

Step 3: Transport of the gas species from the gas-liquid interface through the liquid-film (δ_L), where physical absorption or chemical reaction would take place in the liquid film;

Step 4: Transport of the gas species from the liquid-film to the liquid-bulk; and

Step 5: Transport of the products or the gas species in the reverse directions from the liquid-bulk all the way to the gas-bulk.

According to this two-film theory, the gas-side mass transfer coefficients, $k_G = D_G/\delta_G$, and the liquid-side mass transfer coefficient, $k_L = D_L/\delta_L$, where D_G and D_L are the diffusivities of the gas species in the gas and liquid films, respectively. Also, the mass transfer flux of component A in the gas-film, Equation (2-31), and in the liquid-film, Equation (2-32) are equal.

$$N_A = k_{A,G}(P_A - P_{Ai}) \tag{2-31}$$

$$N_A = Ek_{A,L}(C_{Ai} - C_{Ae}) \tag{2-32}$$

Where E is the enhancement factor due to the chemical reaction and can be defined as the ratio of chemical to physical absorption coefficient. This factor is multiplied to the flux equation (Equation (2-32)) to reduce the complexity of calculating mass flux due to the absorption process where chemical reaction is involved [101].

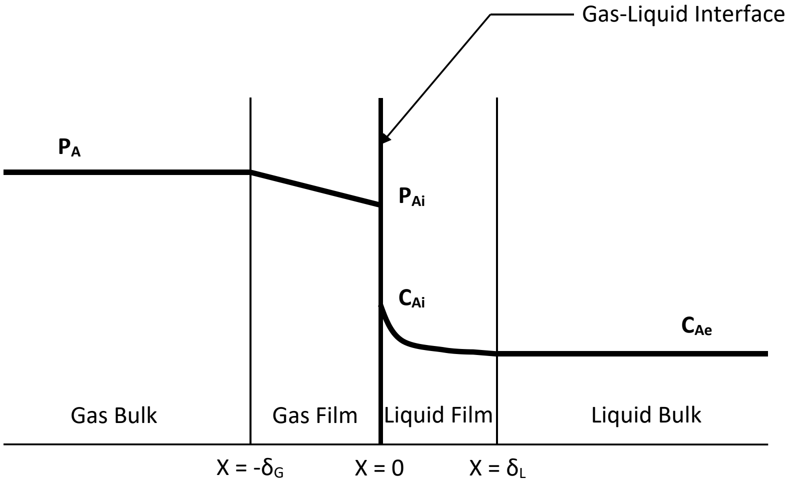

Figure 2-5: A Schematic of Two-Film Theory Schematic Plot

Henry’s law, Equation (2-33), is applicable at the interface:

$$He = \frac{P_{Ai}}{C_{Ai}} \tag{2-33}$$

The partial pressure of gas (A) at the gas-liquid interface could be calculated using Equation (2-34), obtained by coupling Equations (2-31) through (2-33).

$$P_{Ai} = \frac{\left(P_A + \left(\frac{Ek_{A,L}}{k_{A,G}}\right) c_{Ae}\right)}{\left(1 + \frac{E\,k_{A,L}}{k_{A,G}He}\right)} \tag{2-34}$$

Wellek et al. [101] expressed Enhancement factor (E) in rigorous chemical reaction calculations using Equation (2-35).

$$E = 1 + \frac{1}{[\left(\frac{1}{E_i - 1}\right)^{1.35} + (\frac{1}{E_1 - 1})^{1.35}]^{1/1.35}} \tag{2-35}$$

The instantaneous enhancement factor (E_i), the Hatta number (Ha), and E_1 are calculated using Equations (2-36), (2-37) and (2-38), respectively.

$$E_i = 1 + \left(\frac{C_{R,L}\,D_R}{\gamma D_{A,L}\,C_{Ai}}\right) \tag{2-36}$$

$$Ha = \frac{\sqrt{D_{A,L}k_2C_{R,L}}}{k_L} \tag{2-37}$$

$$E_1 = \frac{Ha}{\tanh{(Ha)}} \tag{2-38}$$

If Ha > 2, the reaction is fast, and E = Ha.

The mass transfer coefficients of the gas species in the gas and liquid sides could be predicted using correlations available in the literature. In this study, for CO_2-MEA system, the correlation used to predict the mass transfer coefficients in two-phase flow inside countercurrent packed-beds with Berl Saddle packing are given by Billet and Schultes [4] and Cho [3].

3.0 Model Development for CO_2 Absorption in an Adiabatic Packed-Bed

Modeling of CO_2 absorption in chemical and petroleum processes using packed-bed absorbers has been carried out over many decades. In 1969, Treybal [102] developed a method for steady-state, adiabatic absorption and stripping involving a single solute system. In 1972, Danckwerts [103] developed a rigorous theory for gas absorption with chemical reaction, however, the effort was mainly directed towards developing expressions for local mass transfer coefficients [2]. In 1983, Pandya [1] developed a design method for the gas absorption with chemical reaction in adiabatic packed towers, where the heat of absorption, heat of reaction, solvent evaporation and condensation, chemical reaction in the liquid-phase as well as heat and mass transfer resistances in both phases were considered. Treybal [102] and Pandya [1] argued that the heat losses in industrial gas absorption processes are generally small and adiabatic conditions in the absorbers could be assumed [2]. In 1984, Kelly et. al. [104] conducted experiments to verify the physical absorption of acid gases from coal combustion using methanol. In 1986, De Leyeg and Fromen [105] presented, based on Pandya's method, some numerical results and comparisons for commercial processes. In 1988, Sanyal et al. [106] used a similar approach to model a Benfield absorber to capture CO_2 using hot potassium carbonate solutions.

The analysis method by Pandya [1] includes five components: (1) a solute reactive gas (A), (2) reactant R (MEA), (3) inert carrier gas B (Air), (4) liquid solvent S (Water), and (5) product P (Carbamate). The absorption process was analyzed based on the two-film theory, according to which, the mass transfer flux of component A in the gas-film should equal that in the liquid-film across the interface. The model equations for material and heat balances are written for a differential element (dZ) of the packed-bed as shown in Figure 3-1. The model assumptions and corresponding model equations are discussed in the following sections.

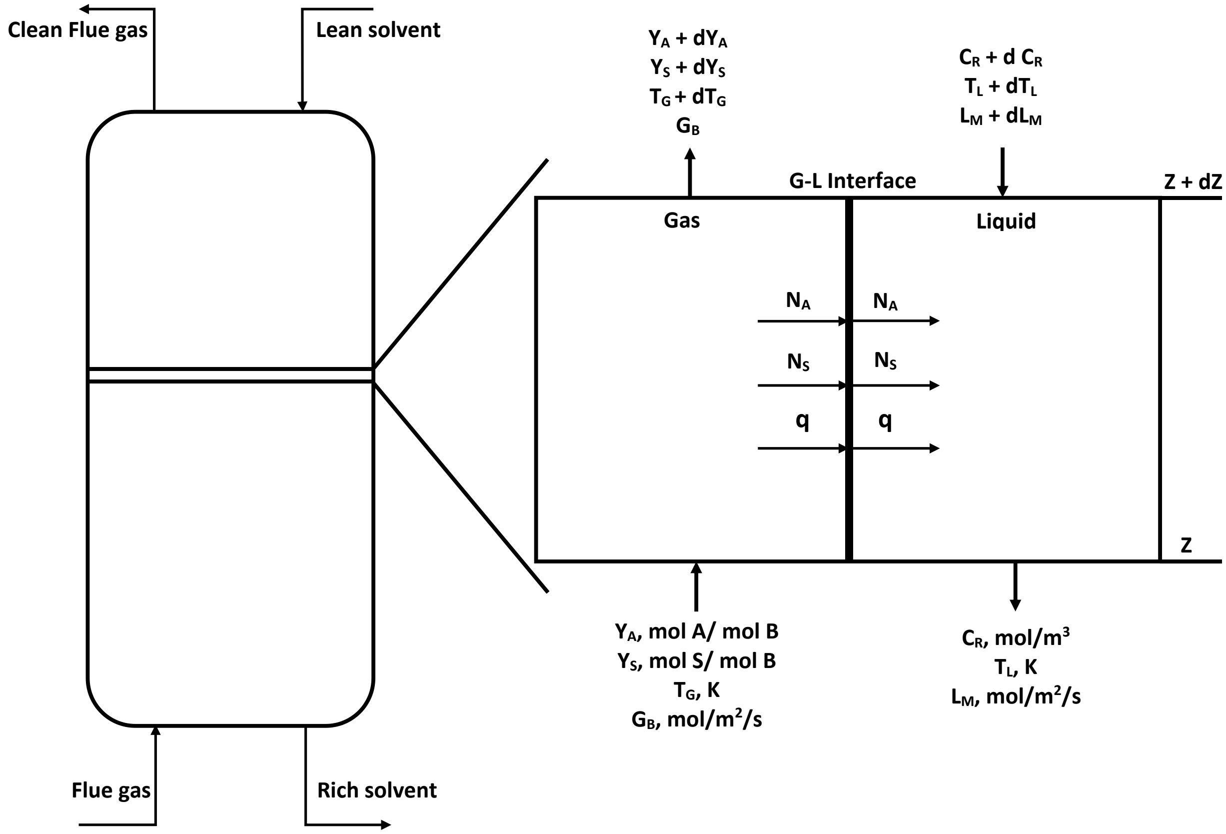

Figure 3-1: Schematic of the Packed-bed Absorber

3.1 Model Assumption

Assumption:

1. The reaction process has been described based on two film theory and considered a second order reaction that is fast enough so that the reaction takes place only in the film. The bulk of the liquid is in equilibrium [1].

2. The system is considered a steady state.
3. The temperature at the interface is the same as liquid bulk [1].
4. Due to a dilute aqueous solution, the liquid phase mass transfer resistance for the volatile solvent is negligible [1].
5. Axial Dispersion has not considered [1].
6. The interfacial area is the same as the heat and mass transfer [2].
7. The packed-bed is adiabatic. This assumption is acceptable because the heat losses due to heat transfer are generally small in industrial absorbers [107].
8. The liquid-phase mass transfer resistance for the volatile solvent (S) is negligible.
9. The carrier gas (B) is inert and does not react with any other component in the mixture [1].
10. The liquid-phase density is homogenous.
11. Rate of bicarbonate formation is insignificant. This assumption is true for an instantaneous second order irreversible reaction [65].

3.2 Model Equations

The material and heat balances in the control volume depicted in Figure 3-2 are required for modeling this adiabatic absorber. These balances allow calculating the molar ratio gradients, and the gas-phase as well as the liquid-phase temperatures.

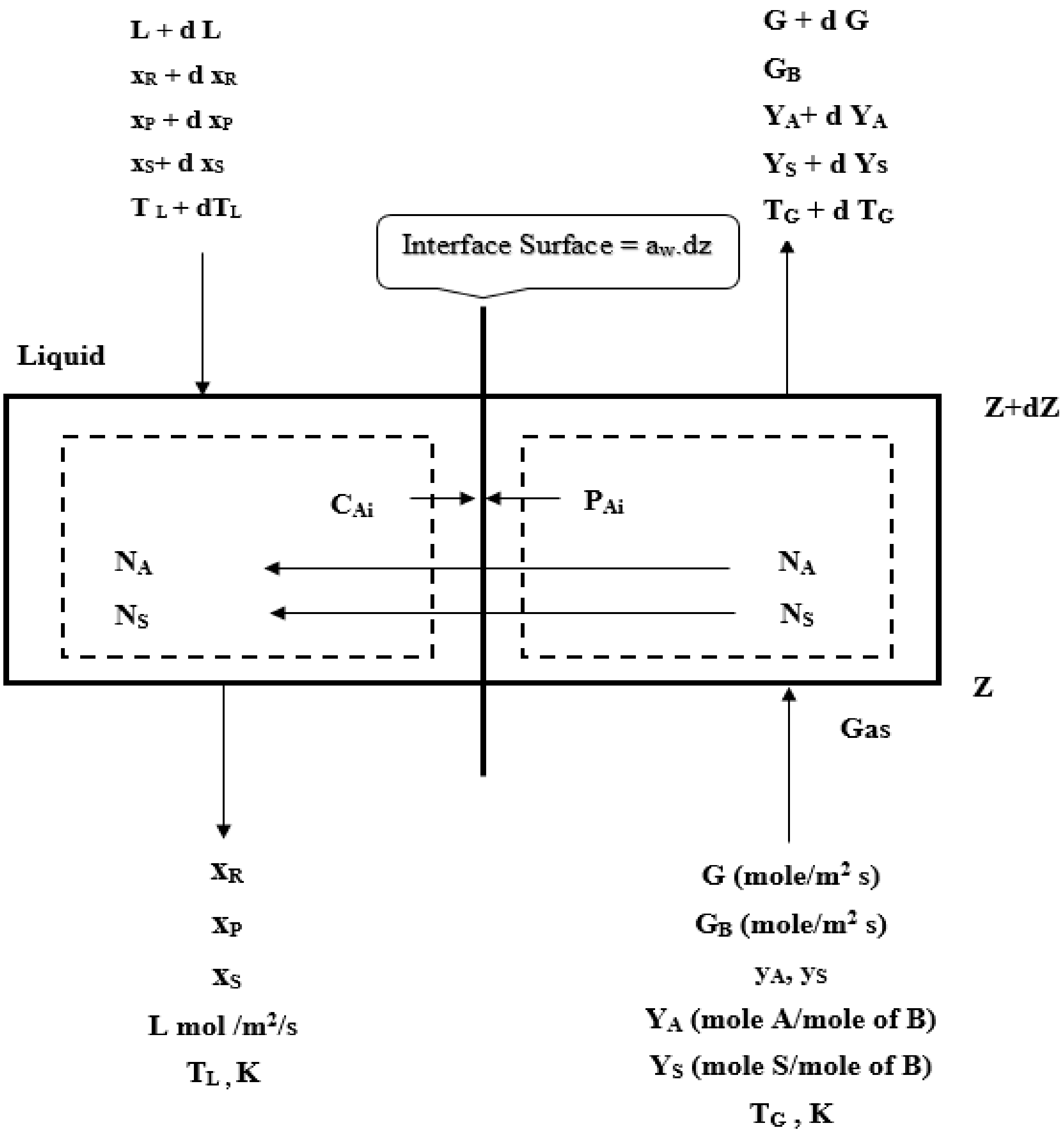

Figure 3-2: Schematic of a Differential Section of the Packed-bed Absorber

3.2.1 Material Balance

According to the reaction mechanism discussed in section 2.1, 1 mole acid gas (A) reacts with 2 mole reactant (R) to produce 1 mole of carbamate (P). It should be emphasized that the stoichiometry of the chemical reaction is considered of the Equation (3-1) as γ where the stoichiometric coefficient (γ) is 2.

$$\mathrm{A\ (g)} + \gamma \mathrm{R\ (aq)} = \mathrm{P\ (aq)} \tag{3-1}$$

According to the stoichiometry of Equation (3-1), the following relationships could be developed:

$$\frac{\mathrm{N_A a_w dz}}{1} = \frac{\frac{\mathrm{L}}{\rho_\mathrm{m}} \mathrm{dn_R}}{\gamma} = \frac{\frac{\mathrm{L}}{\rho_\mathrm{m}} \mathrm{dn_P}}{-1} \tag{3-2}$$

Also, the change in molar concentration of S (H_2O) in solution is related to the flux N_S by Equation (3-3).

$$\frac{\mathrm{N_S a_w dz}}{1} = \frac{\frac{\mathrm{L}}{\rho_\mathrm{m}} \mathrm{dn_s}}{-1} \tag{3-3}$$

$$\mathrm{dn_R} = \gamma \frac{\rho_\mathrm{m}}{\mathrm{L}} \mathrm{N_A a_w dz} \tag{3-4}$$

$$\mathrm{dn_p} = -\frac{\rho_\mathrm{m}}{\mathrm{L}} \mathrm{N_A a_w dz} \tag{3-5}$$

$$\mathrm{dn_s} = -\frac{\rho_\mathrm{m}}{\mathrm{L}} \mathrm{N_s a_w dz} \tag{3-6}$$

In this countercurrent process, the gas side mass transfer equation is unaffected by the liquid phase reaction. A steady-state material balance equation in the differential element (dZ) shown in Equation (3-8).

For the overall material balance across control volume, we can write:

$$(\mathrm{L} + \mathrm{dL}) + \mathrm{G} = \mathrm{L} + (\mathrm{G} + \mathrm{dG}) \tag{3-7}$$

$$\mathrm{dL} = \mathrm{dG} \tag{3-8}$$

3.2.1.1 Material Balance in the Gas-phase

Considering the gas-side control volume shown in Figure 3-3, material balance in the Gas side can be considered.

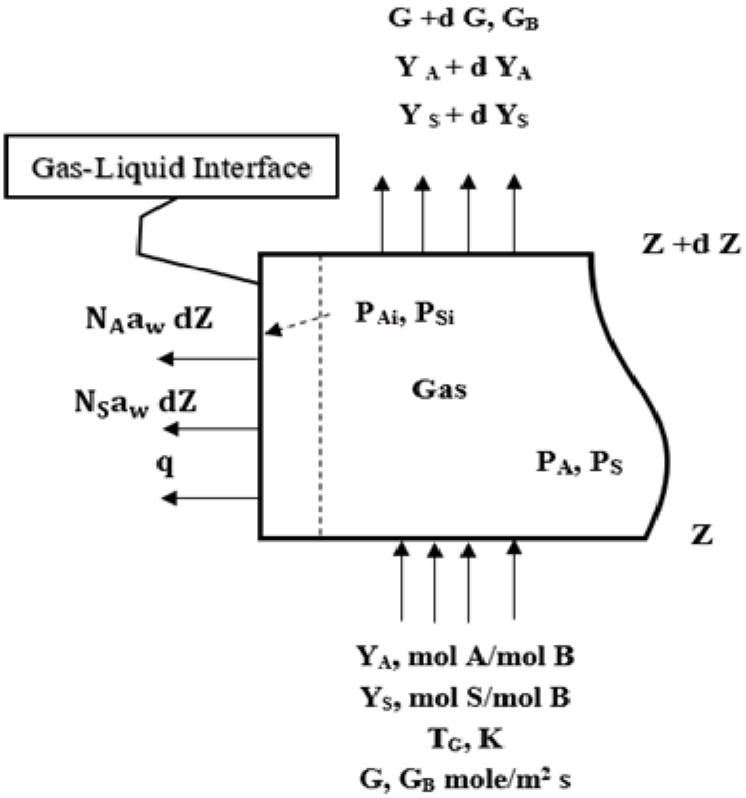

Figure 3-3: Schematic of a Differential Section of the Gas-phase

Applying mass balance across the control volume and can be written as Equation (3-9). Due to the steady state system there is no mass accumulation in the differential element (dZ) for the gas-phase an can be represented by Equations (3-10) through Equation (3-12).

$$\text{Rate of mass in} - \text{Rate of mass out} = \text{Rate of mass accumulation} \tag{3-9}$$

$$\text{Rate of gas mass in} = \text{Rate of gas mass out} \tag{3-10}$$

$$\text{Rate of gas mass in} = \mathrm{G} \tag{3-11}$$

$$\text{Rate of gas mass out} = (\mathrm{G} + \mathrm{dG}) + (\mathrm{N_A a_w dZ} + \mathrm{N_S a_w dZ}) \tag{3-12}$$

Combining Equations (3-11) and (3-12) leads to Equation (3-13).

$$-\mathrm{dG} = \mathrm{N_A a_w dZ} + \mathrm{N_S a_w dZ} \tag{3-13}$$

Since the gas-phase consists of component (A), (B) and (S), the total gas flow rate is expressed as a function of the inert gas (B) flow rate and molar ratios as presented in Equation (3-14).

$$\mathrm{G} = \mathrm{G_B}(1 + \mathrm{Y_A} + \mathrm{Y_S}) \tag{3-14}$$

Differentiating both sides of Equation (3-14) leads to Equation (3-15).

$$-\mathrm{dG} = -\mathrm{G_B dY_A} - \mathrm{G_B dY_S} \tag{3-15}$$

Comparing Equation (3-13) and (3-15) gives Equation (3-16) and (3-17):

$$\mathrm{N_A a_w dZ} = -\mathrm{G_B dY_A} \tag{3-16}$$

$$\mathrm{N_S a_w dZ} = -\mathrm{G_B dY_S} \tag{3-17}$$

According to the two-film theory depicted in Figure 2-5, the mass transfer of components A and S can be written as:

$$N_A a_w dZ = k_{G,A} P(y_A - y_{Ai}) a_w dZ \tag{3-18}$$

$$N_S a_w dZ = k_{G,S} P(y_S - y_{Si}) a_w dZ \tag{3-19}$$

Coupling Equations (3-16), (3-17), (3-18) and (3-19) yields:

$$-G_B dY_A = k_{G,A} a_w P(y_A - y_{Ai}) dZ \tag{3-20}$$

$$-G_B dY_S = k_{G,S} a_w P(y_S - y_{Si}) dZ \tag{3-21}$$

Thus, the molar ratio gradient for component A and S in the gas-phase can be written as follows:

$$\frac{dY_A}{dZ} = -\frac{k_{G,A} a_w P(y_A - y_{Ai})}{G_B} \tag{3-22}$$

$$\frac{dY_S}{dZ} = -\frac{k_{G,S} a_w P(y_S - y_{Si})}{G_B} \tag{3-23}$$

3.2.1.2 Material Balance in the Liquid-phase

Considering the liquid-side control volume shown in Figure 3-4, a steady-state material balance equations in the differential element (dZ) for the liquid-phase is described by Equation (3-24) through Equation (3-26).

$$\text{Rate of liquid mass in} = \text{Rate of liquid mass out} \tag{3-24}$$

$$\text{Rate of liquid mass in} = (\mathrm{L} + \mathrm{dL}) + (\mathrm{N_A a_w dZ} + \mathrm{N_S a_w dZ}) \tag{3-25}$$

$$\text{Rate of liquid mass out} = \mathrm{L} \tag{3-26}$$

Combining Equations (3-25) and (3-26) leads to Equation (3-27).

$$\mathrm{dL} = -\,(\mathrm{N_A a_w dZ} + \mathrm{N_S a_w dZ}) \tag{3-27}$$

Combining with Equation (3-16) and (3-17) gives:

$$\frac{\mathrm{dL}}{\mathrm{dZ}} = \mathrm{G_B}\left(\frac{\mathrm{dY_A}}{\mathrm{dZ}} + \frac{\mathrm{dY_S}}{\mathrm{dZ}}\right) \tag{3-28}$$

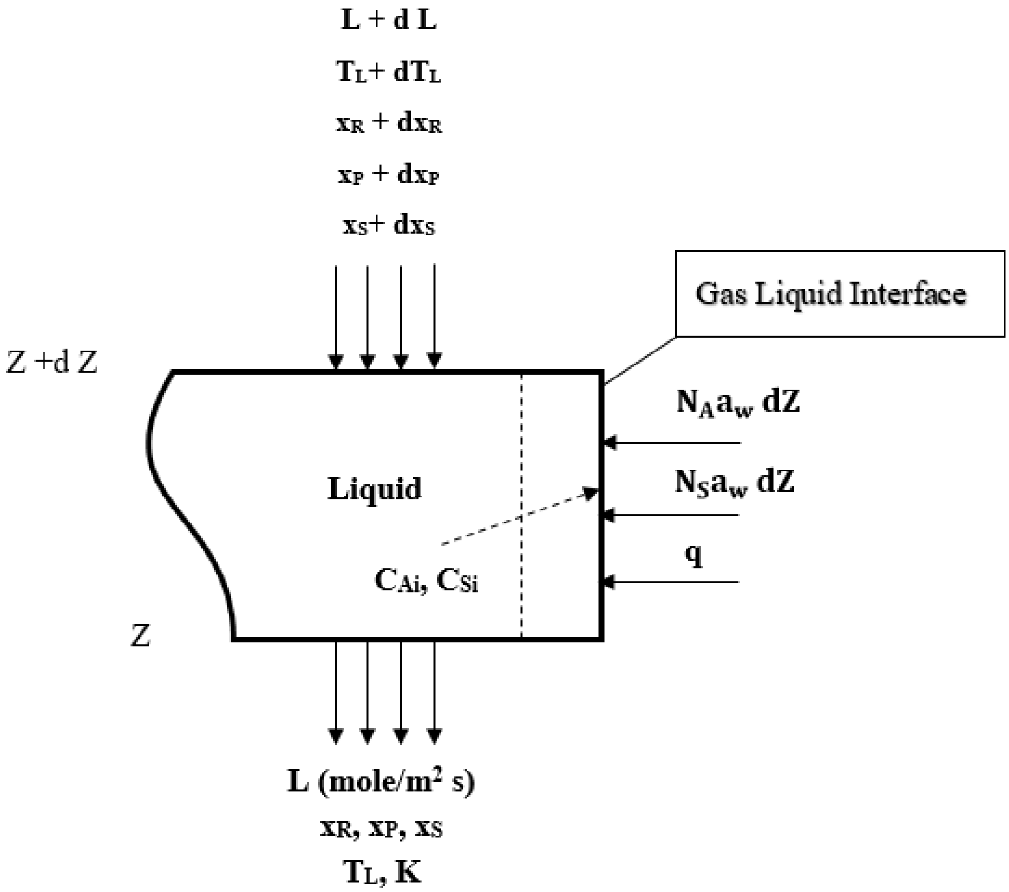

Figure 3-4: Schematic of a Differential Section of the Liquid-phase

The liquid-phase consists of three components (R), (P) and (S). The material balance for R can be expressed by Equations (3-29) through (3-32).

$$\text{Rate of (R) mass in} - \text{Rate of mass comsumed} = \text{Rate of (R) mass out} \qquad (3\text{-}29)$$

$$\text{Rate of liquid mass in} = (L + dL)(x_R + dx_R) \qquad (3\text{-}30)$$

$$\text{Rate of liquid mass consumed} = \gamma N_A a_w dZ \qquad (3\text{-}31)$$

$$\text{Rate of liquid mass out} = Lx_R \qquad (3\text{-}32)$$

Neglecting dL.dx_R and combining Equations (3-30) through (3-32) gives:

$$d(Lx_R) = \gamma N_A a_w dZ \quad (3\text{-}33)$$

Similarly, the mole fraction gradient of the product (P) could be derived:

$$\text{Rate of (P) mass in} + \text{Rate of (P) produced} = \text{Rate of (P) mass out} \quad (3\text{-}34)$$

$$\text{Rate of liquid mass in} = (L + dL)(x_P + dx_P) \quad (3\text{-}35)$$

$$\text{Rate of (P) mass produced} = N_A a_w dZ \quad (3\text{-}36)$$

$$\text{Rate of liquid mass out} = Lx_P \quad (3\text{-}37)$$

$$d(Lx_P) = -\,N_A a_w dZ \quad (3\text{-}38)$$

Similarly, mole fraction gradient of the water (S) could be derived:

$$\text{Rate of (S)mass in} = \text{Rate of (S) mass out} \quad (3\text{-}39)$$

$$\text{Rate of liquid mass in} = (L + dL)(x_S + dx_S) + N_S a_w dZ \quad (3\text{-}40)$$

$$\text{Rate of liquid mass out} = Lx_S \quad (3\text{-}41)$$

$$d(Lx_S) = -\,N_S a_w dZ \quad (3\text{-}42)$$

3.2.2 Energy Balance

Similar to the material balance, an enthalpy balance can be made for both gas and liquid using energy conservation law as mentioned in Equation (3-43).

$$\text{Rate of enthalpy in} - \text{Rate of enthalpy out} = \text{Rate of heat transfer} \qquad (3\text{-}43)$$

3.2.2.1 Energy Balance in the Gas-phase

Considering the gas-side control volume shown in Figure 3-3, the balance of the gas-phase enthalpy (H) per mole of component (B) can be written as follows:

$$\begin{aligned}&\text{Rate of enthalpy in} - \text{Rate enthalpy out}\\ &\qquad = \text{Rate of enthalpy transfer from gas to liquid}\end{aligned} \qquad (3\text{-}44)$$

$$\text{Rate of enthalpy in} = G_B H \qquad (3\text{-}45)$$

$$\begin{aligned}&\text{Rate of enthalpy out}\\ &\qquad = G_B(H + dH) + N_A\, a_w\big[\big(C_{P,A}(T_G - T_o) + H_A^{gas}(T_o, P)\big]dz \qquad (3\text{-}46)\\ &\qquad + N_S\, a_w[(C_{P,S}(T_G - T_o) + H_S^{gas}(T_o, P)]dz\end{aligned}$$

$$\text{Rate of enthalpy transfer from the gas to the liquid} = h'_G(T_G - T_L)a_w dz \qquad (3\text{-}47)$$

Where h'_G is an overall corrected heat transfer coefficient.

Substituting Equations (3-45), (3-46) and (3-47) into Equation (3-44) gives Equation (3-48):

$$\begin{aligned} &-\mathrm{G_B dH} - \mathrm{N_A\, a_w dz}\big[\big(\mathrm{C_{PA}(T_G - T_o)} + \mathrm{H_A^{gas}(T_o, P)}\big] \\ &\qquad - \mathrm{N_S\, a_w dz}\big[\big(\mathrm{C_{PS}(T_G - T_o)} + \mathrm{H_S^{gas}(T_o, P)}\big] = \mathrm{h'_G(T_G - T_L) a_w dz} \end{aligned} \tag{3-48}$$

According to Equation (3-16) and (3-17), Equation (3-48) could be written as Equation (3-49):

$$\begin{aligned} &-\mathrm{G_B dH} + \mathrm{G_B dY_A}\big[\big(\mathrm{C_{P,A}(T_G - T_o)} + \mathrm{H_A^{gas}(T_o, P)}\big] + \mathrm{G_B dY_S}\big[\big(\mathrm{C_{P,S}(T_G - T_o)} + \mathrm{H_S^{gas}(T_o, P)}\big] \\ &\qquad = \mathrm{h'_G(T_G - T_L) a_w dz} \end{aligned} \tag{3-49}$$

The enthalpy of a gas mixture (H) is expressed in Equation (3-50) and the derivative of enthalpy (dH) is shown in Equation (3-51).

$$\begin{aligned} \mathrm{H} = &\big[\big(\mathrm{C_{P,B}(T_G - T_o)} + \mathrm{H_B^{gas}(T_o, P)}\big] + \mathrm{Y_A}\,\big[\big(\mathrm{C_{P,A}(T_G - T_o)} + \mathrm{H_A^{gas}(T_o, P)}\big] \\ &\qquad + \mathrm{Y_S}\,\big[\big(\mathrm{C_{P,S}(T_G - T_o)} + \mathrm{H_S^{gas}(T_o, P)}\big] \end{aligned} \tag{3-50}$$

$$\begin{aligned} \mathrm{dH} = &\ \mathrm{C_{P,B} dT_G} + \mathrm{Y_A C_{P,A} dT_G} + \mathrm{G_B Y_S C_{P,S} dT_G} + \big[\big(\mathrm{C_{P,A}(T_G - T_o)} + \mathrm{H_A^{gas}(T_o, P)}\big]\mathrm{dY_A} \\ &\qquad + \big[\big(\mathrm{C_{P,S}(T_G - T_o)} + \mathrm{H_S^{gas}(T_o, P)}\big]\mathrm{dY_S} \end{aligned} \tag{3-51}$$

Substituting Equation (3-51) into Equation (3-49) and simplifying it gives:

$$-\mathrm{G_B}\left(\mathrm{C_{P,B}} + \mathrm{Y_A C_{P,A}} + \mathrm{Y_S C_{P,S}}\right)\mathrm{dT_G} = \mathrm{h'_G a_w (T_G - T_L) dz} \tag{3-52}$$

Simplifying Equation (3-52) a temperature gradient in differential element for gas-phase is given in Equations (3-53):

$$\frac{\mathrm{dT_G}}{\mathrm{dZ}} = \frac{-\mathrm{h'_G (T_G - T_L) a_w}}{\mathrm{G_B}\left(\mathrm{C_{P,B}} + \mathrm{Y_A C_{P,A}} + \mathrm{Y_S C_{P,S}}\right)} \tag{3-53}$$

3.2.2.2 Energy Balance in the Liquid-phase

Considering the liquid-side control volume shown in Figure 3-4, the balance of the liquid-phase enthalpy ($\mathrm{H_L}$) can be written as follows:

$$\begin{aligned}&\text{Rate of enthalpy in} - \text{Rate enthalpy out}\\ &\qquad = \text{Rate of enthalpy transfer from Liquid to gas}\end{aligned} \tag{3-54}$$

$$\begin{aligned}&\text{Rate of enthalpy in}\\ &\qquad = \mathrm{(L + dL)(H_L + dH_L) + N_A\, a_w}\left[\left(\mathrm{C_{PA}(T_G - T_o) + H_A^{gas}(T_o, P)}\right]\mathrm{dz}\right.\\ &\qquad + \mathrm{N_S\, a_w[(C_{P,S}(T_G - T_o) + H_S^{gas}(T_o, P)]dz}\end{aligned} \tag{3-55}$$

$$\text{Rate of enthalpy out} = \mathrm{LH_L} \tag{3-56}$$

$$\text{Rate of enthalpy transfer from liquid to gas} = -\,h'_G(T_G - T_L)a_w dz \tag{3-57}$$

Substituting Equation (3-52) into Equation (3-57):

$$\text{Rate of enthalpy transfer from liquid to gas} = G_B\left(C_{P,B} + Y_A C_{P,A} + Y_S C_{P,S}\right)dT_G \tag{3-58}$$

Plugging Equations (3-55), (3-56) and (3-58) into Equation (3-54) leads to Equation (3-59):

$$\begin{aligned}(LdH_L) + (H_L dL) + (dLdH_L) + N_A a_w\left[C_{P,A}(T_G - T_O) + H_A^{gas}(T_o, P)\right]dZ \\ + N_s a_w\left[C_{P,S}(T_G - T_O) + H_S^{gas}(T_o, P)\right]dZ \\ = \left[G_B\left(C_{P,B} + Y_A C_{P,A} + Y_S C_{P,S}\right)dT_G\right]\end{aligned} \tag{3-59}$$

Substituting Equation (3-16) and (3-17) into Equation (3-59):

$$\begin{aligned}LdH_L + H_L dL + dLdH_L - G_B dY_A\left[C_{P,A}(T_G - T_o) + H_A^{gas}(T_o, P)\right] \\ - G_B dY_S\left[C_{P,S}(T_G - T_o) + H_S^{gas}(T_o, P)\right] = \left[G_B\left(C_{P,B} + Y_A C_{P,A} + Y_S C_{P,S}\right)dT_G\right]\end{aligned} \tag{3-60}$$

On account of dilute solution where large amount of the volatile solvent (H_2O) exists, the molar density of the liquid is constant. The enthalpy of the solution can be as Equation (3-61).

$$H_L = \frac{1}{\rho_m}\sum_i n_i H_i^{aq}(T_L) = \frac{1}{\rho_m}\sum_i n_i \left[H_i^{aq}(T_0, P) + \int_{T_0}^{T_L} C_{P,i} dT\right] \tag{3-61}$$

Where i represents (A), (R), (P) and (S); ρ_m is molar density of solution, mol/m^3; n_i is molar concentration of species i, mol/m^3. Liquid enthalpy derivative (dH_L) is represented by Equation (3-62).

$$\begin{aligned} dH_L &= \frac{1}{\rho_m} d\left\{\sum_i n_i \left[H_i^{aq}(T_0, P) + \int_{T_0}^{T_L} C_{P,i} dT\right]\right\} \\ &= \frac{1}{\rho_m}\left\{\sum_i \left[H_i^{aq}(T_0, P)\right] dn_i + \sum_i d\left[\int_{T_0}^{T_L} n_i C_{P,i} dT\right]\right\} \end{aligned} \tag{3-62}$$

$C_{P,i}$ is assumed to be an average heat capacity of species i between temperature T_0 and T_L, which is a reasonable assumption hence the heat capacity of the main component (H_2O) is not very sensitive to temperature. Therefore,

$$
\begin{aligned}
dH_L &= \frac{1}{\rho_m}\left\{\sum_i \left[H_i^{aq}(T_0,P)\right]dn_i + \sum_i d\left[n_i C_{P,i}(T_L - T_0)\right]\right\} \\
&= \frac{1}{\rho_m}\sum_i \left[H_i^{aq}(T_0,P)\right]dn_i + \frac{1}{\rho_m}\sum_i n_i C_{P,i} dT_L \qquad (3\text{-}63) \\
&= \frac{1}{\rho_m}\sum_i \left[H_i^{aq}(T_0,P)\right]dn_i + C_L dT_L
\end{aligned}
$$

Expanding Equation (3-63) for all species i and rearranging leads to:

$$
dH_L = \frac{1}{\rho_m}\left[H_A^{aq}(T_0,P)dn_A + H_R^{aq}(T_0,P)dn_R + H_P^{aq}(T_0,P)dn_P + H_S^{aq}(T_0,P)dn_S\right] + C_L dT_L \qquad (3\text{-}64)
$$

In this Equation, dn_A is negligible because (A) is the reactant, its molar concentration in the liquid (n_A) is small for irreversible reaction. Substituting with Equation (3-4), (3-5) and (3-6), Equation (3-65) can be written as:

$$
\begin{aligned}
dH_L = \frac{1}{\rho_m}&\left[H_R^{aq}(T_0,P)\gamma N_A a_w dz\frac{\rho_m}{L} - H_P^{aq}(T_0,P)N_A a_w dz\frac{\rho_m}{L} - H_S^{aq}(T_0,P)N_S a_w dz\frac{\rho_m}{L}\right] \qquad (3\text{-}65) \\
&+ C_L dT_L
\end{aligned}
$$

$$
dH_L = \frac{1}{L}\left[H_R^{aq}(T_0,P)\gamma N_A a_w dz - H_P^{aq}(T_0,P)N_A a_w dz - H_S^{aq}(T_0,P)N_S a_w dz\right] + C_L dT_L \qquad (3\text{-}66)
$$

Therefore, Using Equation (3-16) and (3-17), Equation (3-66) could be rewritten as:

$$\mathrm{dH_L} = \frac{1}{\mathrm{L}}\left[-\gamma \mathrm{H_R^{aq}(T_0,P)G_B dY_A} + \mathrm{H_P^{aq}(T_0,P)G_B dY_A} + \mathrm{H_S^{aq}(T_0,P)G_B dY_S}\right] + \mathrm{C_L dT_L} \tag{3-67}$$

Partially plugging Equation (3-67) into Equation (3-60) resulted as Equation (3-68):

$$\begin{aligned}
&\mathrm{LC_L dT_L} - \gamma \mathrm{H_R^{aq}(T_0,P)G_B dY_A} + \mathrm{H_P^{aq}(T_0,P)G_B dY_A} + \mathrm{H_S^{aq}(T_0,P)G_B dY_S} \\
&\qquad - \mathrm{G_B dY_A}\left[\mathrm{C_{P,A}(T_G - T_o)} + \mathrm{H_A^{gas}(T_o,P)}\right] \\
&\qquad - \mathrm{G_B dY_S}\left[\mathrm{C_{P,S}(T_G - T_o)} + \mathrm{H_S^{gas}(T_o,P)}\right] + \mathrm{(H_L + dH_L)dL} \\
&\qquad = \left[\mathrm{G_B}\left(\mathrm{C_{P,B}} + \mathrm{Y_A C_{P,A}} + \mathrm{Y_S C_{P,S}}\right)\mathrm{dT_G}\right]
\end{aligned} \tag{3-68}$$

Rearranging the above Equation gives:

$$\begin{aligned}
&\mathrm{LC_L dT_L} - \mathrm{G_B dY_A}\left[\mathrm{H_A^{gas}(T_o,P)} + \gamma \mathrm{H_R^{aq}(T_0,P)} - \mathrm{H_P^{aq}(T_0,P)}\right] \\
&\qquad - \mathrm{G_B dY_S}\left[\mathrm{H_S^{gas}(T_o,P)} - \mathrm{H_S^{aq}(T_0,P)}\right] - \mathrm{G_B dY_A C_{P,A}(T_G - T_o)} \\
&\qquad - \mathrm{G_B dY_S C_{P,S}(T_G - T_o)} + \mathrm{(H_L + dH_L)dL} \\
&\qquad = \left[\mathrm{G_B}\left(\mathrm{C_{P,B}} + \mathrm{Y_A C_{P,A}} + \mathrm{Y_S C_{P,S}}\right)\mathrm{dT_G}\right]
\end{aligned} \tag{3-69}$$

Where the term $(\mathrm{H_P^{aq}}(\mathrm{T_0},\mathrm{P}) - \mathrm{H_A^{gas}}(\mathrm{T_o},\mathrm{P}) - \gamma\mathrm{H_R^{aq}}(\mathrm{T_0},\mathrm{P}))$ is the heat of physical absorption and chemical reaction ($\Delta H_{CO2\ in\ solution}$); and the term $(\mathrm{H_S^{gas}}(\mathrm{T_o},\mathrm{P}) - \mathrm{H_S^{aq}}(\mathrm{T_0},\mathrm{P}))$ is the latent heat of vaporization ($\Delta \mathrm{H_{LV}}$). Thus, substituting this in Equation (3-69) , Equation (3-72) can be written :

$$\begin{aligned}
&\mathrm{LC_LdT_L} - \mathrm{G_BdY_A}[-\Delta H_{CO2\ in\ solution}] - \mathrm{G_BdY_S}[\Delta\mathrm{H_{LV}}] - \mathrm{G_BdY_AC_{P,A}}(\mathrm{T_G} - \mathrm{T_o}) \\
&\qquad - \mathrm{G_BdY_SC_{P,S}}(\mathrm{T_G} - \mathrm{T_o}) + (\mathrm{H_L} + \mathrm{dH_L})\mathrm{dL} \\
&\qquad = [\mathrm{G_B}\big(\mathrm{C_{P,B}} + \mathrm{Y_AC_{P,A}} + \mathrm{Y_SC_{P,S}}\big)\mathrm{dT_G}]
\end{aligned} \tag{3-70}$$

$$\begin{aligned}
&\mathrm{LC_LdT_L} + \mathrm{G_BdY_A}[\Delta H_{CO2\ in\ solution}] - \mathrm{G_BdY_S}[\Delta\mathrm{H_{LV}}] - \mathrm{G_BdY_AC_{P,A}}(\mathrm{T_G} - \mathrm{T_o}) \\
&\qquad - \mathrm{G_BdY_SC_{P,S}}(\mathrm{T_G} - \mathrm{T_o}) + (\mathrm{H_L} + \mathrm{dH_L})\mathrm{dL} \\
&\qquad = [\mathrm{G_B}\big(\mathrm{C_{P,B}} + \mathrm{Y_AC_{P,A}} + \mathrm{Y_SC_{P,S}}\big)\mathrm{dT_G}]
\end{aligned} \tag{3-71}$$

Simplifying Equation (3-71) :

$$\begin{aligned}
&\mathrm{LC_LdT_L} + (\mathrm{H_L} + \mathrm{dH_L})\mathrm{dL} \\
&\qquad = \mathrm{G_BdY_A}\big[\mathrm{C_{P,A}}(\mathrm{T_G} - \mathrm{T_o}) - \Delta H_{CO2\ in\ solution}\big] \\
&\qquad + \mathrm{G_BdY_S}\big[\mathrm{C_{P,S}}(\mathrm{T_G} - \mathrm{T_o}) + \Delta\mathrm{H_{LV}}\big] + [\mathrm{G_B}\big(\mathrm{C_{P,B}} + \mathrm{Y_AC_{P,A}} + \mathrm{Y_SC_{P,S}}\big)\mathrm{dT_G}]
\end{aligned} \tag{3-72}$$

$$\begin{aligned}
&\mathrm{LC_LdT_L} + (\mathrm{H_L} + \mathrm{dH_L})\mathrm{dL} \\
&\qquad = \mathrm{G_B}\Big[\mathrm{dY_A}\big[\mathrm{C_{P,A}}(\mathrm{T_G} - \mathrm{T_o}) - \Delta H_{CO2\ in\ solution}\big] \\
&\qquad + \mathrm{dY_S}\big[\mathrm{C_{P,S}}(\mathrm{T_G} - \mathrm{T_o}) + \Delta\mathrm{H_{LV}}\big] + \big[\big(\mathrm{C_{P,B}} + \mathrm{Y_AC_{P,A}} + \mathrm{Y_SC_{P,S}}\big)\mathrm{dT_G}\big]\Big]
\end{aligned} \tag{3-73}$$

As dH_LdL is very small, ignoring this term from the above, the resulted Equation can be expressed as Equation (3-74):

$$\begin{aligned} \mathrm{LC_L dT_L + H_L dL} \\ &= \mathrm{G_B}\Big[\mathrm{dY_A}\big[\mathrm{C_{P,A}(T_G - T_o)} - \Delta H_{CO2\ in\ solution}\big] \\ &+ \mathrm{dY_S}\big[\mathrm{C_{P,S}(T_G - T_o) + \Delta H_{LV}}\big] + \big[\big(\mathrm{C_{P,B} + Y_A C_{P,A} + Y_S C_{P,S}}\big)\mathrm{dT_G}\big]\Big] \end{aligned} \tag{3-74}$$

Simplifying Equation (3-74), a temperature gradient in differential element for liquid-phase is given in Equations (3-75).

$$\begin{aligned} \frac{\mathrm{dT_L}}{\mathrm{dZ}} = \frac{\mathrm{G_B}}{\mathrm{LC_L}}\Bigg[&\left[\big(\mathrm{C_{P,B} + Y_A C_{P,A} + Y_S C_{P,S}}\big)\frac{\mathrm{dT_G}}{dZ}\right] + \big[\mathrm{C_{P,A}(T_G - T_O)} - \Delta H_{CO2\ in\ solution}\big]\frac{\mathrm{dY_A}}{\mathrm{dZ}} \\ &+ \big[\mathrm{C_{P,S}(T_G - T_O) + \Delta H_{LV}}\big]\frac{\mathrm{dY_S}}{dZ}\Bigg] - \left(\frac{\mathrm{H_L}}{\mathrm{LC_L}}\right)\frac{\mathrm{dL}}{dZ} \end{aligned} \tag{3-75}$$

Also, using Equation (3-52), Equation (3-75) can also be written as :

$$\begin{aligned} &\mathrm{LC_L dT_L} = \\ &-\mathrm{h'_G a_w (T_G - T_L) + G_B\big[C_{P,A}(T_G - T_O) - \Delta H_r\big]dY_A + G_B\big[C_{P,S}(T_G - T_O) + \Delta H_{LV}\big]dY_S - H_L dL} \end{aligned} \tag{3-76}$$

3.2.3 Solution Method

It should be noted that even though the model based on Pandya's approach [1] has been used in the various literature by the above-mentioned authors for CO_2 absorption from CO_2-air mixture using MEA solutions, many equation parameters (physico-chemical data of the gas and liquid phases) are not mentioned and a small number of experimental errors also reported in the CO_2 material balance calculations by Tontiwachwuthikul et al. [2], made the task of replicating the model predictions more difficult than expected.

Enhancement factor (E) is a function of the interfacial concentration of A (C_{Ai}), the partial pressure of A at the interface, mass transfer coefficient (k_La) and the bulk composition of the liquid. As C_{Ai} and P_{Ai} are implicit, can be determined by a trial and error method.

The iteration method follows below steps and details of the trial and error method is shown in Figure 3-5.

Step 1 : Assume the mole fraction of component A at the interface (y_{Ai-1}).

Step 2 : Calculate P_{Ai} by applying Dalton's Law of partial pressure using equation (2-34).

Step 3 : Plug in calculated P_{Ai} (from step 2) in Henry's law of solubility (equation (2-33)) to get the concentration at interface (C_{Ai}).

Step 4 : The enhancement factor (E) is calculated using equation (2-35).

Step 5 : The mass transfer flux N_A is calculated from equation (2-32).

Step 6 : The partial pressure of A is obtained from equation (2-31).

Step 7 : The new mole fraction of A at the interface (y_{Ai-2}) is then calculated to compare with the assumed (y_{Ai-1}). A deterministic loop has been used to compare the values. If y_{Ai-1}

$\neq y_{Ai-2}$, the program will assign the value of y_{Ai-2} to y_{Ai-1} and repeat the above calculation steps. The correct mole fraction of A at the interface (y_{Ai}) will be obtained when the deterministic expression turns to be true i.e. ($y_{Ai-1} = y_{Ai-2}$).

In this connection, it can be noted that the initial assumption of y_{Ai} should be reasonable to get a reliable value through trial and error.

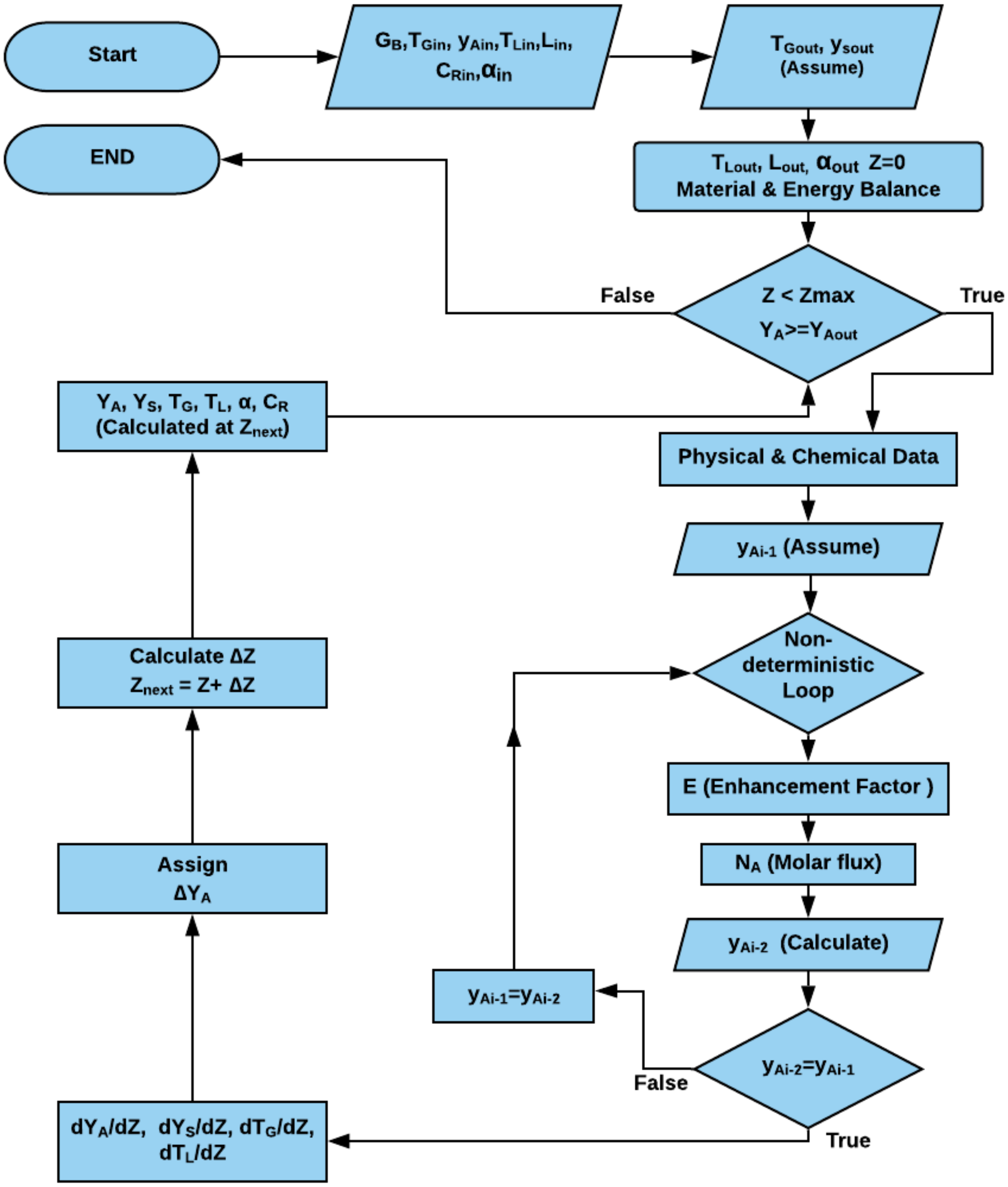

Figure 3-5: **Algorithm for Gas Absorption in a Packed-bed** [108]

3.3 Model Equation Parameter

The preceding section indicated that in order to solve the model equations of combined material and energy balances, the equation parameters including, a_w, $k_{A,L}$, $k_{A,G}$, $k_{S,G,}$ $D_{A,L,}$ $D_{R,L}$, He, k_2, H_L, $C_{P,A}$, $C_{P,S}$, $C_{P,B}$, T_O, ΔH_{LV} and ΔH_r, are needed under given boundary conditions. It should be noted that the gas-phase is a mixture (CO_2, carrier inert gas, and volatile H_2O vapor) and the liquid-phase is also a mixture (MEA, volatile liquid solvent (H_2O) and the reaction liquid products (bicarbonate or carbamates)). Therefore, calculating the physiochemical properties of the gas and liquid phases require the knowledge of the specific properties of each species in the mixture.

3.3.1 Density of Gas and Mixing Rule for Gas mixture density

The cubic Peng-Robinson (P-R) Equation of State (EOS) [109] is used to calculate the gas density which is a function of pressure, temperature and gas composition. From the theory of thermodynamics, the cubic equation will have three roots. Among these three roots, the real positive root (highest in value- for vapor phase) were considered for calculating the molar volume of the gases. The P-R EOS can be written as:

$$\mathrm{P} = \frac{\mathrm{RT}}{\mathrm{v} - \mathrm{b}} - \frac{\mathrm{a}}{\mathrm{v}^2 + 2\mathrm{vb} - \mathrm{b}^2} \tag{3-77}$$

$$\mathrm{k} = (0.37464 + 1.54226\omega - 0.26992\omega^2) \tag{3-78}$$

$$\mathrm{a(T)} = 0.45724\left(\frac{\mathrm{R}^2\, \mathrm{T_c}^2}{\mathrm{P_c}}\right)\left\{1 + \mathrm{k}\left[1 - \left(\frac{\mathrm{T}}{\mathrm{Tc}}\right)^{0.5}\right]\right\}^2 \tag{3-79}$$

$$b = 0.07780 \frac{RT_c}{P_c} \tag{3-80}$$

Where ω is an acentric factor, Tc is critical temperature and Pc is critical pressure.

The values of these parameters for different gases (CO_2, H_2O, Air), used in this study, is summarized in Table 3-1. In Equation (3-77), a and b are the attraction parameter and van der Waals co-volume, respectively.

Table 3-1: Critical Properties for selected gas [110, 111]

	Critical Pressure (P_c), bar	**Critical Temperature (T_c), K**	**Acentric Faction (ω)**
CO_2	73.8	304.1	0.225
Water Vapor	220.5	647.15	0.344
Air	37.858	132.63	0.036

Due to inlet gas to the absorption column is a mixture of CO_2 and air, the necessity of calculating mixture gas density is evident. In order to use the P-R EOS for multicomponent system, the following mixing rules published by Shibata et al.[112] in 1989 are used:

$$a_m = \sum_{i=1}^{NC} \sum_{j=1}^{NC} y_i \, y_j \, a_{ij} \tag{3-81}$$

$$b_m = \sum_{i=1}^{NC} y_i \, b_i \tag{3-82}$$

$$a_{ij} = \left(a_{ii} \, a_{jj}\right)^{\frac{1}{2}} (1 - k_{ij}) \tag{3-83}$$

Where a_m and b_m are the attraction parameter and Van der Waals co-volume for the mixture, respectively, y_i is the mole fraction of species i, NC is the number of components in the mixture, and k_{ij} is the binary interaction parameters between the i^{th} and j^{th} components.

It is assumed that $k_{ij} = k_{ji}$ and $k_{ii} = k_{jj} = 0$. By solving equation (3-77), the gas mixture molar volume (v) at a specific temperature and pressure can be obtained. The gas mixture density can then be calculated using Equation (3-84).

$$\rho = \frac{\mathrm{AMW}}{\mathrm{v}} \tag{3-84}$$

Where AMW is the apparent molecular weight of the gas mixture = $\sum y_i \, Mw_i$

3.3.2 Viscosity of Gas and Mixing Rule for Gas mixture viscosity

As viscosity of gases changes with temperature, in 1986, Zografos et.al. [113] published various thermodynamic property correlation of few common fluids in order to solve the problems of fluid dynamics and heat transfer in computer application. Equation (3-85) and (3-86) were used to calculate the viscosity of CO_2 and water vapor respectively. Also, Sutherland [114] proposed Equation (3-87) to calculate the viscosity of air. The values of Sutherland's constant and the reference temperature and viscosity for the air used from the LMNO Engineering calculation [115]. Figure 3-6 shows predicted viscosities for these three gases as a function of temperature.

$$\mu_{CO2} = (-1.1188 \times 10^{-11} \cdot T^2 + 5.0256 \text{ x } 10^{-8} \cdot T - 9.3761 \text{ x } 10^{-7}) \quad (3\text{-}85)$$

$$\mu_{H2O} = (4.0724 \times 10^{-8} \cdot T - 3.0948 \text{ x } 10^{-6}) \quad (3\text{-}86)$$

$$\mu_{Air} = 0.01827 \times 10^{-3} \left(\frac{410.85885}{0.999\ T + 120}\right) \left(\frac{1.8\ T}{524.07}\right)^{3/2} \quad (3\text{-}87)$$

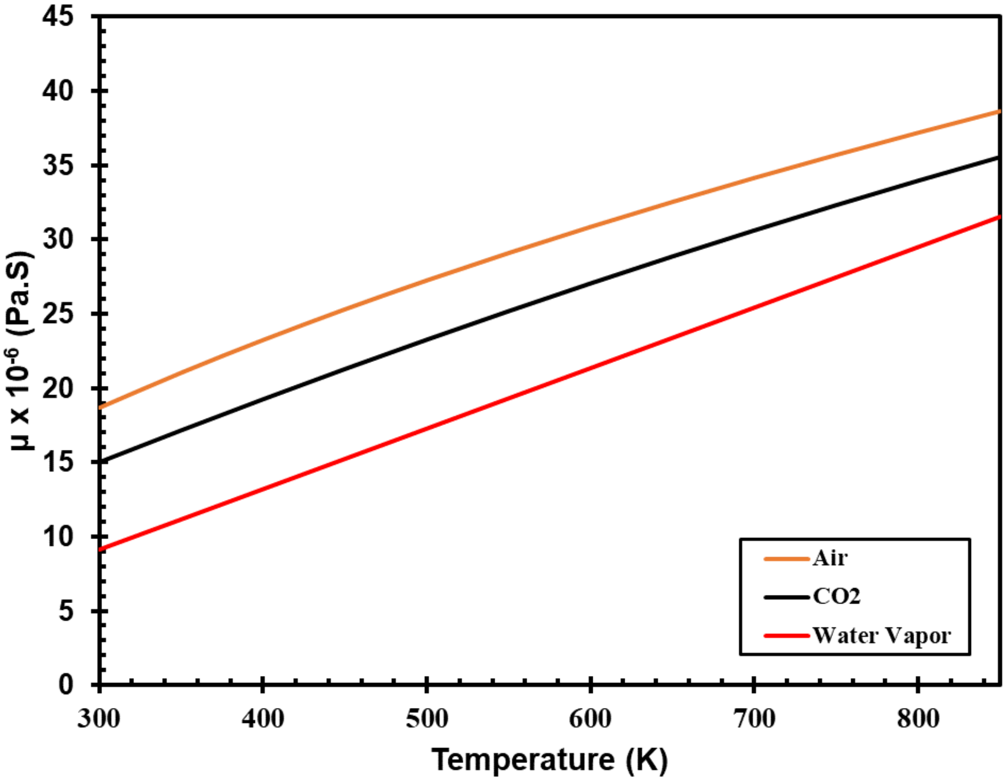

Figure 3-6: Viscosity of Gases as a Function of Temperature

For calculating the viscosity of a mixture of gases, there are a variety of equations available. The simplest model is Graham's model as mentioned by Thomas Davidson [116] in his investigation report of finding simple and accurate method for calculating the viscosity of gaseous mixture. Davidson [116] mentioned that the Graham model approximated the viscosity of mixture gases by summing the products of the viscosities (μi) of the individual components and their mole fractions (y_i) and shown in Equation (3-88).

$$\mu_{mix} = \sum_{i} \mu_i y_i \tag{3-88}$$

However, this model is inadequate where the components have not nearly the same molecular weight or molecular weight ratio is different from unity, mixtures can deviate from its behavior greatly [116]. In 1936, Herning and Zipperer [117] proposed Equation (3-89) based on the sum of partial viscosities (μ_i), weighted by the square root of the molecular weight for each species. Davidson [116] validated that the reported accuracy of Equation (3-89) for hydrocarbon mixtures is 1.5% average deviation and 5% maximum deviation, except for hydrogen-rich mixtures.

$$\mu_{mix} = \frac{\sum\left(\mu_i\, y_i \sqrt{}\mathrm{Mw}_i\right)}{\sum y_i \sqrt{\mathrm{Mw}_i}} \tag{3-89}$$

Where Mw_i is the molecular weight the i^{th} component and y_i is the mole fraction.

Also, Buddenberg and Wilke [118] suggested Equation (3-90) to calculate the viscosity of a gas mixture within 2.57% deviation:

$$\mu_{mix} = \sum_{i=1}^{n} \frac{\mu_i}{1 + \frac{1.385\mu_i}{y_i\rho_i} \sum_{\substack{j=1 \\ j\neq i}}^{n} \frac{y_i}{D_{ij}}} \quad (3\text{-}90)$$

Where ρ is the density (g/m^3); μ is the viscosity (cP); D is the diffusivity (cm^2/s); y is the mole fraction.

3.3.3 Thermal Conductivity of Gases and Gas mixture

Thermal conductivity of the gas mixture is needed to estimate the gas-side heat transfer coefficient. Equation **(**3-91**)** by Zografos et al. [113] was used to calculate the thermal conductivity of CO_2. The thermal conductivity of air was calculated using Equation (3-92) obtained from Sanyal et al. [119]. The thermal conductivity of H_2O vapor was calculated using Equation (3-93) obtained from reference [120]. It should be mentioned that Equation (3-93) is applicable at T > 326 K. At low temperatures, the thermal conductivity of water vapor is negligible. Figures 3-7 and 3-8 show the thermal conductivities of the gases as a function of temperature.

$$\lambda_{CO2} = -2.0203 \times 10^{-8}T^2 + 9.8510 \times 10^{-5}T - 1.0992 \times 10^{-2} \quad (3\text{-}91)$$

$$\lambda_{Air} = 1.5207 \times 10^{-11}T^3 - 4.8574 \times 10^{-8}T^2 + 1.018 \times 10^{-4}T - 3.933 \times 10^{-4} \quad (3\text{-}92)$$

$$\lambda_{H2O} = -2.56076 \times 10^{-11}T^3 + 9.3938 \times 10^{-8}T^2 + 2.3642 \times 10^{-5}T + 3.9539 \times 10^{-3} \quad (3\text{-}93)$$

Lindsay and Bronmley [121] proposed a generalized correlation for the thermal conductivity, Equation (3-94) which is similar to that of the viscosity, Equation (3-90) derived by Buddenberg and Wilke [118]:

$$\lambda_{\mathrm{mix}} = \sum_{i=1}^{n} \left(\frac{\lambda_i}{\frac{1}{y_i} \sum_{j=1}^{n} A_{ij} y_i} \right) \tag{3-94}$$

Where A_{ij} can be calculated using Equation (3-95):

$$A_{ij} = \frac{1}{4} \left\{ 1 + \left[\frac{\mu_i}{\mu_j} \left(\frac{Mw_j}{Mw_i} \right)^{3/4} \frac{(1 + \frac{S_i}{T})}{(1 + \frac{S_j}{T})} \right]^{1/2} \right\}^2 \frac{(1 + \frac{S_{ij}}{T})}{(1 + \frac{S_i}{T})} \tag{3-95}$$

Where μ_i/μ_j could be evaluated from Eucken Equation **(**3-96**)** [122] if the viscosity data are not available.

$$\frac{\mu_i}{\mu_j} = \frac{\lambda_i (C_{pj} + 1.25\ R/Mw_j)}{\lambda_j (C_{pi} + 1.25\ R/Mw_i)} \tag{3-96}$$

R is the universal gas constant. S is the Sutherland constants taken as a function of the boiling point in Kelvin which is available in Table 3-2:

$$S = 1.5T_B \tag{3-97}$$

Table 3-2: Typical Gases Boiling Point

Elements	T_B (K)
CO_2	194.65
Air	78.8
H_2O	373.15

If both molecules are nonpolar, S_{ij} is the geometric mean of Sutherland constant of each component:

$$S_{ij} = \sqrt{S_i S_j} \tag{3-98}$$

If one of constituents is polar, another coefficient, Equation **(**3-98**)** is required:

$$S_{ij} = 0.733\sqrt{S_i S_j} \tag{3-99}$$

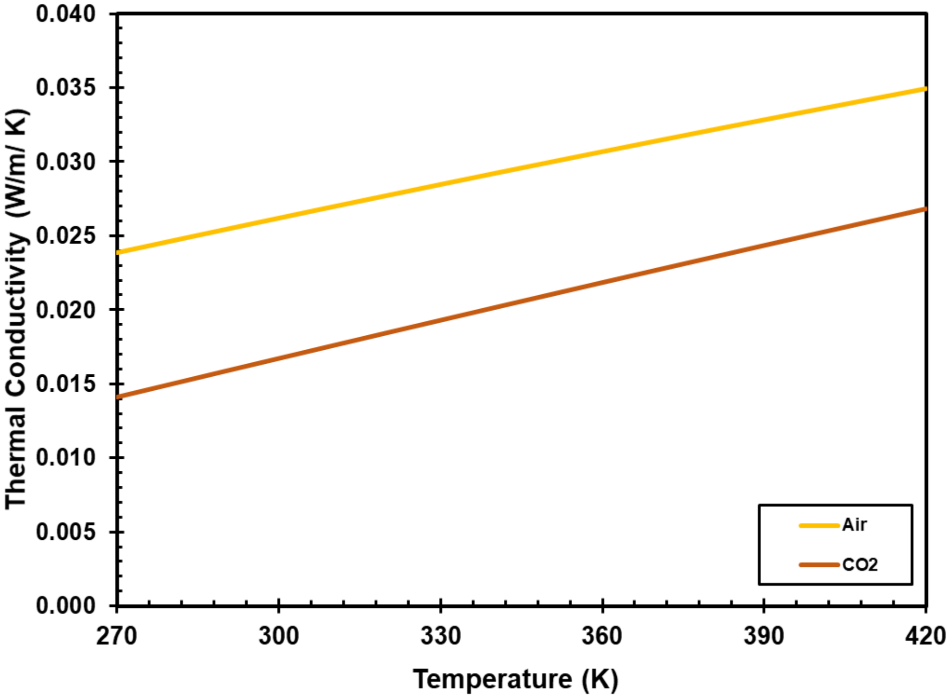

Figure 3-7: Thermal Conductivity of Gases (CO_2 and Air) as a Function of Temperature

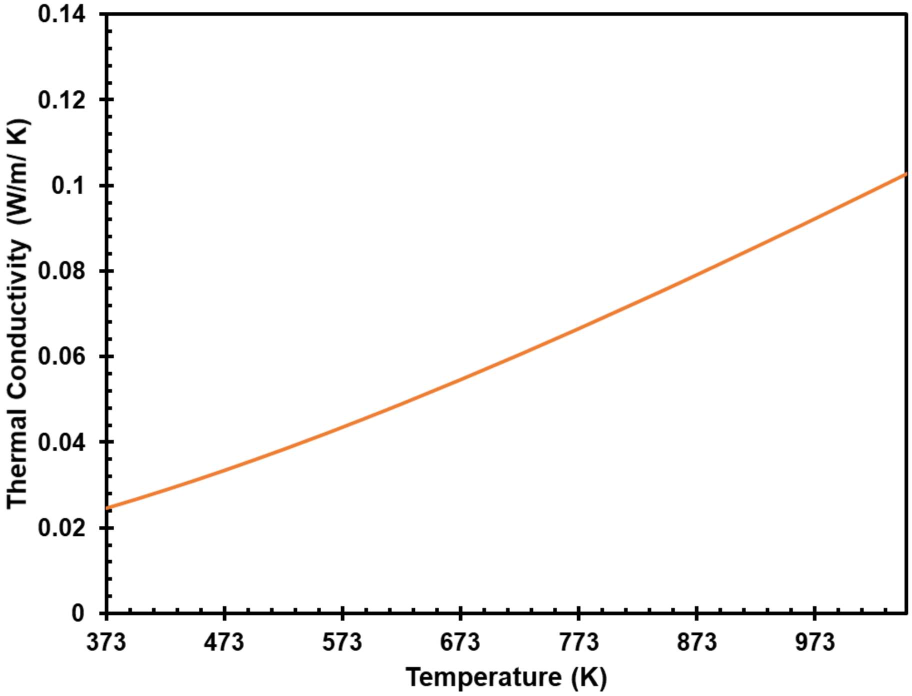

Figure 3-8: Thermal Conductivity of Water Vapor as a Function of Temperature

3.3.4 Gas/Gas Binary and Mixture Diffusivities

The gas/gas diffusivity is needed for calculating the gas-side mass transfer coefficient in gas mixtures. The gas composition includes the reactive component A, the volatile liquid component S and the inert gas component B. In order to obtain the mass transfer coefficient of a single gas component into the gaseous mixture, the binary gas diffusion coefficients should be determined. These binary gas diffusion coefficients include D_{AB}, D_{AS} and D_{BS}. Fuller et al. [123] proposed a method to predict the binary gas-phase diffusion coefficients as summarized in Equation (3-100), (3-101) and (3-102).

$$\mathrm{D_{A,B}} = \mathrm{D_{B,A}} = \frac{1 \times 10^{-3}\mathrm{T}^{1.75}(1/\mathrm{Mw_A} + 1/\mathrm{Mw_B})^{1/2}}{\mathrm{P}\left[(\sum_\mathrm{A}\mathrm{v_i})^{1/3} + (\sum_\mathrm{B}\mathrm{v_i})^{1/3}\right]^2} \tag{3-100}$$

$$\mathrm{D_{A,S}} = \mathrm{D_{S,A}} = \frac{1 \times 10^{-3}\mathrm{T}^{1.75}(1/\mathrm{Mw_A} + 1/\mathrm{Mw_S})^{1/2}}{\mathrm{P}\left[(\sum_\mathrm{A}\mathrm{v_i})^{1/3} + (\sum_\mathrm{S}\mathrm{v_i})^{1/3}\right]^2} \tag{3-101}$$

$$\mathrm{D_{B,S}} = \mathrm{D_{S,B}} = \frac{1 \times 10^{-3}\mathrm{T}^{1.75}(1/\mathrm{Mw_S} + 1/\mathrm{Mw_B})^{1/2}}{\mathrm{P}\left[(\sum_\mathrm{S}\mathrm{v_i})^{1/3} + (\sum_\mathrm{B}\mathrm{v_i})^{1/3}\right]^2} \tag{3-102}$$

$\sum_A v_i$ is the summation of the diffusion volume of each atom of the component A molecule. Similarly, the diffusion volumes for components B and S can be calculated. Fuller et al. [123] gave several diffusion volumes of typical molecules as listed in Table 3-3. As for the diffusion volumes of alkanes, ethane (C_2H_6) for instance, the summation of diffusion volumes of all atoms is needed. In this case, two carbon atoms and six hydrogen atoms lead to a diffusion volume of 44.88.

Table 3-3: Atomic Diffusion Volume and Diffusion Volume of Typical Molecules [123]

Atom	Atomic Diffusion Volume	Substance	Diffusion volume of Molecules
C	16.5	CO_2	26.9
H	1.98	N_2	17.9
O	5.48	O_2	16.6
N	5.69	H_2O	12.7
Cl	19.5	Air	20.1
S	17.0	He	2.88
Aromatic rings	-20.2	H_2	7.07

Also, for multicomponent gas mixture, Fairbanks and Wilke [124] suggested using Equation (3-103) for calculating the diffusivity of a single component A in the gas mixture. Equations (3-104) and (3-105) are also similar for component B and S, respectively.

$$\mathrm{D_{Am}} = \frac{1-\mathrm{y_A}}{\frac{\mathrm{y_B}}{\mathrm{D_{A,B}}}+\frac{\mathrm{y_S}}{\mathrm{D_{A,S}}}} \tag{3-103}$$

$$\mathrm{D_{Bm}} = \frac{1-\mathrm{y_B}}{\frac{\mathrm{y_A}}{\mathrm{D_{B,A}}}+\frac{\mathrm{y_S}}{\mathrm{D_{B,S}}}} \tag{3-104}$$

$$\mathrm{D_{Sm}} = \frac{1-\mathrm{y_S}}{\frac{\mathrm{y_B}}{\mathrm{D_{S,B}}}+\frac{\mathrm{y_A}}{\mathrm{D_{S,A}}}} \tag{3-105}$$

Where y_A, y_B, y_S are the mole fractions of components A, B, S; and D_{Am}, D_{Bm}, D_{Sm} are effective diffusivity of component A, B, S in the gas mixture, respectively.

3.3.5 Heat Capacity of the Gases

Aly and Lee [125] correlated the heat capacities as a function of temperature for over fifty different gaseous species. Equations (3-106) and (3-107) represent their correlations for CO_2 and H_2O vapor respectively. The correlated heat capacity of air as a function of temperature is regressed with high accuracy ($R^2 = 0.9998$) based on the data of Thermopedia data engine [126] and expressed as Equation (3-108). Figure 3-9 shows the heat capacities for these three gases as a function of temperature.

$$C_{P,A} = 4.184\left\{7.54056 + 7.51625\left[\frac{1442.7/T}{\sinh(1442.7/T)}\right]^2 + 5.38023\left[\frac{647.502/T}{\cosh(647.502/T)}\right]^2\right\} \qquad \text{(3-106)}$$

$$C_{P,S} = 4.184\left\{7.97183 + 6.27078\left[\frac{2572.63/T}{\sinh(2572.63/T)}\right]^2 + 2.0501\left[\frac{1156.72/T}{\cosh(1156.72)}\right]^2\right\} \qquad \text{(3-107)}$$

$$C_{P,B} = 8 \times 10^{-12}T^4 - 3 \times 10^{-8}T^3 + 4 \times 10^{-5}T^2 - 0.0165T + 31.133 \qquad \text{(3-108)}$$

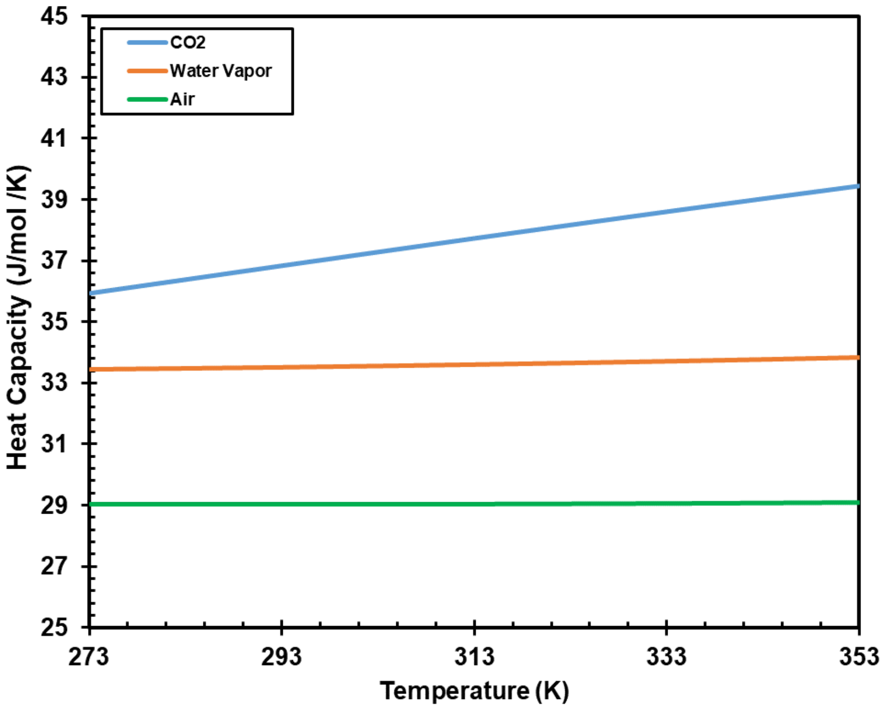

Figure 3-9: Heat Capacity of Gases as a Function of Temperature

3.3.6 Henry’s Law constant

According to Henry’s law, at a given temperature, the solubility of a gas (in terms of mole fraction of the solution) is proportional to the partial pressure of the gas. Applying this law, the solubility of the gas into liquid solution can be found provided the molecular state of solute must be in the same state of the gas and in the solution (physical absorption). As CO_2 reacts with MEA in CO_2 absorption process, Henry’s law cannot be applied directly to find the solubility of CO_2 in MEA solution. Therefore, the solubility must be estimated from corresponding data of more or less similar non-reacting gases in MEA solution. According to Versteeg and Swaaij et al. [127], Laddha et al. [128] was first investigated the solubility of N_2O and CO_2 in aqueous solutions of organic compounds that are non-reacting with respect to both solutes. Due to the similarities with regard to configuration, molecular weight (44) and electronic structure, it was concluded that the ratio of the solubility of these two components remained constant for the various solutions and the "N_2O analogy" may be applied to estimate the solubility of CO_2 in aqueous MEA solutions.

In 1988, Versteeg and Swaaij et al. [127] proposed equations for calculating Henry's Law constants for N_2O and CO_2 in water. In this study, the Henry's Law constant for N_2O in aqueous MEA solution is calculated by regressing with high accuracy ($R^2 = 0.981$) the experimental data by Tsai et al. [129] and shown in Equation (3-111). In 2000, Tsai et al. [129] and in 2005, Mandal et al. [130] used the N_2O analogy to estimate Henry's law constants for CO_2 in aqueous MEA solutions. In this study, Equations (3-109) - (3-112) were used to calculate the Henry's law constants of CO_2 in aqueous MEA solution.

Figure 4-4 shows Henry's law constant as function of temperature for solubility of CO_2 and N_2O in water and N_2O in Aqueous MEA solution. Figure 4-5 shows that Henry's constant of CO_2 as function of temperature using N_2O Analogy and Aspen Plus property.

$$\mathbf{He}_{\mathbf{N_2O,Water}} = \mathbf{8.547 \times 10^6 \, exp\,(-2284 / T)} \tag{3-109}$$

$$\mathbf{He}_{\mathbf{CO_2,Water}} = \mathbf{2.8249 \times 10^6 \, exp\,(-2044 / T)} \tag{3-110}$$

$$\mathbf{He}_{\mathbf{N_2O,Aqueous\,MEA}} = \mathbf{8.547 \times 10^6 \, exp} \left[-\frac{\mathbf{2284}}{\mathbf{T}} + \frac{\mathbf{C_R}}{\mathbf{484167.7}} + \left(\frac{\mathbf{C_R}}{\mathbf{34643.79}} \right)^{\mathbf{2}} \right] \tag{3-111}$$

$$\mathbf{He}_{\mathbf{CO_2,Aqueous\,MEA}} = \mathbf{He}_{\mathbf{N_2O,Aqueous\,MEA}} \left(\frac{\mathbf{He}_{\mathbf{CO_2,water}}}{\mathbf{He}_{\mathbf{N_2O,water}}} \right) \tag{3-112}$$

Where C_R is the concentration of MEA in mol /m^3 and T is in K.

3.3.7 Gas/Liquid Diffusivity

Gas /liquid diffusivity refers to the diffusivity of CO_2 in MEA solution. Similar to the solubility discussed in section 3.3.6, N_2O analogy can be also applied in the calculation of diffusivity for the same reason and expressed as Equation (3-116). N_2O and CO_2 diffusivity in water are calculated using correlation provided by Versteeg and Swaaij [127] shown as Equations (3-113) and (3-114). The diffusivity of N_2O in aqueous MEA solution was calculated by using the correlation provided by Wang and Lin et al. [131] and expressed as Equation (3-115). The coefficients of the Equation (3-115) are given in Table 3-4 and the concentration of MEA (C_R) is in kmol/m^3 .

$$\mathbf{D_{N_2O,Water} = 5.07 \times 10^{-6} \exp\left(\frac{-2371}{T}\right)} \tag{3-113}$$

$$\mathbf{D_{CO_2,Water} = 2.35 \times 10^{-6} \exp\left(\frac{-2119}{T}\right)} \tag{3-114}$$

$$\mathbf{D_{N_2O,MEA(aq)} = \left[b_0 + b_1 C_R + b_2 {C_R}^2\right] \exp\left[\frac{b_3 + b_4 C_R}{T}\right]} \tag{3-115}$$

$$\mathbf{D_{CO_2,MEA(aq)} = D_{N_2O,MEA(aq)} \left(\frac{D_{CO_2,Water}}{D_{N_2O,Water}}\right)} \tag{3-116}$$

Where all diffusivities are in m^2/s and T is in K

Table 3-4: Coefficients Used in Equation (3-115)

Parameter	Value
b_0	5.07E-06
b_1	8.65E-07
b_2	2.78E-07
b_3	-2.371E+03
b_4	-9.34E+01

Figure 3-10 to Figure 3-13 show the diffusivity of CO_2 and N_2O in water and N_2O in Aqueous MEA solution and diffusivity of CO_2 in Aqueous MEA solution as function of temperature respectively.

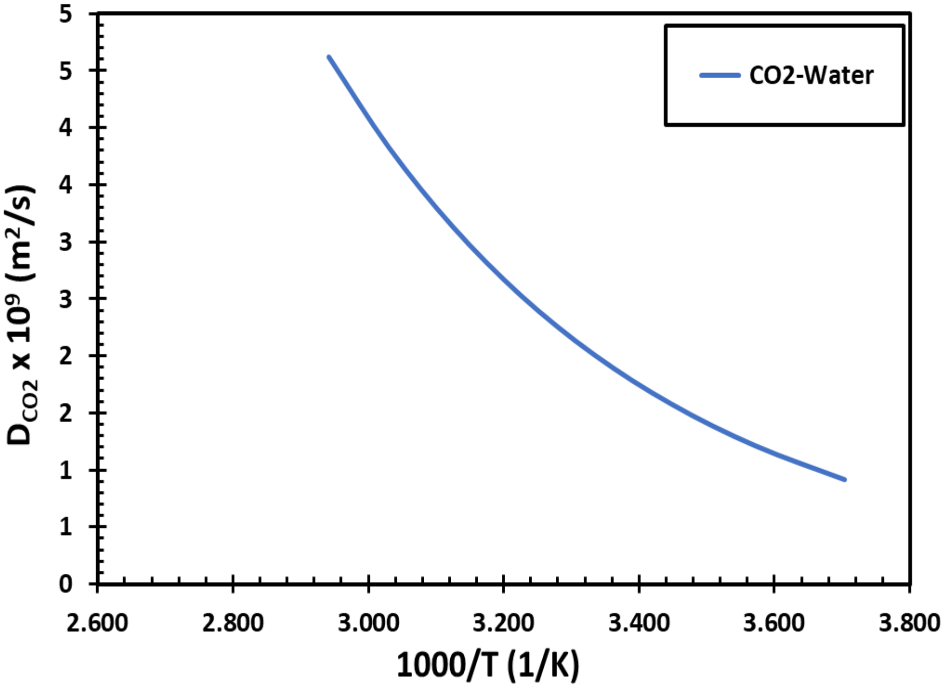

Figure 3-10: Diffusivity of CO_2 in Water as a Function of Temperature

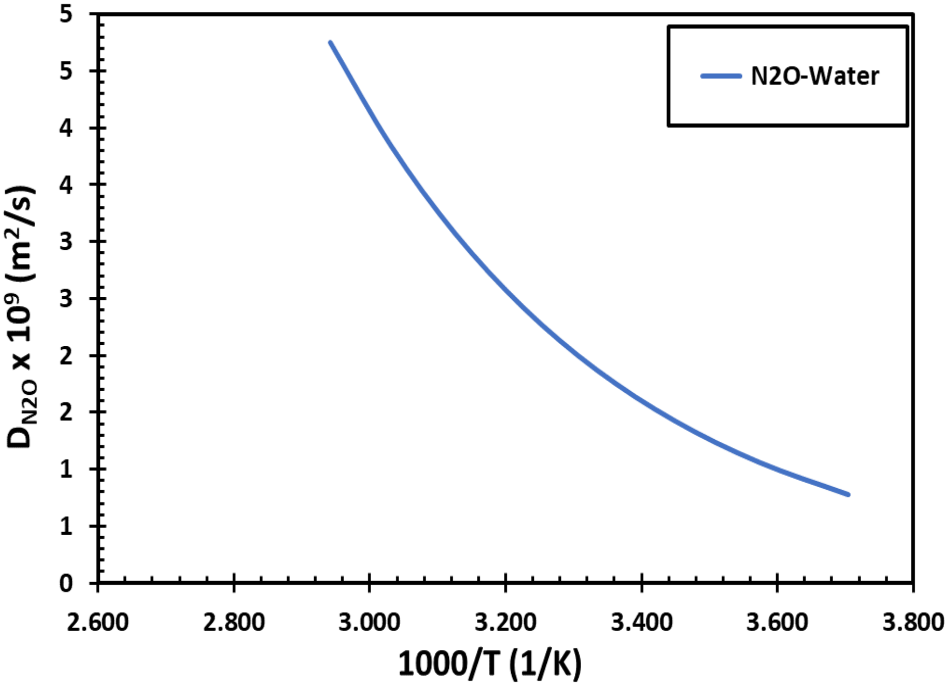

Figure 3-11: Diffusivity of N_2O in Water as a Function of Temperature

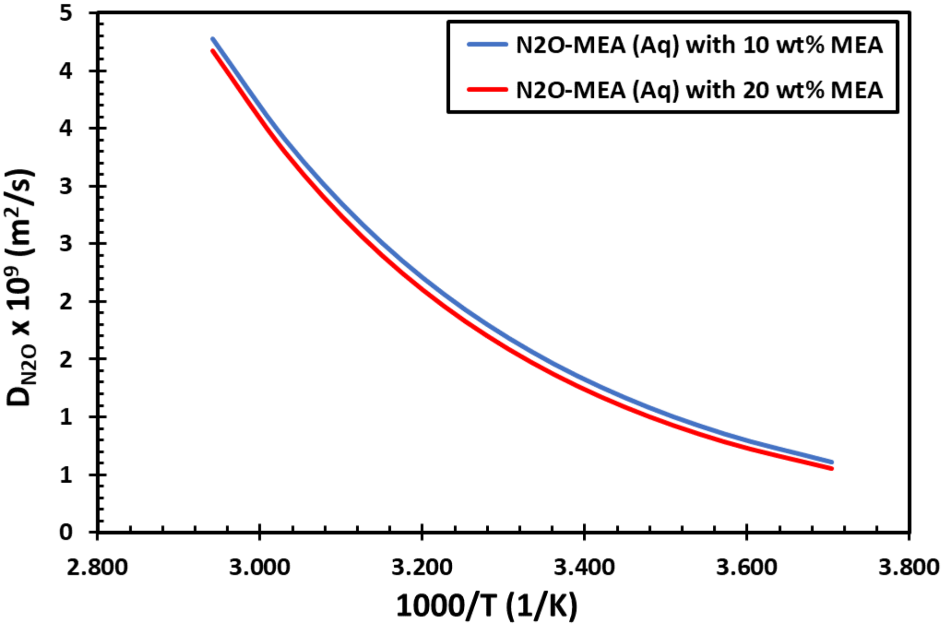

Figure 3-12: Diffusivity N_2O in Aqueous MEA solution as a Function of Temperature

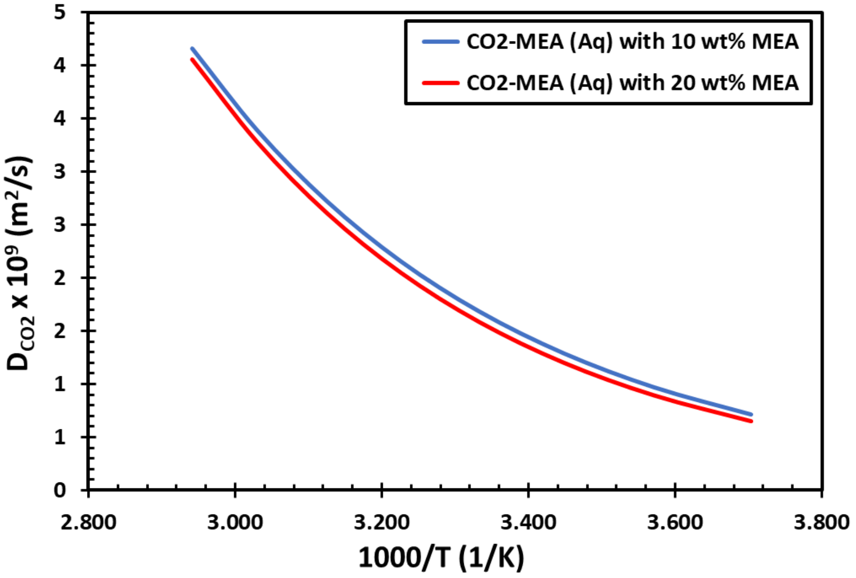

Figure 3-13: Diffusivity of CO_2 in Aqueous MEA solution as a Function of Temperature

3.3.8 Liquid/Liquid Diffusivity

Liquid/liquid diffusivity is essential for calculating the instantaneous Enhancement Factor expressed as Equation (2-36). For calculating diffusivity of MEA into the water, the Wilke and Chang [132] equation was used for predicting liquid diffusivities. The respective Equation (3-117) is given below:

$$D_{R,S} = 1.17282 \times 10^{-16} \left(\frac{T(\varphi \cdot Mw_s)^{1/2}}{\mu_S v_R^{0.6}} \right) \tag{3-117}$$

Where φ is the association coefficient (φ = 2.6 for water); T in K; $D_{R,S}$ in m^2/s; μ_S in Pa.s and v_R is the molar volume of MEA at its normal boiling point in m^3/kmol (v_R for MEA = 0.07186 m^3/kmol).

3.3.9 Water Vapor Pressure

There are many published literatures available for approximate calculation of water vapor pressure. In 2008, Monteith and Unsworth [133] published Tetens' Equation for temperatures above 0 °C and expressed in Equation (3-118). Figure 3-14 shows water vapor pressure as function of temperature using Tetens' Equation.

$$P_{vap} = 610.78 \exp\left(\frac{17.27(T - 273.15)}{T - 35.85}\right) \qquad (3\text{-}118)$$

Where T is in K

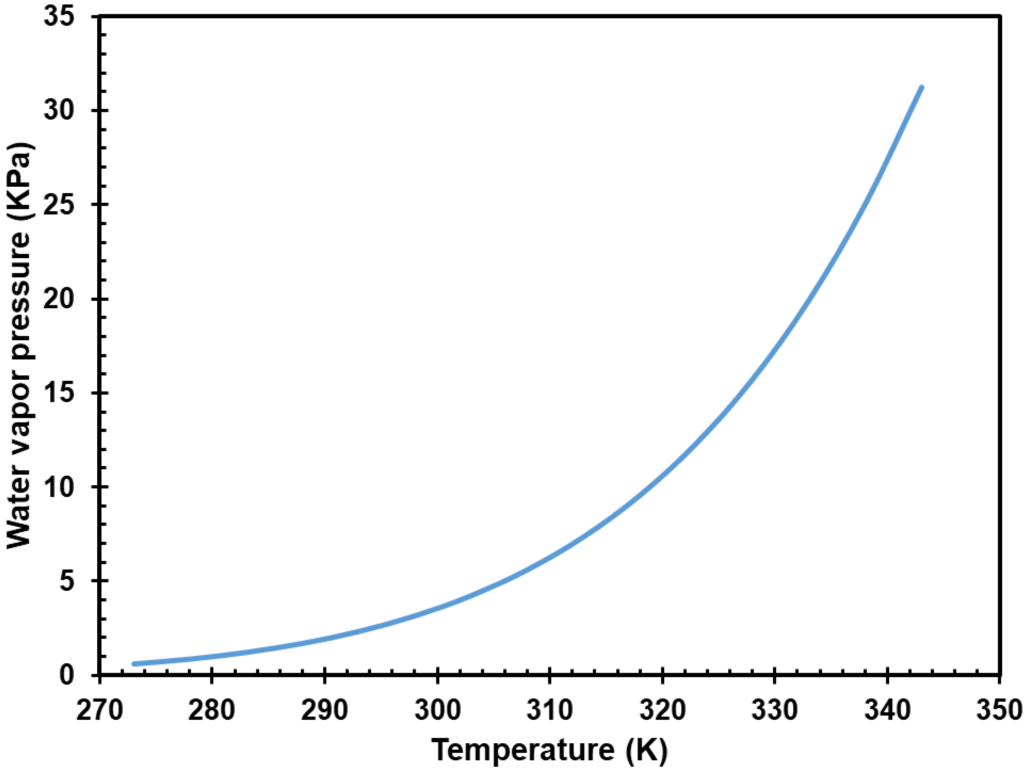

Figure 3-14: Water vapor pressure as a Function of Temperature

3.3.10 Latent Heat of Water Vaporization

The enthalpy of vaporization or (latent) heat of vaporization, is the amount of energy (enthalpy) that must be added to a liquid substance to vaporize. In CO_2 absorption system, the exothermic reaction between MEA and CO_2 generates heat which will increase the temperature for both the gas and liquid. There will be no heat will dissipate outside as per our initial consideration of the adiabatic process. In this regard, the necessity of calculating the amount of heat is to be consumed for vaporization of volatile solvent (water) is evident to utilize that information in the enthalpy balance for the system. Clausius- Clapeyron equation has been used in this regard and shows in Equation (3-119).

$$\frac{\mathrm{dlnP}}{\mathrm{dT}} = \frac{\Delta \mathrm{H_{LV}}}{\mathrm{RT}^2} \tag{3-119}$$

Integrating both sides and applying a limit, we get:

$$\ln\left(\frac{P_2}{P_1}\right) = -\frac{\Delta H_{LV}}{R}\left[\frac{1}{T_2} - \frac{1}{T_1}\right] \tag{3-120}$$

Or

$$\Delta H_{LV} = -\frac{R.\ln\left(\frac{P_2}{P_1}\right)}{\left[\frac{1}{T_2} - \frac{1}{T_1}\right]} \tag{3-121}$$

Where P_1 and P_2 are the vapor pressure (Pa) of water at temperature T_1 and T_2 (K), ΔH_{LV} is the heat of vaporization (J/mole) and R is Universal gas constant (8.314 $J \cdot K^{-1} \cdot mol^{-1}$).

3.3.11 Enthalpy of CO_2 Absorption and Reaction in the Liquid Solution

Conventionally, the total heat of solution represents the combined enthalpy change due to the physical absorption and chemical reaction as expressed by Equation (3-122).

$$\Delta(H)_{CO2\ in\ Solution} = \Delta(H)_{absorption} + \Delta(H)_{reaction} \tag{3-122}$$

The heat of reaction ($\Delta(H)_{reaction}$) can be calculated from the heat of formation of the products and reactants at the standard condition (298.15 K) according to Equation (3-123).

$$\Delta(H)_{reaction} = \sum_{i}^{k} \Delta(H_i)_{formation-products} - \sum_{i}^{k} \Delta(H_i)_{formation-reactants} \tag{3-123}$$

In 2012, Heintz [134] proposed Equation (3-124) to calculate the heat of CO_2 absorption ($\Delta(H)_{absorption}$) through Henry's Law constant (*He*).

$$\frac{\partial(\ln(He))}{\partial(\frac{1}{T})} = \frac{\Delta(H)_{absorption}}{R} \tag{3-124}$$

where R is the universal gas constant = 8.314472 J/mol.K and $\Delta(H)_{absorption}$ is in J/mol.

In the literature on CO_2 absorption in amines, the total heat of CO_2 physical absorption followed by a chemical reaction was often estimated as the enthalpy change due to the combined physical absorption and chemical reaction through the Gibbs-Helmholtz energy. In 2005, Gabrielsen et al. [135] calculated the total heat of solution for CO_2-MDEA, CO_2-DEA and CO_2-MEA systems using Equation (3-125), which is the Gibbs-Helmholtz energy, where K_{CO2} is the combined Henry's law and chemical reaction rate constant. They also proposed Equation (3-126) to represent the relationship between K_{CO2} and CO_2 equilibrium partial pressure (P_{CO2}) using CO_2 loading (α) and the unreacted and reacted CO_2 mole fraction in the liquid-phase (X_{CO2}). They also proposed equation (3-127) to calculate K_{CO2} for all three amines. By inserting Equation (3-125) into is Equation (3-127), the heat of absorption of CO_2 in MEA can be estimated using Equation (3-128).

$$\frac{\partial(ln(K_{CO2}))}{\partial(\frac{1}{T})} = \frac{\Delta H_{CO2\ in\ solution}}{R} \tag{3-125}$$

$$K_{CO2} = (\frac{(1-2\alpha)^2}{\alpha})(\frac{P_{CO2}}{X_{CO2}}) \tag{3-126}$$

$$ln(K_{CO2}) = 30.96 - \frac{10{,}584}{T} - 7.187\ (\alpha\ X_{R,initial}) \tag{3-127}$$

$$\Delta H_{CO2\ in\ solution} = 10{,}584\ (R) \tag{3-128}$$

Where $X_{R,initial}$ is the mole fraction of MEA in aqueous MEA solution.

In 2012, Hiwale et al. [136] modeled CO_2-MEA system for a laminar jet absorbers and packed beds using the total heat of solution; and Mathias and O'Connell [137] used Gibbs-

Helmholtz energy equation to calculate the heat of solution for the CO_2-MEA system. Also, in 2014, Hopkinson et al. [138] calculated the total heat of solution for CO_2-MEA, CO_2-DEA and CO_2-MDEA systems using the Gibbs-Helmholtz energy by Equation (3-125). It should be noted that Equation (3-128) shows that the heat of absorption of CO_2 in MEA solutions is constant. In 2011, however, McCann et al. [139] calculated the heat of solution for CO_2-MEA and CO_2-MDEA systems at 313 K and found large deviation in calculating the heat of absorption for CO_2-MEA system using Equation (3-125). This was further validated by the experimental data reported in 2014 by Kim et al. [140-142] where the total heat of solution of CO_2-MEA system (includes the heat of dissolution of CO_2 and the heat of reaction of CO_2 and MEA) was not constant. It was dependent on MEA mass percent, liquid temperature and CO_2 loading. Therefore, in this study, the heat of absorption for CO_2-MEA system was calculated by regressing the experimental data by Kim et al. [140-142] and expressed in Equation (3-129) .

$$\Delta H_{\mathrm{CO2\ in\ Solution}} = [4.1042 - 7.24\,(w_R) - 47.3710\,(\alpha) + 0.2926\,(T)] \times 1000 \qquad (3\text{-}129)$$

$(\Delta H)_{absorption}$ is in J/mol, w_R is mass fraction of MEA and T is in K

3.3.12 Enthalpy of MEA and H_2O in Solution

The enthalpy of the liquid solution is defined as shown in Equation (3-130) [1].

$$H_L^{aq}(T_L) = \sum_i x_i H_i^{aq}(T_o) + \int_{To}^{TL} C_{p,L}\, dT \tag{3-130}$$

Where i stands for dissolved A (CO_2), R (MEA), S (H_2O), and P (Carbamate), H_i and x_i are the molar enthalpy and mole fraction of the corresponding species i, respectively.

In order to calculate the enthalpy of CO_2 in solution (H_{CO2}), the dissolution (dissolving) enthalpy of CO_2 and heat of absorption of CO_2 were considered. Equation (3-131) proposed by McCann et al. [139] for aqueous MEA solution shows the excess molar enthalpy. Also, the partial molar enthalpy of MEA and water in solution were calculated using Equations (3-132) and (3-133) proposed by Mathonat et al. [143], which were obtained by differentiating of Equation (3-131):

$$H^E = x_R(1 - x_R) \sum A_n (1 - 2\, x_R)^{n-1} \tag{3-131}$$

$$H_R = H^E + (x_R)(\partial H^E / \partial x_R)_{P,T} \tag{3-132}$$

$$= (1 - x_R)^2 \sum A_n (1 - 2\, x_R)^{n-1} - 2\, x_R (1 - x_R)^2 \sum A_n (n-1)(1 - 2\, x_R)^{n-2}$$

$$H_S = H^E + (1 - x_R)(\partial H^E / \partial x_R)_{P,T} \tag{3-133}$$

$$= x_R^2 \sum A_n (1 - 2\, x_R)^{n-1} + 2\, x_R^2 (1 - x_R) \sum A_n (n-1)(1 - 2\, x_R)^{n-2}$$

Where H^E, H_R and H_S are in j/mol and n represents the coefficients in Equations (3-132) and (3-133) reported by Maham et al. [144] are listed in Table 3-5.

Table 3-5: Coefficients in Equations (3-132) and (3-133) [144]

Parameter	Value
A_1	9260.7
A_2	-3395.8
A_3	-601.3
A_4	491.0
A_5	977.6

McCann et al. [139] reported that the enthalpy of carbamate formation was constant between 293 K and 346 K and estimated -33 ± 2 kJ/mol, which was found from NMR titrations published by Ballard et al. [145] and Barth et al.[146]. McCann et al. [139] also reported that the enthalpy of carbamate formation was constant in the temperature range from 273 K to 423 K from vapor-liquid-equilibria (VLE) measurements according to Park et al. [147] and Jou et al. [148]. Therefore, in this study, the enthalpy of formation of the carbamate was assumed to be constant with -33 kJ/mol.

3.3.13 Reaction Rate Constant

The overall reaction order for CO_2 absorption in aqueous MEA solutions has an order of two because it has an order of one with respect to CO_2 and an order of one with respect to MEA. This indicates that the deprotonation of the zwitterion by the base present in the solution is very fast compared to the rate of the reverse reaction to CO_2 and amine [149].

Blauwhoff et al. [150] expressed the second order reaction rate constant for CO_2-MEA system by Equation (3-134), which is plotted as a function of temperature in Figure 3-15.

$$\log \mathrm{k}_2 = 10.99 - \frac{2152}{\mathrm{T}} \tag{3-134}$$

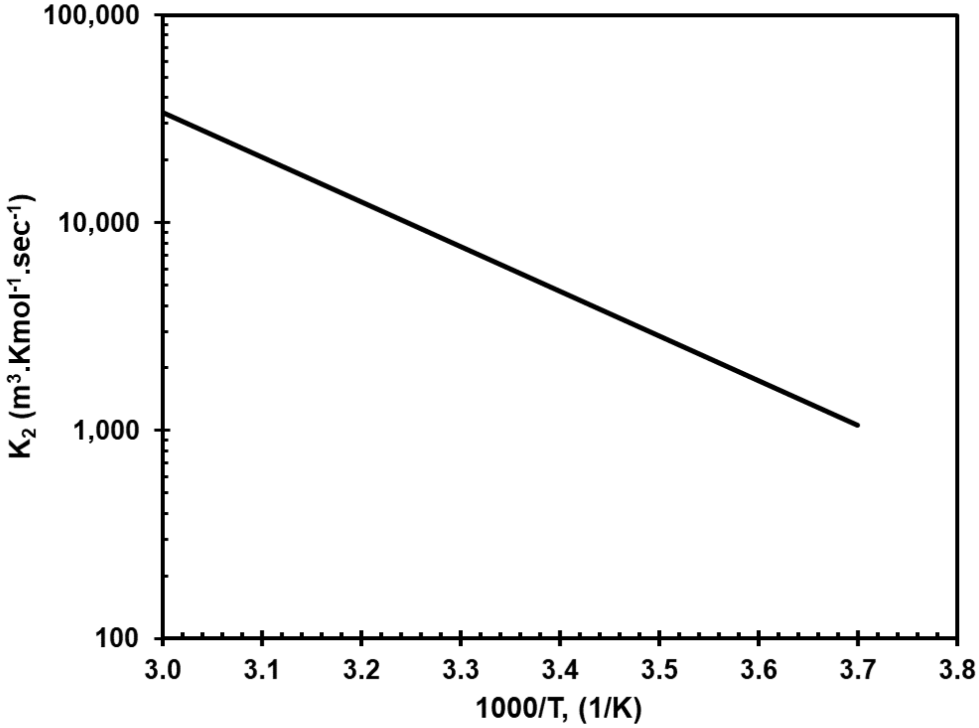

Figure 3-15: Reaction Rate Constant for CO_2 in Aqueous MEA System [150]

3.3.14 Density of Aqueous MEA Solution

The density of aqueous MEA solutions were calculated using the Equations (3-135) - (3-137) developed by Weiland et. al. [151] based on literature data by Ho et al. [116] for partially carbonated MEA.

$$\boldsymbol{\rho = (x_R Mw_R + x_S Mw_S + x_A Mw_A)/V} \tag{3-135}$$

$$\mathbf{V = x_R V_R + x_S V_S + 0.047 x_A - 1.821 x_R x_S} \tag{3-136}$$

$$\mathbf{V_R = \frac{M_R}{-5.351(T)^2 + (-4.514)(T) + 1.194}} \tag{3-137}$$

Where V is the molar volume of solution in unit of mL·mol^{-1}, ρ is density in unit of g·mL^{-1} and T is temperature in unit of K. x_i and M_i are the mole fractions and molecular weight of components respectively.

For an ideal solution, it can be assumed that the molar volume of a solution is the sum of the partial molar volumes of its components multiplied by their respective mole fractions. However, in CO_2-MEA system, the assumption of ideal solutions would not be correct due to the ionization reaction. This assumption would be accurate if the CO_2 would exist as free CO_2 and not as its carbamate or reaction product [151]. For this nonideal behavior of loaded amine solutions, an additional term requires to account for the interaction between amine and water along with the molar volume of dissolved CO_2, unrelated to its pure component.

In Equation (3-136) by Weiland et. al. [151], the molar volume of CO_2 was 0.047 ($mL \cdot mol^{-1}$) and the molar volume associated with the interaction between water and amine was -1.821 ($mL \cdot mol^{-1}$). Weiland et. al. [151] also mentioned that the molar volume of pure MEA was given in 1989 by Al-Ghawas et al. [119] and in 1992 by DiGuillo et al. [152] and is expressed as Equation (3-137).

This correlation was developed to allow the calculation of alkanolamine solution density as a function of amine concentration, CO_2 loading, and temperature for single-amine solutions. Figure 3-16 shows the density of 2M MEA solution as function of temperature and loading.

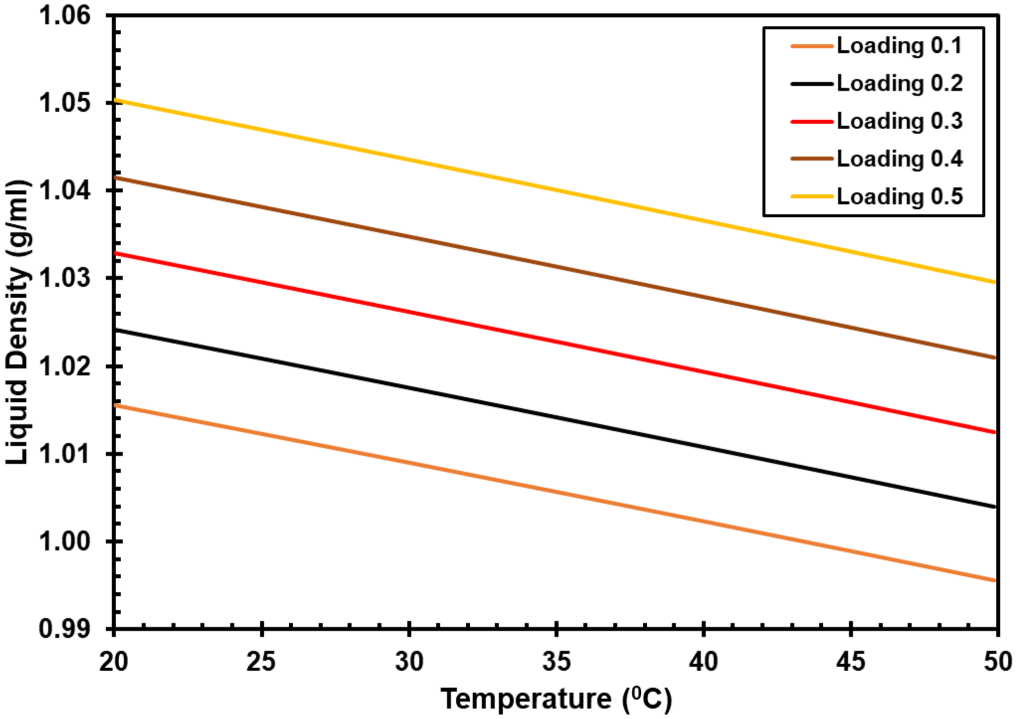

Figure 3-16: Density of 2M MEA Aqueous Solution as Function of Temperature and CO_2 Loading

3.3.15 Viscosity of Aqueous MEA Solution

Weiland et. al. [151] combined the data by Al-Ghawas et al. [119], DiGuillo et al. [152], Ho et al. [116] and Snidjer et al. [153] and proposed Equation (3-138) to calculate the viscosity of MEA solutions at a given temperature, MEA concentration, and CO_2 loading [151].

The viscosity of water was calculated using semi-empirical relation available at Dortmund Data Bank [154] as function of temperature, Equation (3-139).

Figure 3-17 shows the viscosity of 2M concentrated MEA Aqueous solution as function of temperature and CO_2 loading. Figure 3-18 shows the viscosity of pure water as function of temperature.

$$\frac{\mu_L}{\mu_{H2O}} = \exp\left[\frac{[(21.186 w_R + 2373)][\alpha(0.01015 w_R + 0.0093T - 2.2589) + 1] w_R}{T^2}\right] \tag{3-138}$$

$$\mu_{H2O} = 0.001 \exp\left(-3.7188 + \frac{578.919}{T - 137.546}\right) \tag{3-139}$$

Where w_R is the MEA mass fraction, T is temperature in unit of K

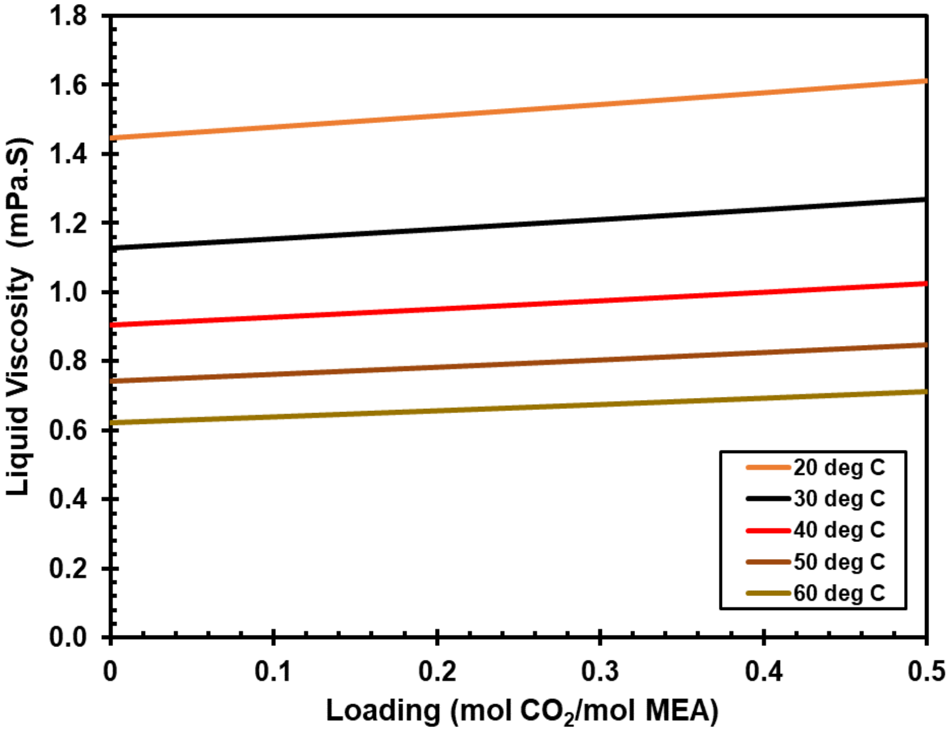

Figure 3-17: Viscosity of 2M MEA Aqueous Solution as Function of Temperature and CO_2 Loading

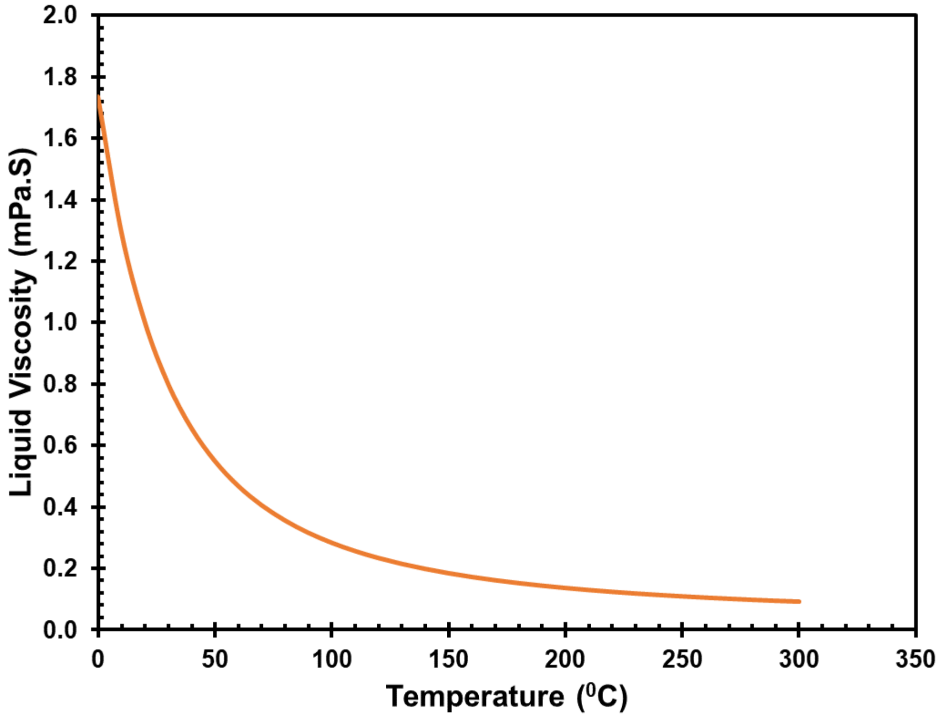

Figure 3-18: Viscosity of water as Function of Temperature

3.3.16 Surface Tension of Aqueous MEA Solution

Dong et al. [155] measured the surface tension of aqueous MEA solutions from 293.15 K to 323.15 K using an automatic surface tensiometer and studied the effect of temperature, MEA concentration, and CO_2 loading (α) on the surface tension. They also proposed Equation (3-140) to express the surface tension of aqueous MEA solutions. This equation shows the solution surface tension (σ_L) is the summation of surface tension of unloaded solution (σ_{aq}), surface tension contributed from the hydrolysis of ion (σ_{ion}) and $[e\alpha w_R/T]$, which is the contribution from hydrolysis of ions, residual MEA, and the interaction between ions and water [155]. Equations (3-141) and (3-143) can be used to calculate σ_{aq} and σ_{ion}, respectively.

Dong et al. [155] measured the maximum CO_2 loading (α_{max}) at different temperatures and MEA mass fraction. Then α_{max} is regressed as a function of temperature and MEA mass fraction in Equation (3-145). According to Dong et al. [155], at a given MEA concentration α_{max} decreases monotonically with the increase of temperature. And, at a given temperature α_{max} decreases with increase of MEA concentration [155]. These relationships can be seen in Figure 3-19.

$$\boldsymbol{\sigma_L = \sigma_{aq} + \sigma_{ion} - e\alpha(w_R^*)/T} \quad (3\text{-}140)$$

$$\boldsymbol{\sigma_{aq} = x_R\sigma_R + x_S\sigma_S + \emptyset(T, w_R)x_Rx_S} \quad (3\text{-}141)$$

$$\boldsymbol{\emptyset(T, w_R) = (a + bw_R + cw_R{}^2)T} \quad (3\text{-}142)$$

$$\boldsymbol{\sigma_{ion} = (fw_{ion} + gw_{ion}^2)/T} \quad (3\text{-}143)$$

$$\boldsymbol{w_{ion} = \alpha w_R(M_A/M_R + 1/\alpha_{max})/M_t} \quad (3\text{-}144)$$

$$\boldsymbol{\alpha_{max} = 1.801849 - 0.00333T - 0.7525w_R} \tag{3-145}$$

$$\mathbf{M_t = 1 + (\alpha w_R M_A)/M_R} \tag{3-146}$$

$$\mathbf{w_R^* = \left(1 - \frac{\alpha}{\alpha_{max}}\right) w_R/M_t} \tag{3-147}$$

Where σ_L, $\sigma_{aq}, \sigma_{ion}, \sigma_R, \sigma_S, e\alpha(w_R^*/T)$ and $\emptyset(T, w_R)$ are in mN/m; w_R and w_{ion} are the mass fraction of MEA and ions, respectively; and M_A and M_R are the molecular weight of CO_2 and MEA. The coefficients for surface tension calculation are given in Table 3-6.

Table 3-6: Coefficients for Surface Tension Calculation

a	b	c	e	f	g
-0.567	1.05	-0.552	-27494.72	6175.83	2828.87

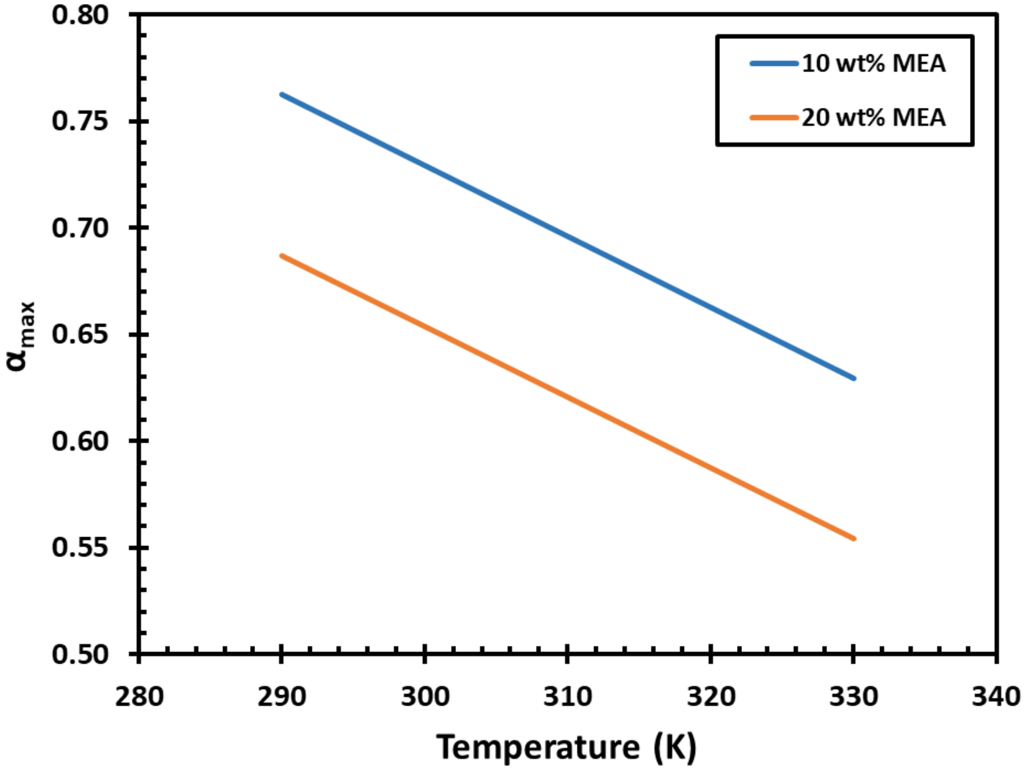

Figure 3-19: Dependency of α_{max} on MEA Concentration and Temperature

Surface tension of pure MEA was calculated using correlation provided by Han et al. [156] and expressed as Equation (3-148). Surface tension of pure water was calculated using Equation (3-149) available at Dortmund Data Bank [157]. Figure 3-20 shows the surface tension of pure water as function of temperature.

$$\boldsymbol{\sigma_R = 0.001\,[0.05146 - 0.0001158\,(T - 273.15)]} \qquad (3\text{-}148)$$

$$\boldsymbol{\sigma_S = 134.15\left(1 - \frac{T}{647.3}\right)^{1.6146 - 2.035\left(\frac{T}{647.3}\right) + 1.5598\left(\frac{T}{647.3}\right)^2}} \qquad (3\text{-}149)$$

Figure 3-21 shows the surface tension of Aqueous MEA solution at different concentration of MEA without CO_2 loading and as function of temperature.

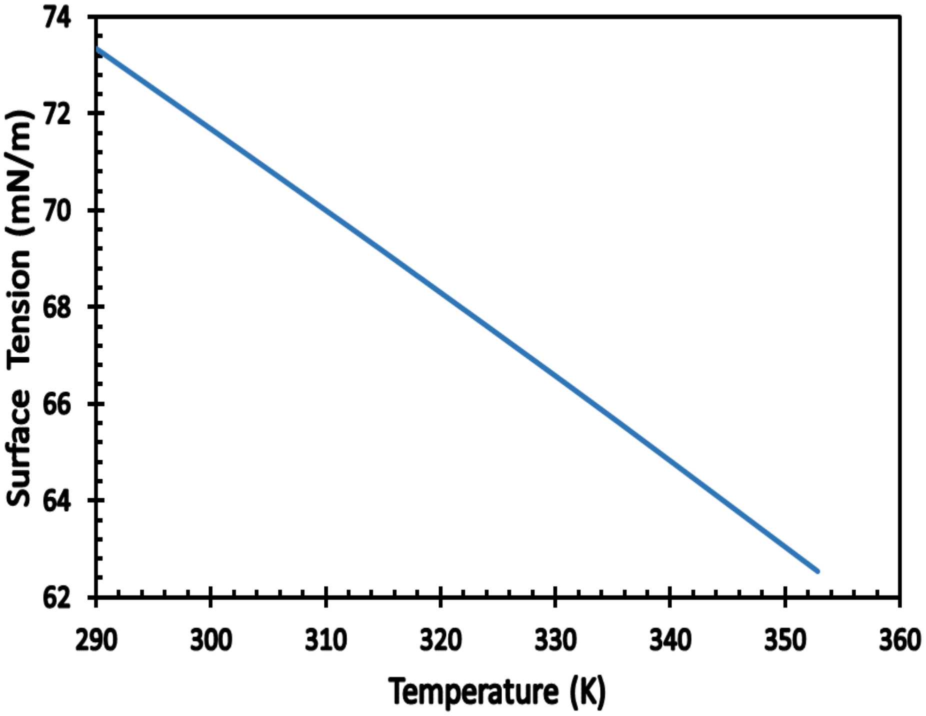

Figure 3-20: Surface Tension of Water as function of Temperature

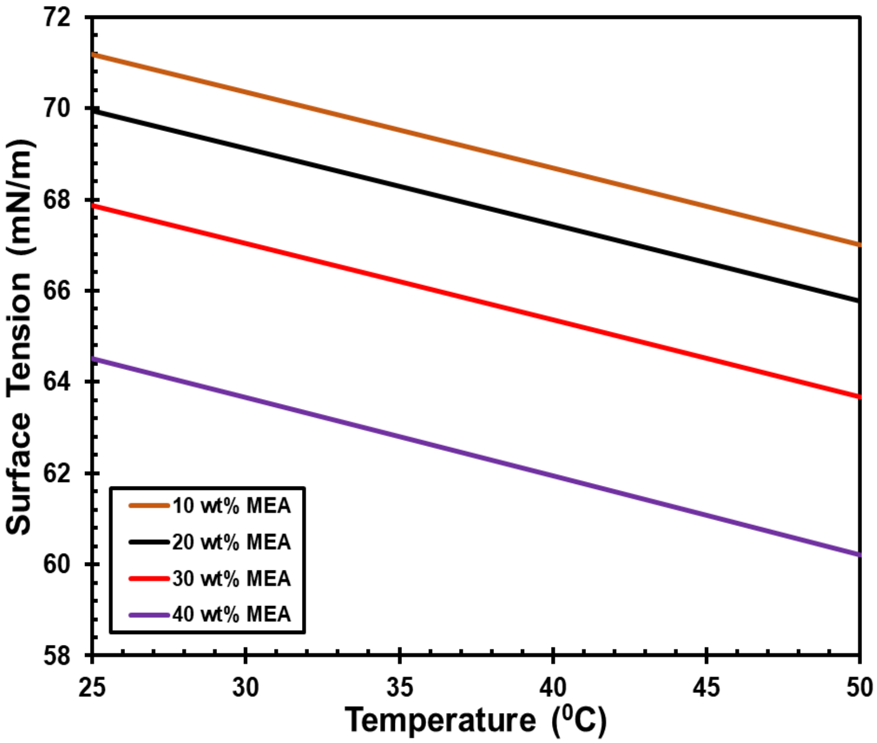

Figure 3-21: Surface Tension of Aqueous MEA Solution as Function of Temperature at No Loading Conditions

Figure 3-22 shows the surface tension of carbonated MEA solution at a given temperature as function of CO_2 loading with 10wt% MEA concentration.

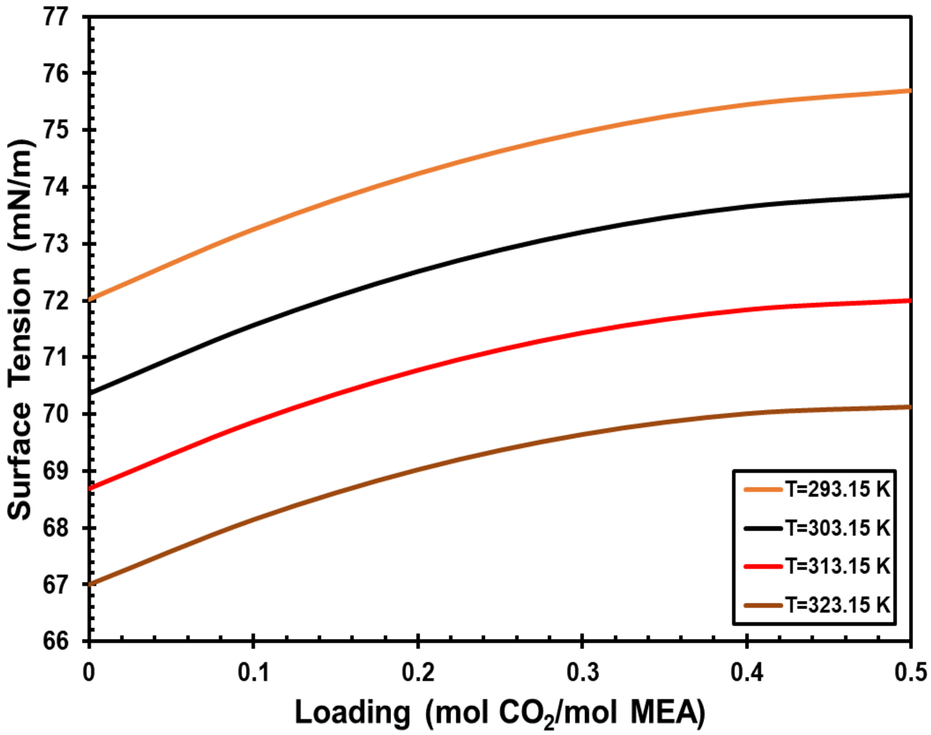

Figure 3-22: Effects of Temperature and CO_2 loading on the surface tension of Carbonated MEA Aqueous Solutions with w_R = 0.1.

3.3.17 Heat Capacity of Aqueous MEA Solution

Heat capacity of a liquid solution is a temperature dependent physical property which defines the amount of heat energy required to raise the temperature of the liquid solution. This information is necessary to perform the liquid side enthalpy balance. In 1994, Linde and Kehiaian [158] expressed the Equation (3-150) for calculating the molar heat capacity of mixture. In 2001, Chen and Li [159] showed their experimental result of eight binary systems for calculating heat capacities including aqueous MEA solution as a function of mole fraction of amine and temperature which fitted very well with the predicted result using Equation (3-150).

$$C_{P,R} = C_p^E + \sum_{i=1}^{n} x_i C_{pi} \tag{3-150}$$

Where xi is the mole fraction of each component, Cpi is molar heat capacity of pure components and Cp^E is excess molar heat capacity.

For binary system, Chiu et al. [160] mentioned the Redlich and Kister Equation shown as Equation (3-151) to calculate the excess molar heat capacity.

$$C_p^E = x_1 x_2 \sum_{i=1}^{n} A_i (x_1 - x_2)^{i-1} \tag{3-151}$$

The Temperature-dependent Ai is assumed to follow the equation (3-152) by Chiu et al. [160] and the values of coefficients are given in Table 3-7.

$$A_i = a_{i,0} + a_{i,1}(T/K) \tag{3-152}$$

Table 3-7: Parameter of heat capacity of aqueous MEA solution [160]

System	$a_{1,0}$	$a_{1,1}$	$a_{2,0}$	$a_{2,1}$
MEA+H_2O	-148.90	0.492	28.033	-0.096

The molar heat capacity of pure MEA was calculated by using equations (3-153) by regressing the experimental data published by Chiu et al. [160] with high accuracy (R^2=0.998). The molar heat capacity of pure water as function of temperature was calculated using Equation (3-154) which is available in National Institute of Standards and Technology (NIST) webbook [161].

$$C_{P_R} = 78.58 + 0.2927 * T \tag{3-153}$$

$$C_{p_S} = -203.6060 + 1523.29t - 3196.413t^2 + 2474.455t^3 + \frac{3.855326}{t^2} \tag{3-154}$$

Where t=Temperature T(K)/1000

Figure 3-23 shows the heat capacity of MEA aqueous solutions as a function of MEA mole fraction at different temperatures.

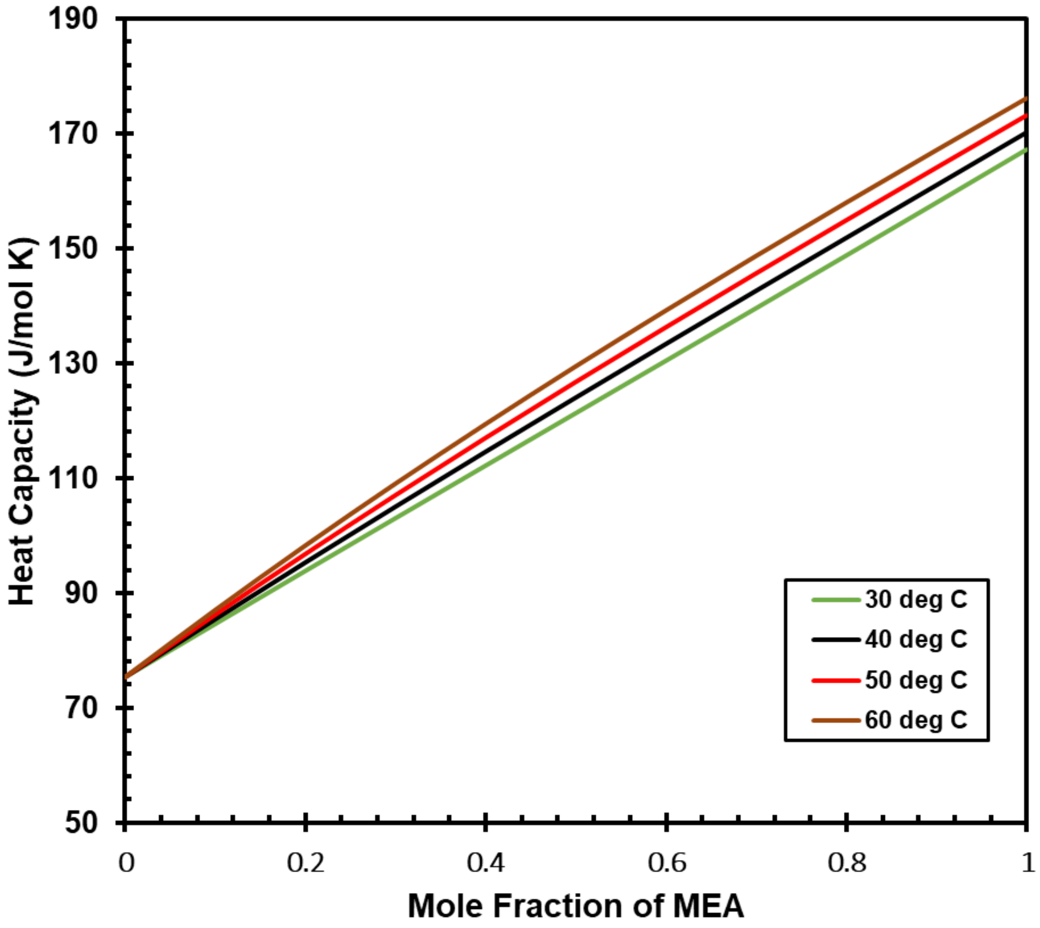

Figure 3-23: Heat Capacity of Aqueous MEA solution as a Function of Mole Fraction of MEA and Temperature.

3.3.18 Mass Transfer Coefficients

In 1995, Billet and Schultes [4] updated their correlation for mass transfer coefficients with small deviation from experimental results based on one of the largest experimental database in the world at that time. They suggested the following Equations (3-155) - (3-157) to predict the specific gas-liquid interfacial area as well as the volumetric gas-side and liquid-side mass transfer coefficients. Equation (3-158) was used to calculate the gas-side mass transfer coefficient in (m.s^{-1}) mentioned in overall corrected heat transfer coefficient calculation in section 3.3.19:

$$\frac{a_w}{a} = 1.5(ad_h)^{-0.5}\left(\frac{u_L d_h}{\nu_L}\right)^{-0.2}\left(\frac{u_L^2 \rho_L d_h}{\sigma_L}\right)^{0.75}\left(\frac{u_L^2}{g d_h}\right)^{-0.45} \tag{3-155}$$

$$k_L = C_L 12^{\frac{1}{6}}\left(\frac{u_L}{\beta_L}\right)^{1/2}\left(\frac{D_L}{d_h}\right)^{1/2} \tag{3-156}$$

$$k_G = \frac{C_G}{RT}\frac{D_G}{(\varepsilon - \beta_L)^{1/2}}\left(\frac{a^{1/2}}{{d_h}^{1/2}}\right)\left(\frac{u_G}{a\nu_G}\right)^{3/4}\left(\frac{\nu_G}{D_{i,G}}\right)^{1/3} \tag{3-157}$$

$$\dot{k_G} = k_G\ (R\ T) \tag{3-158}$$

Where i could be CO_2, H_2O or inert gas. a_w is the specific wetted area; a is the specific packing area; ε is the bed porosity; C_L, C_G are the characteristic parameters of different packings; D_G and D_L is the gas and liquid diffusivities, d_h is hydraulic diameter of the packing which is defined by Equation (3-159); and β_L is liquid hold up which could be determined using Equation (2-19).

$$d_h = 4\left(\frac{\varepsilon}{a}\right) \tag{3-159}$$

The characteristic parameters of packing, including, C_G and C_L, are listed in Table 3-8.

Table 3-8: Characteristic Parameters for Packing [4]

Packing	Nominal Size, mm	Void Fraction, ε	Specific Area, m^{-1}	C_L	C_G
Ceramic Berl Saddle	13	0.65	545	1.364	0.232
Ceramic Berl Saddle	25	0.68	260	1.246	0.387

In this study, Equations (3-160) through (3-163) by Cho [3] were used to calculate the specific wetted area (a_w) as well as the liquid-side mass transfer coefficient (k_L) and Equation (3-157) by Billet and Schultes [4] was used for calculating the gas-side (k_G) mass transfer coefficient.

Cho's [3] correlation is developed based on the surface renewal rate from Danckwerts' theory and the effective interfacial area between gas and liquid per unit packing volume in a packed absorption tower were evaluated for the absorption of carbon dioxide into carbonate/bicarbonate buffer solution accompanied by a pseudo-first order chemical reaction [3].

Cho's [3] correlation is also developed based on the Berl saddle packing and resulted the surface renewal rate and specific wetted area is the function of Reynolds number (Re). Equation (3-163) defined by Faramarzi et al. [162] . S is surface renewal rate (sec^{-1}) defined by Cho [3].

$$a_w = 25\ Re^{0.61} \qquad 13 \leq Re \leq 30 \tag{3-160}$$

$$S = 0.74\ Re^{0.37} \qquad 13 \leq Re \leq 30 \tag{3-161}$$

$$k_L = (D_L S)^{0.5} \tag{3-162}$$

$$Re = \left(\frac{\rho_L u_L d_h}{\mu_L}\right) \tag{3-163}$$

3.3.19 Heat Transfer Coefficient

The heat transfer coefficient plays a significant role for calculating the gas-phase and liquid-phase temperatures in the absorber. Due to the similarities in molecular transport process of momentum, heat and mass transfer, the molecular diffusion equation of Newton's law of momentum is similar with Fourier's law for heat and Fick's law for mass transfer [163].

However, theses similarities are not well defined mathematically or physically and are more difficult to relate each other [163]. To understand this further, method of dimensional analysis and use of dimensionless numbers are important. The experimental data for mass transfer coefficients obtained using various kinds of fluids, different velocities and different geometries are correlated by the dimensionless numbers [163] which later can be used to calculate other properties of molecular transportation. A consolidated list of dimensionless number related to heat and mass transfer has been provided in Table 3-9 with Equation from (3-164) to (3-167).

Over the decades, researchers made huge effort to develop analogies among these three transport processes so that an unknown transfer coefficient can be predicted when one of the other coefficients are known [163]. In this case also heat transfer coefficient can be calculated from mass transfer data through heat transfer analogy.

Table 3-9: List of Dimensionless numbers related to Heat and Mass Transfer

Dimensionless no	Definition
Schmidt number (Sc)	$\frac{\text{Momentum Diffusivity}}{\text{Mass Diffusivity}}$
Prandtl number (Pr)	$\frac{\text{Momentum Diffusivity}}{\text{Thermal Diffusivity}}$
Stanton number (St_H) (for heat transfer)	$\frac{\text{Heat transfer into fluid}}{\text{Therml capacity of the Fluid}}$
Stanton number (St) (for mass transfer)	$\frac{\text{Convective Mass Resistance}}{\text{Mass average vlocity}}$

$$\mathrm{Sc} = \frac{\mu_G}{\rho_G\, D_G} \tag{3-164}$$

$$\mathrm{Pr} = \frac{C_P\, \mu_G}{\lambda} \tag{3-165}$$

$$\mathrm{St_H} = \frac{h_G}{\rho_G\, C_P\, u_G} \tag{3-166}$$

$$\mathrm{St} = \frac{\dot{k}_G}{u_G} \tag{3-167}$$

Even though Reynolds was the first to note similarities in transport processes and relate turbulent momentum and heat transfer, known as Reynolds analogy, the most successful and most widely used analogy is the Chilton and Colburn J factor analogy [163]. This analogy is based on experimental data for gases and liquids in both the laminar and turbulent flow regions and is written as follows by Equation (3-168) [163] :

$$\frac{f}{2} = J_H = St_H(Pr)^{\frac{2}{3}} = J_D = St\,(Sc)^{\frac{2}{3}} \tag{3-168}$$

Where f is friction factor, J_H and J_D are the dimensionless factor for heat and mass transfer respectively. For the flow where drag force is present, like the flow in packed bed absorber, f/2 is much higher than J_H or J_D and often $J_H \cong J_D$ [163]. Therefore, Equation (3-168) can be simplified into Equation (3-169):

$$St_H(Pr)^{\frac{2}{3}} = St(Sc)^{\frac{2}{3}} \tag{3-169}$$

Plug in Equation (3-164) to (3-167) in equation (3-169), heat transfer coefficient of gas phase (h_G) can be calculated using Equation (3-170).

$$h_G = \overline{\dot{k}_G}\rho_G C_p \left(\frac{\lambda}{\rho_G C_p \overline{D_G}}\right)^{2/3} \tag{3-170}$$

It should be mentioned that all properties in the Equation (3-170) are average properties for the gas mixture. These average properties are defined in ASPEN PLUS under "Chilton and Colburn Methodology" [164] and were obtained by using Equations (3-171) and (3-172).

$$\overline{D}_G = \frac{\sum_{i=1}^{nc-1}\sum_{k=i+1}^{nc}(y_i + \delta)\,(y_k + \delta)D_{ik}}{\sum_{i=1}^{nc-1}\sum_{k=i+1}^{nc}(y_i + \delta)\,(y_k + \delta)} \tag{3-171}$$

$$\overline{\dot{k}_G} = \frac{\sum_{i=1}^{nc-1}\sum_{k=i+1}^{nc}(y_i + \delta)\,(y_k + \delta)\dot{k}_{ik}}{\sum_{i=1}^{nc-1}\sum_{k=i+1}^{nc}(y_i + \delta)\,(y_k + \delta)} \tag{3-172}$$

Where $\delta = 0.0001$, taken from ASPEN PLUS (Rate based setup) [164], y_i is assumed to be the mole fraction of gas component into mixture gas, and nc is number of gas components.

In this connection this should be also noted that there is a difference between momentum transfer and heat transfer. This is due to the change in boundary condition of molecule transpiration at the shear surface. In 2006, Ambrosini et al. [165] discussed these differences and mentioned that these differences are the result of the average transversal motion of mass transfer, temperature and concentration profile in the boundary layers. Therefore, a correction factor, known as Ackermann 1937 correction for heat transfer coefficients have been applied to account this phenomenon [165]. The expression of Ackermann 1937 correction factor recommended by Pandya [108] and shown in equation (3-173).

$$h_G{}' a_w = \frac{-G_B(C_{P,A}\frac{dY_A}{dZ} + C_{P,S}\frac{dY_S}{dZ})}{1 - \exp\left\{G_B(C_{P,A}\frac{dY_A}{dZ} + C_{P,S}\frac{dY_S}{dZ})/h_G a_w\right\}} \tag{3-173}$$

Where h_G is the original heat transfer coefficient and h_G' is the corrected heat transfer coefficient.

4.0 Model Validation with Pilot-Plant Study by Tontiwachwuthikul et al.[2]

In, 1989, Tontiwachwuthikul et al. [64] built the experimental setup schematically shown in Figure 4-1 and recorded the results of CO_2 concentration and liquid temperature profiles along the column using NaOH, MEA and AMP as solvents. The experiments were carried in a packed-bed with 0.1 m ID and 7.2 m height containing 0.5 inch ceramic Berl Saddle packing, the packed-bed consisted of six sections (each 1.2 m) and due to liquid redistribution between the sections, the effective packed height in each section was 1.1 m, leading to a total of 6.6 m packing height. The flow rates of the solvents and CO_2-air mixture were measured using rotameters and the inlet gas and liquid temperatures were using a constant temperature bath. An infrared gas analyzer was employed to measure the gas-phase composition [64]. In 1992, an extended version of this pilot plant study of Tontiwachwuthikul et al. [2] was published where the author reported the liquid temperature, CO_2 loading and CO_2 mole fraction in the gas-phase at each section. They also modeled their experimental results with MEA based on the procedure by Pandya [1] and reported that their model predictions were in agreement with the experiment results.

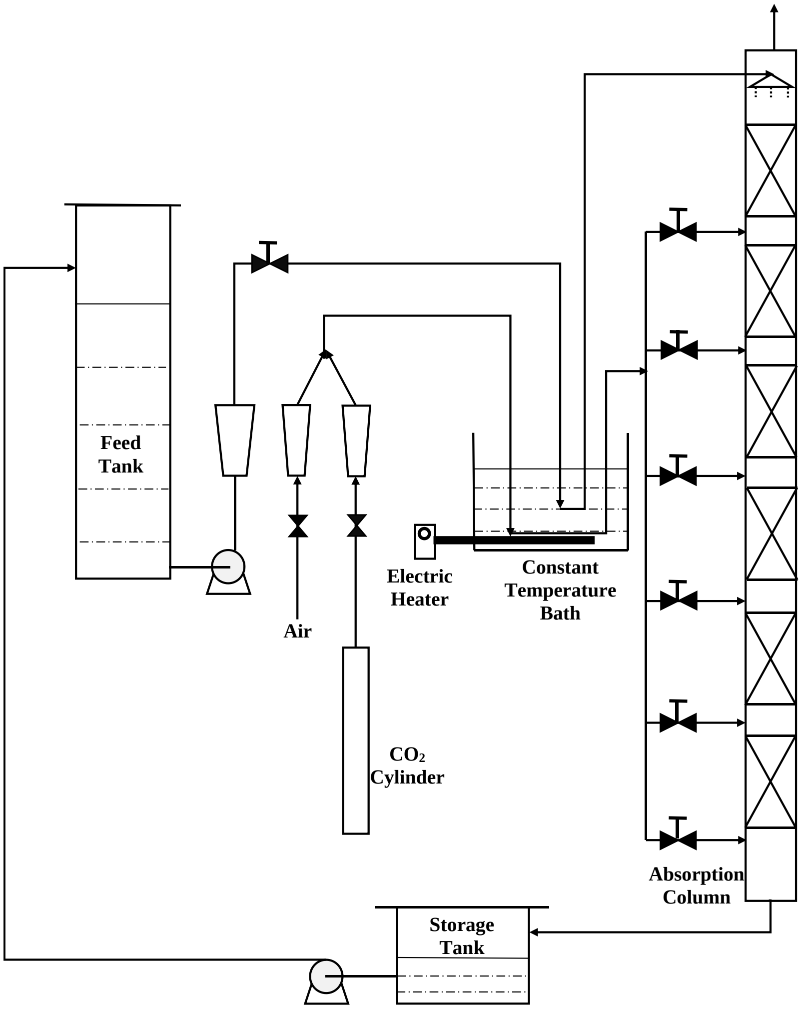

Figure 4-1: A Schematic of the Experimental Setup Used for CO$_2$ Absorption by Tontiwachwuthikul et al. [64]

The experimental data by Tontiwachwuthikul et al. [2] for CO$_2$ absorption from a mixture with air in aqueous MEA solutions using an adiabatic packed-bed absorber were used to validate the model predictions. Tontiwachwuthikul et al. [2] carried out a total of 10 different runs for CO$_2$ absorption using MEA aqueous solutions in a small-scale (0.1 m ID) adiabatic absorber packed with a 12.7 mm ceramic Berl Saddles to a height of 6.55m. It should be mentioned that some runs were replicates to ensure reproducibility, and other runs exhibited errors in the CO$_2$ material balance. In this study, runs (T13, T15, T19 and T22) carried out at 1 atm (1.01325 bar) were considered for model validation. The boundary conditions of the individual streams of these experimental runs are given in Table 4-1.

Table 4-1: Inlet and outlet Stream Conditions from Pilot-Plant Study

Inlet Parameters	T13	T15	T19	T22
Liquid Flow (m^3/m^2 h)	13.5	13.5	13.5	9.5
MEA Feed Concentration ($kmol/m^3$)	2.00	2.03	2.00	3.00
Liquid Feed Temperature, °C	19	19	19	19
Air Flow Rate ($mole/m^2$ s)	14.8	14.8	14.8	14.8
Inlet Gas Temperature, °C	19	19	19	19
CO_2 Mole Fraction (at inlet)	0.153	0.195	0.115	0.191
CO_2 Removal (%)	100	100	100	100
Packed Height (m)	6.55	6.55	6.55	6.55

Also, It should be noted that due to the unavailability of the packing characteristics for 12.7 mm ceramic Berl Saddles in the literature, a 13-mm nominal size ceramic Berl Saddles packing with the characteristics shown in Table 4-2 was used in the present model.

Table 4-2: Characteristics of the Packed-bed Absorber and Packing Used in the Present Model

Packing Type	Ceramic Berl Saddle
Packing Nominal Size, mm	13
Void Fraction (ε), %	65
Specific Area (a), m^{-1}	545
Packed Height, m	6.55
Column ID, m	0.10

All the equation parameters discussed in the previous sections were inserted in the model equations, which were implemented in MATLAB 2016a to solve the combined material and energy balance equations under different boundary conditions. Another model on Aspen plus was also developed using Rate based Model of CO_2-MEA system.

4.1 Hydraulics of the Four Runs

The hydraulics of the four runs (T13, T15, T19 and T22) listed in Table 4-1, including flooding, irrigated pressure drops and liquid holdup, were evaluated. Figures 4-2 and 4-3 were used to check for flooding and interpolate for the two-phase irrigated pressure drop. The two-phase irrigated pressure drops were also predicted using the correlations by Billet and Schultes [96] and Stichlmair et al. [99]. The liquid holdup values were predicted using the correlations by Billet and Schultes [96] and Stichlmair et al. [99]. Figures 4-2 and 4-3 show that the four points corresponding to the four runs are below the flooding line, indicating that flooding did not occur during the operation. The calculated values of k_L, k_G, β_L and ΔP_{irr} for the four runs are given in Table 4-3, and as can be observed the correlations by Billet and Schultes [4] and Stichlmair et al. [99] predict pressure drops which are in very close to each other, however, these predicted values are almost double those interpolated using the graphs by Leva [90] and GPDC [94].

Table 4-3: Hydraulic Results and Mass/Heat Transfer Coefficients of the Four Runs Used in the Model Validation

Run #	T13	T15	T19	T22
Flooding				
	No	No	No	No
Pressure Drop - Psi/ft (Pa/m)				
Leva [90]	9.31×10^{-3} (211)	10.16×10^{-3} (230)	8.64×10^{-3} (196)	8.01×10^{-3} (181)
GPDC [94]	7.80×10^{-3} (167)	8.67×10^{-3} (196)	6.50×10^{-3} (142)	6.94×10^{-3} (177)
Billet and Schultes [4]	18.02×10^{-3} (408)	19.9×10^{-3} (450)	16.6×10^{-3} (375)	19.32×10^{-3} (437)
Stichlmair et al. [99]	22.78×10^{-3} (515)	25.48×10^{-3} (576)	20.7×10^{-3} (469)	20.0×10^{-3} (453)
Aspen Plus	8.63×10^{-3} (195)	9.90×10^{-3} (224)	7.84×10^{-3} (177)	8.39×10^{-3} (190)
Liquid Holdup (%)				
Billet and Schultes [4]	7.50	7.37	7.64	5.99
Stichlmair et al. [99]	10.02	10.04	10.00	7.97
Mass Transfer Coefficients				
$k_{A,L}$ (Cho [3]) (m/s)	7.09×10^{-5}	7.85×10^{-5}	6.44×10^{-5}	7.47×10^{-5}
$k_{A,G}$ (Billet and Schultes [4]) (mol/Pa/m^2/s)	1.29×10^{-5}	1.35×10^{-5}	1.24×10^{-5}	1.34×10^{-5}
$k_{S,G}$ (Billet and Schultes [4]) (mol/Pa/m^2/s)	1.73×10^{-5}	1.80×10^{-5}	1.67×10^{-5}	1.79×10^{-5}
$k_{B,G}$ (Billet and Schultes [4]) (mol/Pa/m^2/s)	$1. 13 \times 10^{-5}$	1.17×10^{-5}	1.09×10^{-5}	1.34×10^{-5}
a_w (m^{-1}) (Cho [3])	164.54	164.00	148.35	125.3
a_w (m^{-1}) (Billet and Schultes [4])	64.67	64.76	64.70	59.99
h_G, (W/m^2/K) (Chilton-Colburn analogy [164])	40.20	39.88	40.54	39.78

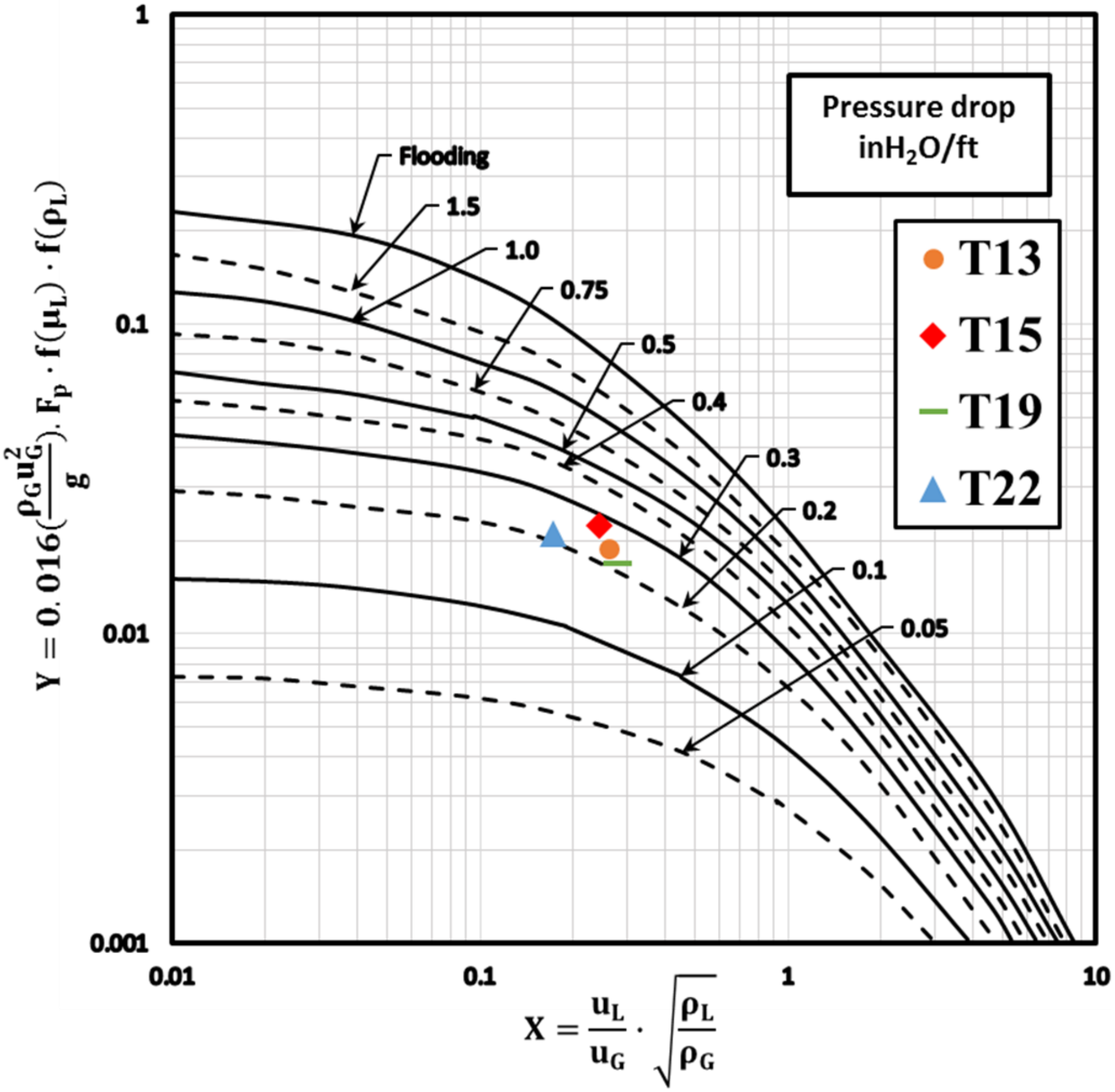

Figure 4-2: Flooding and Pressure Drop Graph by Leva [90]

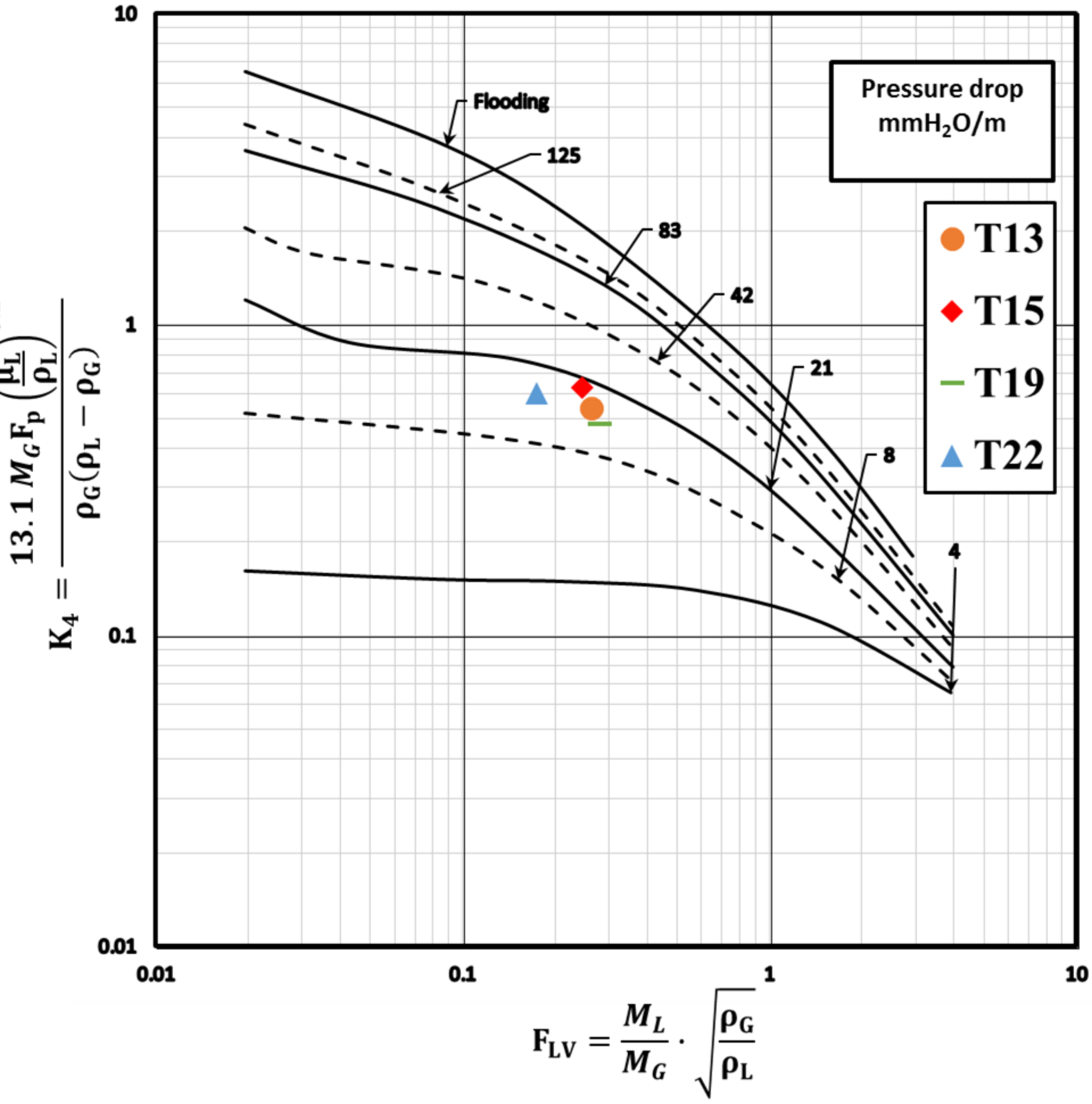

Figure 4-3: Generalized Pressure Drop Correlation (GPDC) [94]

4.2 Predictions of Henry's Law Constant and Diffusivity of CO_2 in MEA Aqueous Solutions

4.2.1 CO_2 Henry's Law Constant (He)

Figure 4-4 shows a good agreement between the He values calculated through N_2O analogy shown in Equation (3-109) - (3-112) for N_2O-MEA aqueous solution and experimental data from literature data [127, 129, 166]. Also, Figure 4-5 shows the comparison between the He values calculated using and N_2O analogy [127, 129, 166] and those obtained from Aspen Plus [167] for CO_2-MEA system. As can be seen in this figure, at 0 wt% MEA, He values calculated using the N_2O analogy are lower than those obtained from Aspen Plus. This behavior, however, is reversed at higher MEA concentrations (10 wt% - 30 wt%), where the He values obtained from Aspen Plus are systematically smaller than those calculated using the N_2O analogy. This behavior could be related to the ionic effect of the MEA solution at higher concentration, which was not considered in the development of N_2O analogy [127, 166].

.

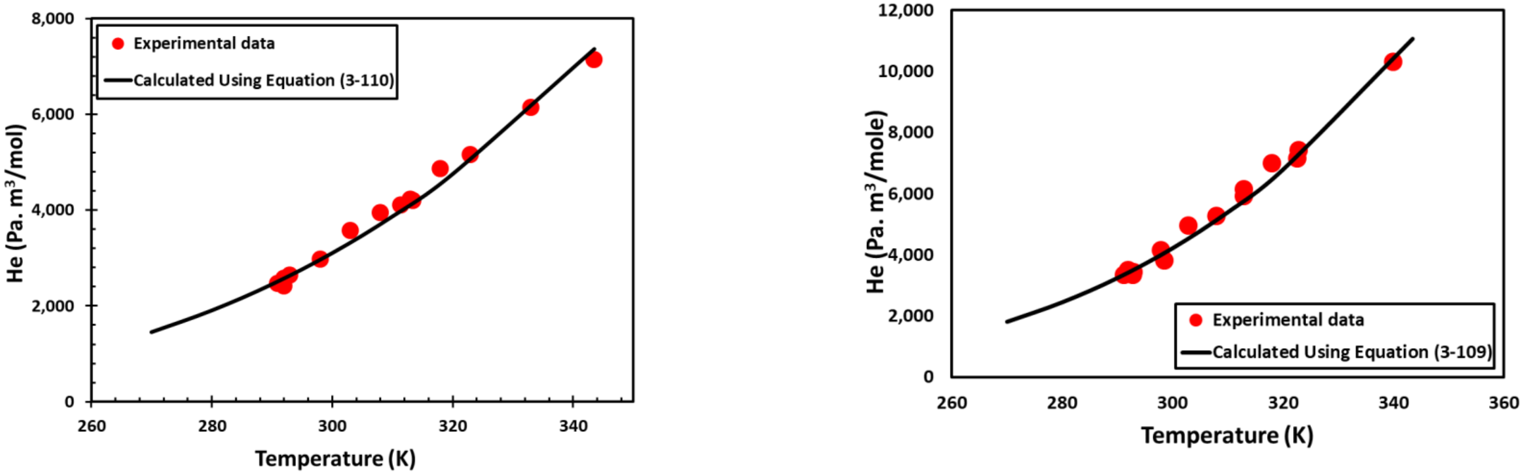

Henry's Law constant of CO_2 in water [127, 130, 166]

Henry's Law constant of N_2O in water [127, 130, 166]

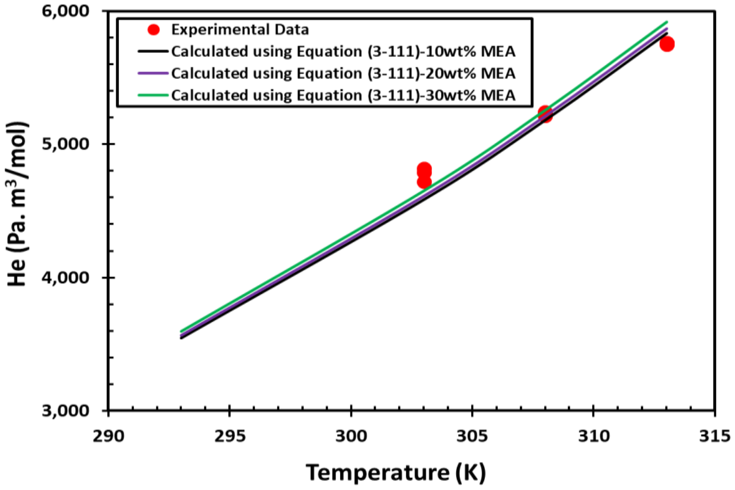

Henry's Law constant of N_2O in Aqueous MEA [129]

Figure 4-4: Henry's Law constant vs. Temperature

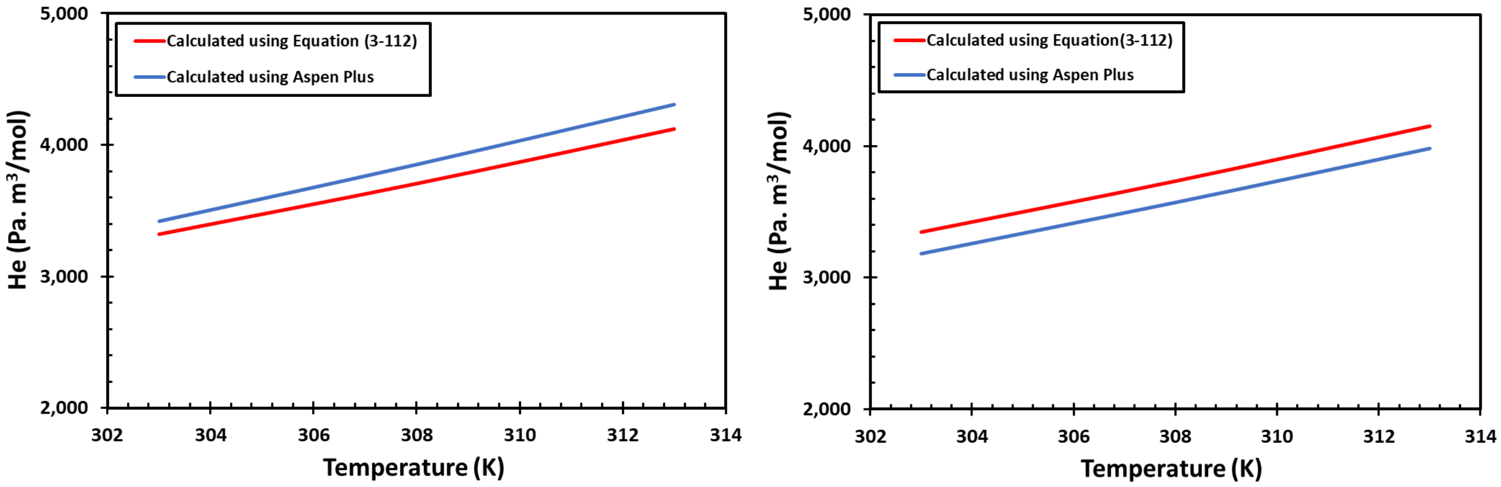

Henry's Constant comparison of 0 wt % MEA

Henry's Constant comparison of 10 wt % MEA

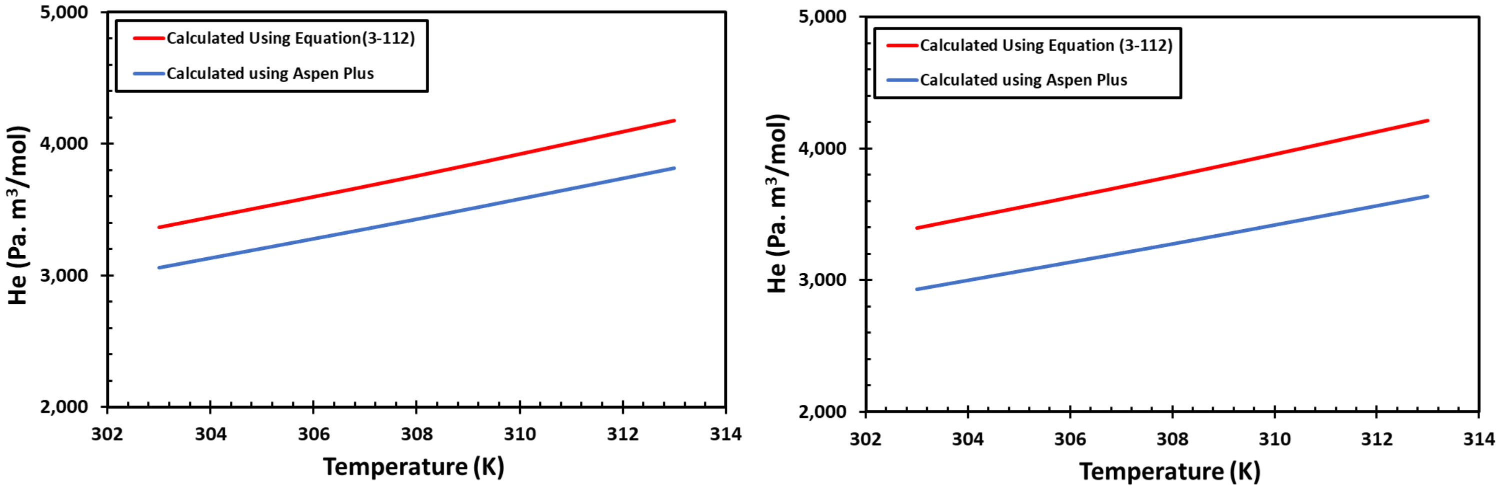

Henry's Constant comparison of 20 wt % MEA

Henry's Constant comparison of 30 wt % MEA

Figure 4-5: Henry's Law constant of CO_2 vs. Temperature using N_2O Analogy and Aspen Plus

4.2.2 CO_2 Diffusivity (D_A)

Figure 4-6 shows the diffusivity values of CO_2 in MEA aqueous solutions calculated using the N_2O analogy [130, 166] and those calculated using Equation (3-117) by Wilke and Chang [132]. As can be seen in this figure the diffusivity values in water (0 wt% MEA) calculated using the two methods are in good agreement. Significant deviations are observed at higher MEA concentrations, which can be attributed to the fact that Aspen Plus uses the Wilke and Chang [132] correlation (Equation (3-117)) to calculate the diffusivity of CO_2 in aqueous MEA solutions, which is a reactive system. This is fundamentally incorrect since CO_2 readily reacts with MEA and the CO_2 solubility as well as diffusivity will be corrupted by the chemical reaction between CO_2 and MEA. In fact, wrong diffusivity values lead to a wrong mass transfer coefficient since according to the Penetration Theory of gas-liquid mass transfer, the mass transfer coefficient (k_L) is proportional to the square root of the gas diffusivity ($k_L \alpha (D_L)^{0.5}$). It should be emphasized that since the reaction between CO_2 and MEA is fast with an enhancement factor greater than 10, the overall mass transfer rate is solely dependent on the specific wetted area (a_w) and is independent of the liquid-side mass transfer coefficient (k_L). Therefore, in the case of CO_2-MEA system, a wrong diffusivity would not have direct impact on the overall mass transfer rate.

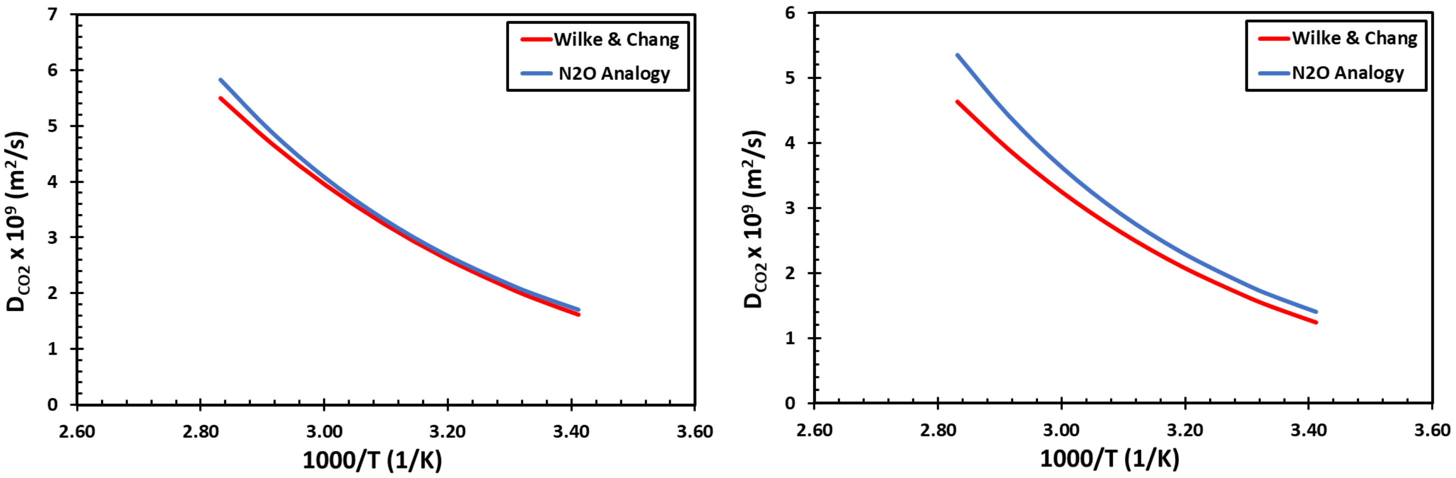

Diffusivity Comparison -0 wt% MEA

Diffusivity Comparison -10 wt% MEA

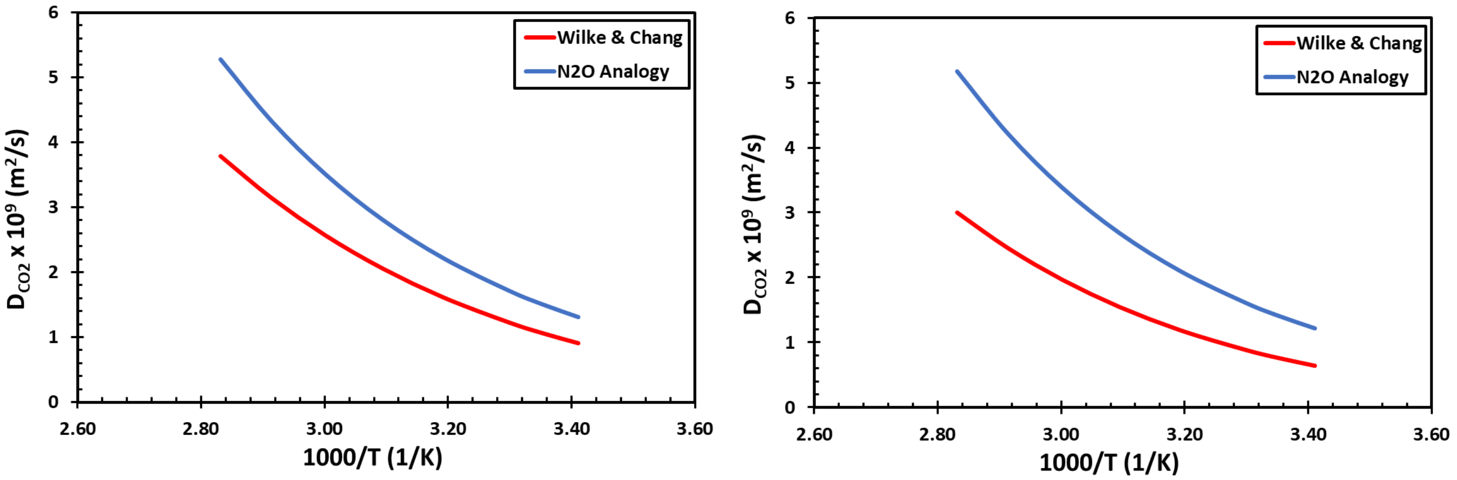

Diffusivity Comparison -20 wt% MEA

Diffusivity Comparison -30 wt% MEA

Figure 4-6:Diffusivity of CO_2 in MEA vs. Temperature Using Wilke and Chang [132] and N_2O Analogy [127, 130, 166]

4.3 Matlab Model Prediction of the Enhancement Factor Profiles

For absorber design in countercurrent mode, the temperature and composition of the lean absorbent and raw feed gas composition are generally given, while the CO_2 concentration of the exit gas is specified. The temperature and moisture content of exit gas is generally not known. In this scenario, these two points boundary value problem can be solved by assuming that temperature of the exit gas is in equilibrium with entering lean absorbent [2]. This is based on Pandya's [1] procedure and according to his suggestion, this assumption is valid for most of the cases [2]. By using this assumption, the composition of the rich solvent, exiting from the bottom of the absorber can be estimated.

Figure 4-7 shows the enhancement factor profile along with the absorber height calculated using Matlab model. As can be observed, the enhancement factor values are between 28 and 67 for run T13, between 10 and 67 for run T15, between 41 and 67 for run T19 and between 18 and 88 for run T22, all indicating a very fast reaction between CO_2 and aqueous MEA solutions.

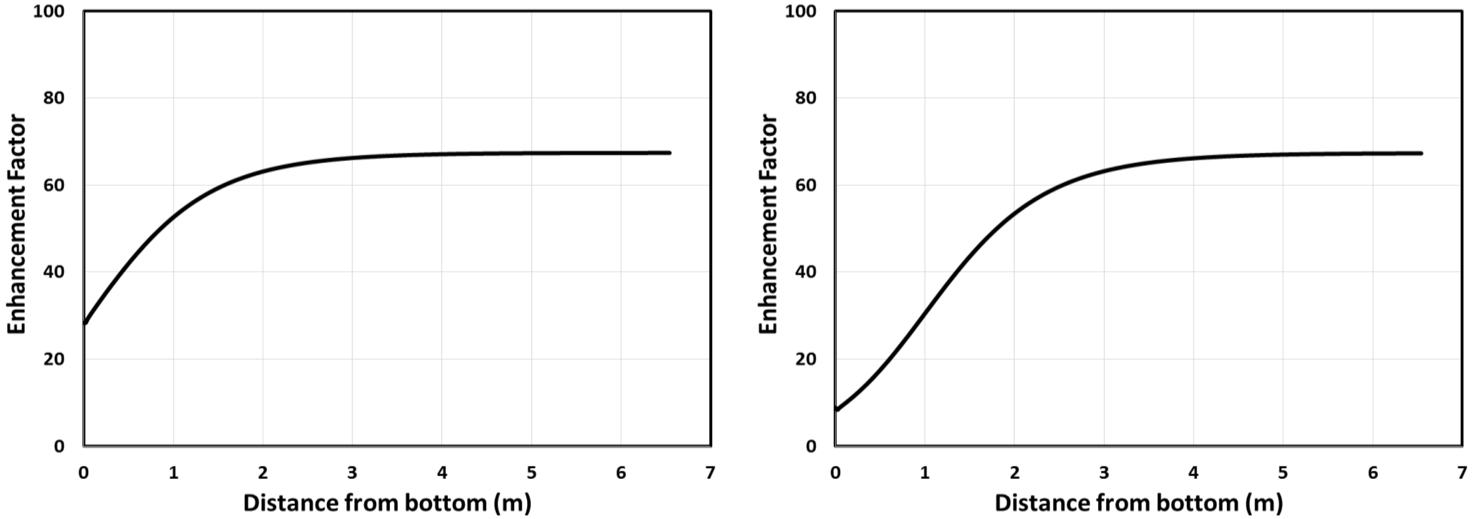

Run –T13

Run –T15

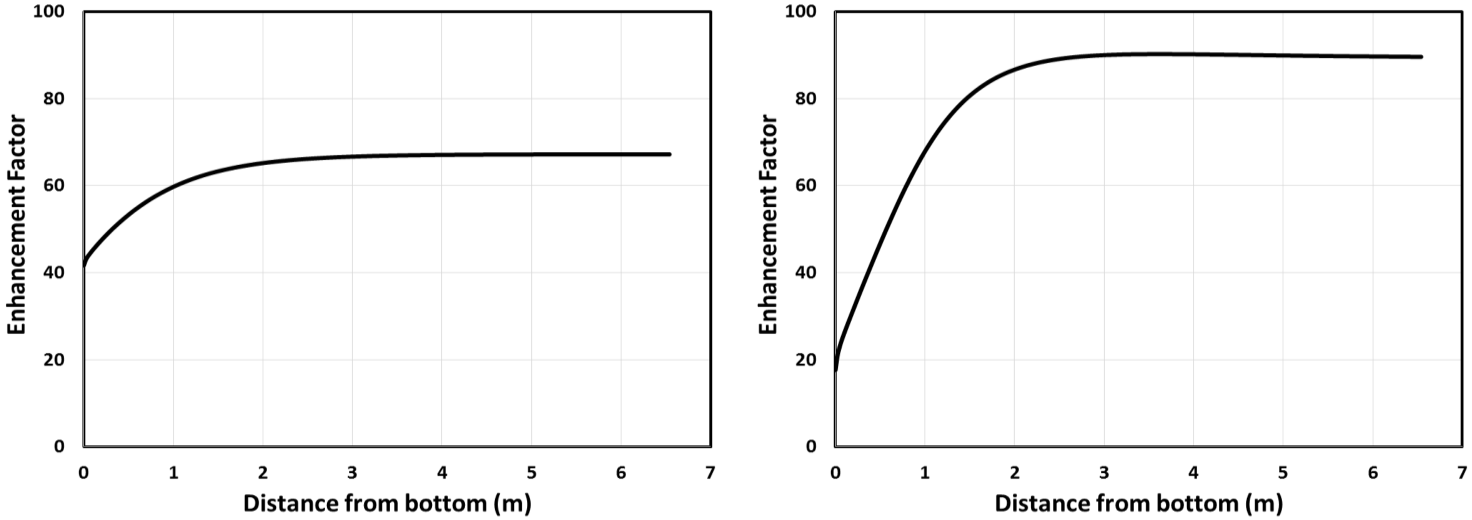

Run –T19

Run –T22

Figure 4-7: Enhancement Factor Profiles for the 4 Experimental Runs of Tontiwachwuthikul et al. [2] used in this study

4.4 Models Prediction of the Experimental CO_2 Mole Fraction Profiles

Figure 4-8 shows the experimental CO_2 mole fraction profiles for runs T13, T15, T19, and T22 by Tontiwachwuthikul et al. [2] along with the predicted values by the Matlab model and by Aspen Plus (Discrxn model). As can be seen in Figure 4-8, the Matlab and Aspen Plus model predictions are in a good agreement with the experimental results. Under all operating conditions used, the reaction of CO_2 with aqueous MEA was fast, as enhancement factors greater than 10 were calculated, and consequently the overall mass transfer rates were dependent on the specific wetted gas-liquid interfacial area (a_w) and independent of the liquid-side mass transfer coefficient (k_L). In the Matlab model, the correlations by Cho [3] were used to calculate the specific wetted area (a_w) and the liquid-side mass transfer coefficient (k_L); and the model predictions were in a good agreement with the experimental data. Whereas in the Aspen Plus model, the correlations by Billet and Schultes [4] were used to calculate (a_w) and the liquid-side mass transfer coefficient (k_L); and the model predictions could not well predict the experimental data. The reason for this behavior was attributed to the small a_w values calculated using the correlations by Billet and Schultes [4] when compared with those using the correlations by Cho [3] . Therefore, an interfacial area correction factor of 3 was introduced into the Aspen Plus model; and as a result, a good agreement was possible between the corrected model predictions and the experimental data. Actually, the maximum deviation between the predicted values using the corrected Aspen Plus model and experimental data, which can be observed for run T13 and T19, are 2.36% and 4.58%, respectively.

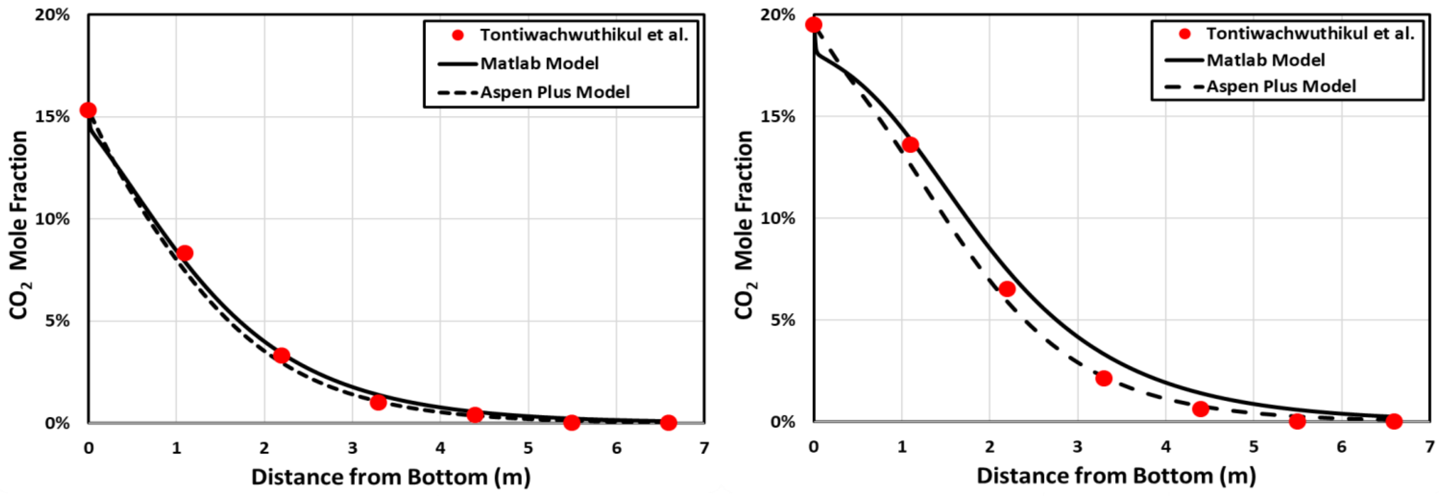

Run –T13

Run –T15

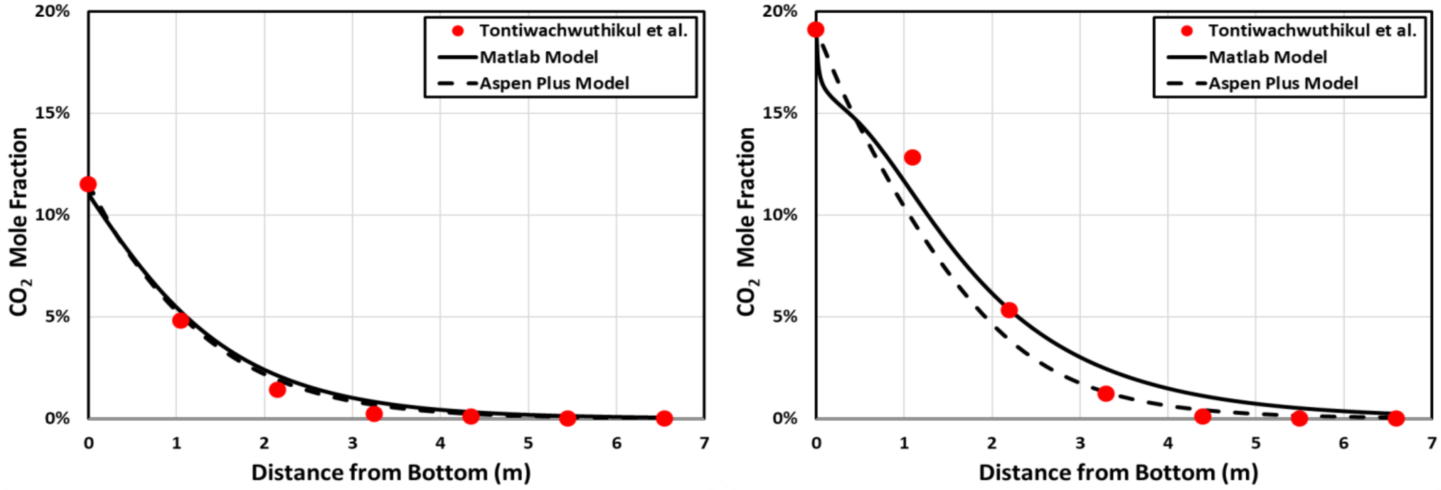

Run –T19

Run –T22

Figure 4-8: Comparison of Axial CO_2 Mole Fraction Profiles Between the Matlab and Aspen Plus models and the Experimental data of Tontiwachwuthikul et al. [2]

4.5 Models Prediction of the Experimental Liquid Temperature Profiles

Figure 4-9 shows the experimental axial liquid temperature profiles for runs T13, T15, T19, and T22 by Tontiwachwuthikul et al. [2] and the predicted values by the Matlab and Aspen Plus models. A good agreement between the predictions of the Matlab and Aspen Plus model and the experimental results can be observed.

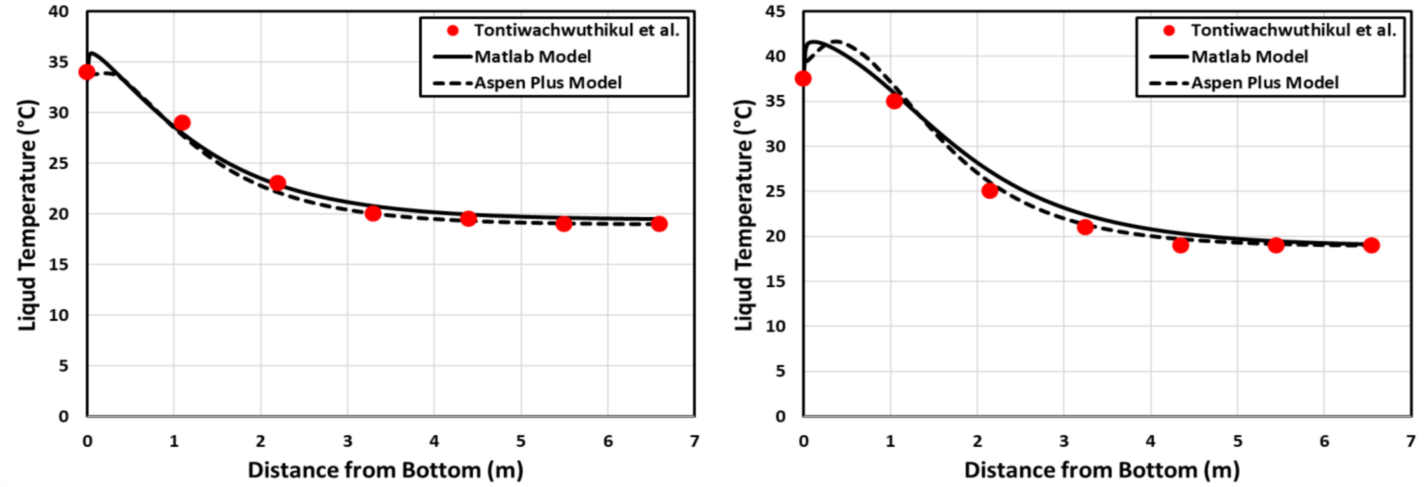

Run –T13

Run –T15

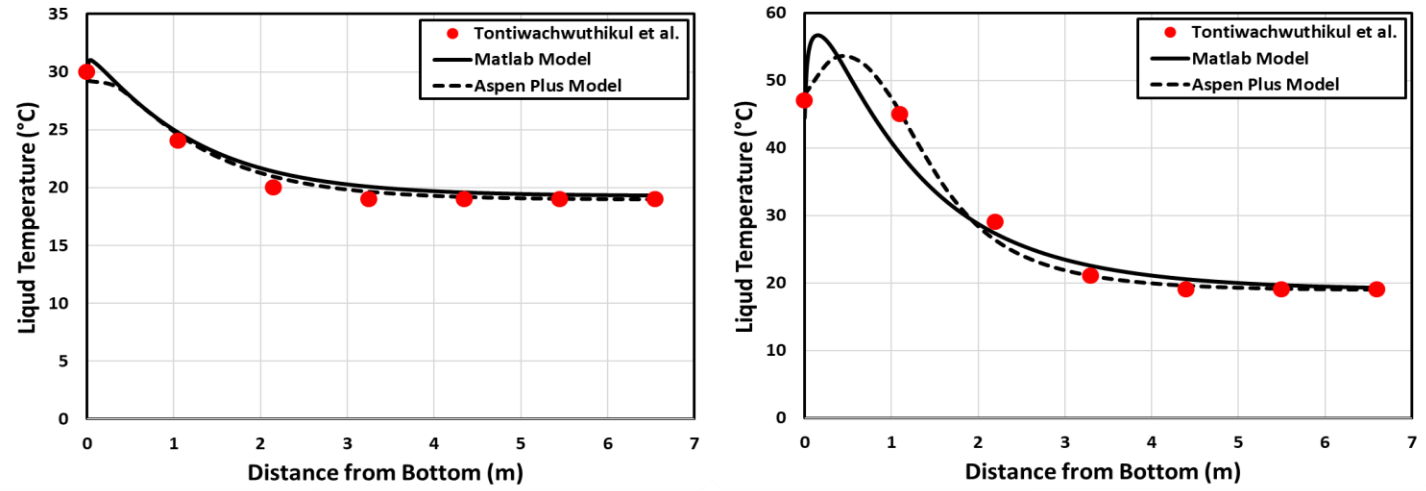

Run –T19

Run –T22

Figure 4-9: Comparison among Liquid Temperature Profiles Between the Matlab and Aspen Plus models and the Experimental data of Tontiwachwuthikul et al. [2]

4.6 Models Prediction of the Experimental CO_2 Loading Profiles

Figure 4-10 shows a comparison between the experimental CO_2 loading (mole of CO_2/initial mole of MEA) profiles for runs T13, T15, T19, and T22 by Tontiwachwuthikul et al. [2] and the predicted values by the Matlab and Aspen Plus models. As can be seen in this figure, the predicted values using Matlab model and Aspen Plus model are in a good agreement, particularly for the run T13 and T19 and the small deviation from runs T15 and T22 can be attributed to the experimental errors reported by Tontiwachwuthikul et al.[2].

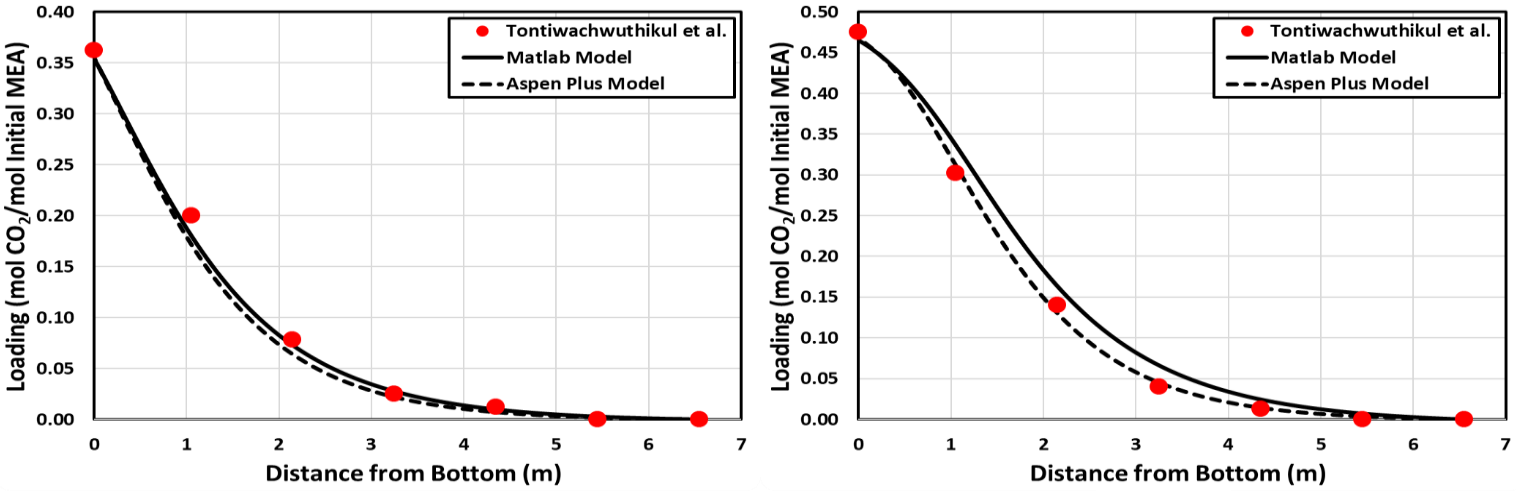

Run –T13

Run –T15

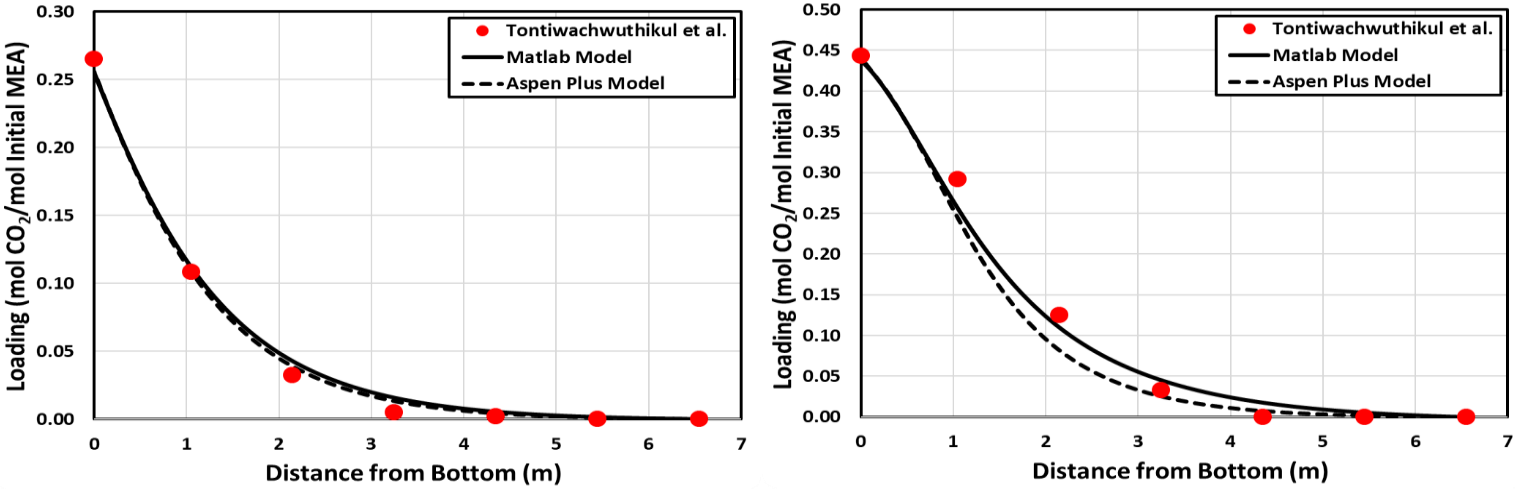

Run –T19

Run –T22

Figure 4-10: CO_2 Loading Profile Comparison Between the Matlab and Aspen Plus models and the Experimental data of Tontiwachwuthikul et al. [2]

4.7 Models Prediction of the CO_2 Absorption Efficiency

The Matlab model and the Aspen Plus model were used to calculate the CO_2 absorption efficiency defined using Equation (4-1) and the model results are illustrated in Figure 4-11 for Runs T13, T15, T19 and T22.

$$\mathrm{CO_2 Absorption\ Efficiency} = \left(1 - \frac{N_{CO2-out}}{N_{CO2-in}}\right) \tag{4-1}$$

Where N_{CO2} is the number of moles of CO_2

As can be seen in this figure, Aspen Plus and Matlab model predict over 95% of the CO_2 absorption efficiency at a packing height of about 5 m from the bottom of the absorber for the four runs.

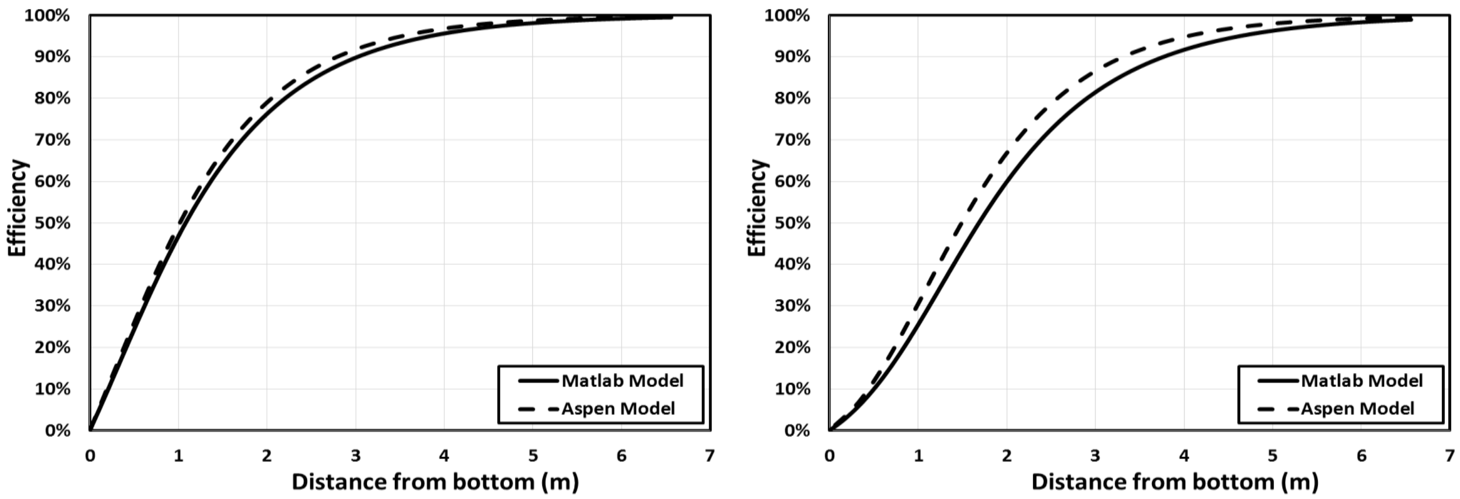

Run –T13

Run –T15

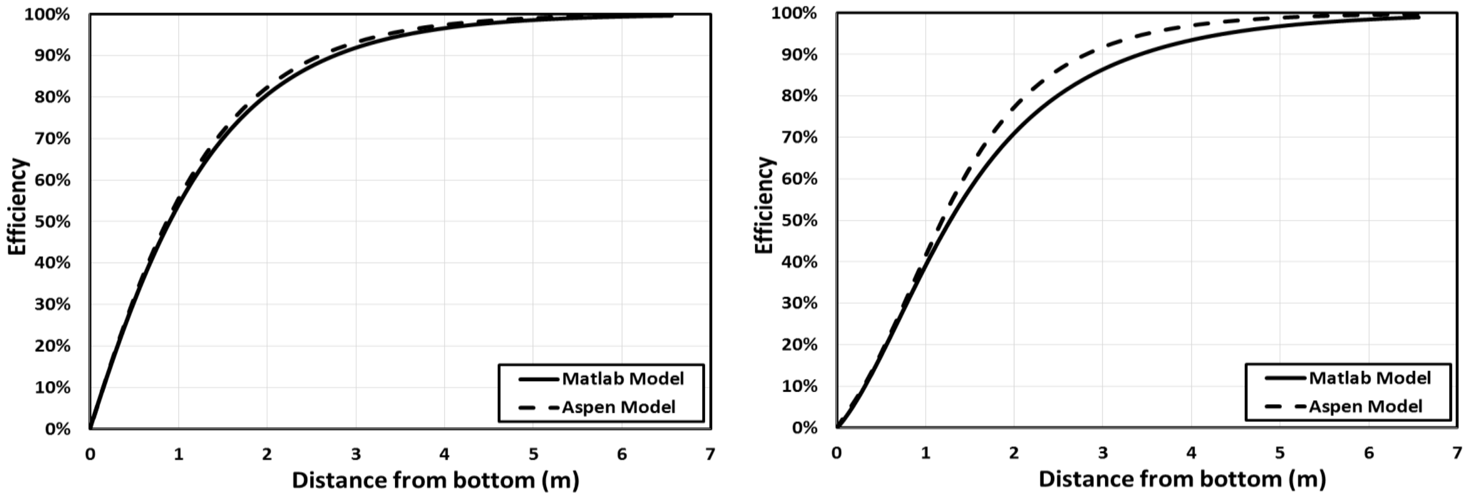

Run –T19

Run –T22

Figure 4-11: CO_2 Absorption Efficiency Axial Profiles as Predicted by the Matlab and Aspen Plus Models

4.8 Models Prediction of the Gas Temperature Profiles

Tontiwachwuthikul et al. [2] did not show the gas temperature profiles for all the four runs. In this study, the gas temperature profiles were predicted using Matlab and Aspen Plus models. Figure 4-12 shows the axial gas temperature profiles for all the runs and as can be observed the temperatures in the bottom half of the column are noticeably higher, which is due to the fact that the majority of CO_2 absorption occurs in the bottom half of the column, which causes a rapid variation of gas temperature due to the exothermic reaction between CO_2 and the aqueous MEA solution. The gas then continues to react and exchange heat with the liquid to as it moves to the top of the absorber. In all the cases, the Matlab and Aspen Plus models predicted that the gas exits the column at about 19 ^{o}C, which is the liquid inlet temperature.

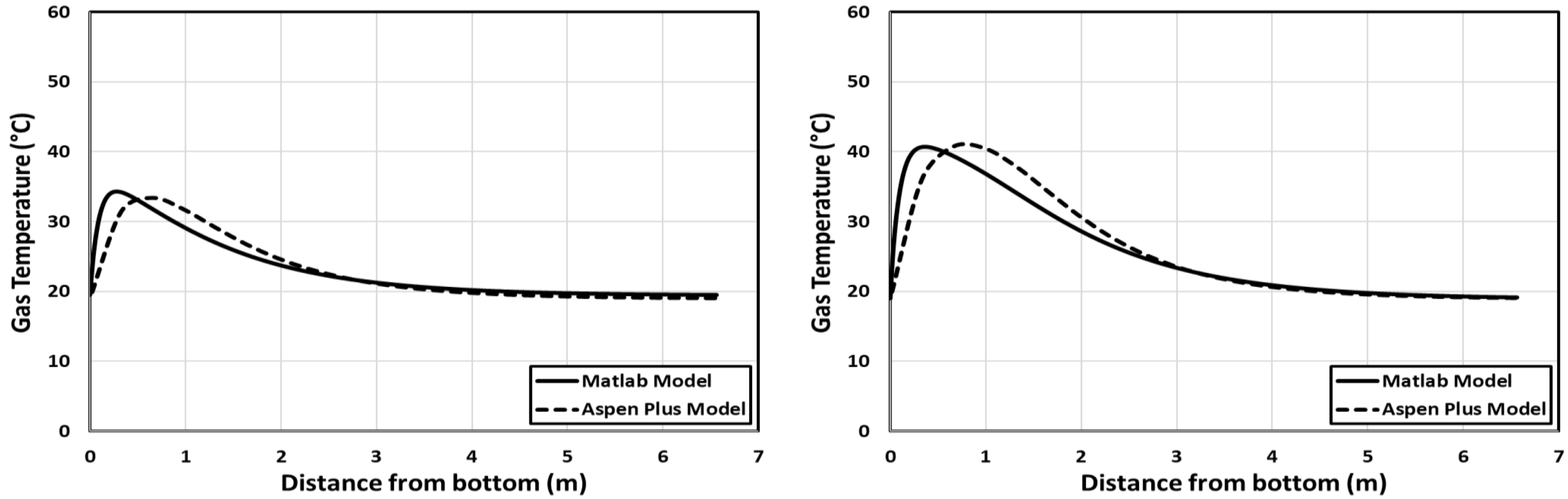

Run –T13

Run –T15

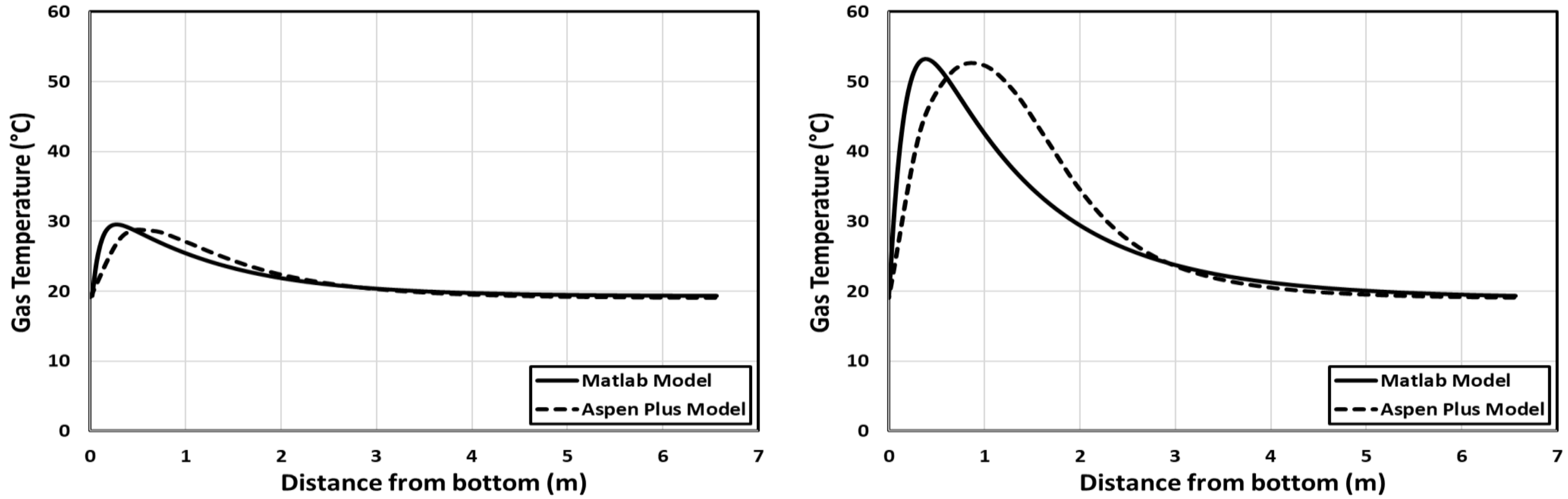

Run –T19

Run –T22

Figure 4-12: Axial Gas Temperature Profiles as Predicted by the Matlab and Aspen Plus Models

5.0 Concluding Remarks

A five-components (CO_2, air, MEA, H_2O, and carbamates) mathematical model was developed in Matlab (R2016a) based on the rigorous procedure for adiabatic gas absorption into liquids with second-order chemical reaction by Pandya [1]. The material and energy balance equations were derived for the five components present in the absorber. The absorber was operated under ambient conditions, representative of the post-combustion CO_2 capture applications. The equation parameters, including reaction kinetics of CO_2 with aqueous MEA solutions, physicochemical properties of the five components and heat as well as mass transfer coefficients of the gases in the solvents required for model solution were obtained from the literature. In Matlab model, Henry's Law constants and diffusivity of CO_2 in MEA solutions were calculated using N_2O analogy. Also, a rate-based discretized reaction model (Discrxn model) for CO_2 absorption in aqueous MEA solutions using the same absorber was implemented in Aspen Plus (v.8.8). The Matlab and Aspen Plus models were used to predict the experimental results for CO_2 capture from a mixture of air using aqueous MEA solutions in a 0.10 m ID, 6.55 m height packed-bed absorber with 12.7 mm Berl Saddles by Tontiwachwuthikul et al. [2]. The Matlab and Aspen Plus models were used to predict the experimental results and the following concluding remarks can be made:

1. Under all operating conditions used in the four runs, no flooding occurred in the counter-current absorber. The irrigated two-phase pressure drops, and liquid holdup were calculated and graphically interpolated for each run.

2. The specific wetted interfacial area (a_w); liquid-side (k_L) and gas-side (k_G) mass transfer coefficients; and heat transfer coefficients (h_G) were also calculated. No unusual behavior in the calculated results can be reported. The specific wetted interfacial areas predicted with correlations by Cho [3] were greater than those predicted with the correlations by Billet and Schultes [4].
3. Due to the fast-chemical reaction between CO_2 and MEA with enhancement factors greater than 10, the overall mass transfer rate was dependent of the specific wetted interfacial area (a_w) and independent of liquid-side mass transfer coefficient (k_L).
4. The predicted mole fraction, liquid-phase temperature, and CO_2 loading axial profiles using the Matlab model including the specific wetted area calculated using the correlations by Cho [3] were in good agreement with the experimental data under all the experimental conditions used.
5. The predicted mole fraction, liquid-phase temperature, and CO_2 loading axial profiles using the Aspen Plus model including the corrected specific wetted interfacial area calculated using the correlations by Billet and Schultes [4] were in good agreement with the experimental data under all the experimental conditions used. A specific wetted area correction factor of 3 was necessary to fit the experimental data.
6. Almost 70 – 80 mole% of CO_2 was captured within the first two meters from the bottom of the absorber and since the CO_2-MEA reaction is exothermic, peaks in the axial liquid and gas phase temperature profiles occur within this region. After two meters, the gas-phase continues to cool as it rises upwards and exits the top of the absorber at a similar temperature to that of the inlet liquid-phase, due to the adiabatic behavior of the absorber.

Bibliography

[1] J. D. Pandya, "Adiabatic gas absorption and stripping with chemical reaction in packed towers," *Chemical Engineering Communications,* vol. 19, pp. 343-361, 1983.

[2] P. Tontiwachwuthikul, A. Meisen, and C. J. Lim, "CO_2 absorption by NaOH , Monoethanolamine, 2-amino-2-methyl-1-propanol solutions in a packed column," *Chemical Engineering Science,* vol. 47, no. 2, pp. 381-390, 1992.

[3] J. S. Cho, "Gas Absorption in a Countercurrent Packed Tower: (1) Absorption with Simultaneous Chemical Reaction (2) Absorption into Varying Viscous Solutions," *Ph.D. Thesis. Oregon Sate University,* 1987.

[4] R. Billet and M. Schultes, "Prediction of mass transfer columns with dumped and arranged packings: updated summary of the calculation method of Billet and Schultes," *Chemical Engineering Research and Design,* vol. 77, no. 6, pp. 498-504, 1999.

[5] A. Kothandaraman, "Carbon Dioxide Capture by Chemical Absorption : A Solvent Comparison Study," *PhD thesis,* pp. 144-184, 2010.

[6] GISS, *Global Temerature* (http://ossfoundation.us/projects/environment/global-warming/temperature).

[7] NASA. (2020). *Global Climate Change*.

[8] NASA, *Global Climate Change(NASA)*.

[9] E. Ozdemir, K. Schroeder, and B. I. Morsi, "Global warming: Carbon dioxide sequestration in coal seams," *American Chemical Society,* vol. 42, pp. 310-317, 2002.

[10] IPCC, "Contribution Of Working Group III to 5th Assessment Report Of The Intergovernmental Panel on Climate Change," 2014.

[11] M. Meinshausen *et al.*, "Greenhouse-gas emission targets for limiting global warming to 2 C," vol. 458, no. 7242, p. 1158, 2009.

[12] J. Farrel, "Carbon Capture," *Journal of SciencePolicy & Governanc (JSPG),* vol. 12, no. 1, February, 2018 2018.

[13] E. I. A. (EIA). (2009). *International Energy Outlook, US Department of Energy*.

[14] M. Tubman, Center for Climate and Energy Solutions: Washington, DC, USA, "President Obama’s Climate Action Plan: Two Years Later," 2015.

[15] D. Reichle, J. Houghton, B. Kane, and J. Ekmann, "Carbon sequestration research and development," Oak Ridge National Lab., TN (US); National Energy Technology Lab …1999.

[16] A. B. Rao and E. S. Rubin, "A technical, economic, and environmental assessment of amine-based CO2 capture technology for power plant greenhouse gas control," *Environmental science technology,* vol. 36, no. 20, pp. 4467-4475, 2002.

[17] J. Dyment and S. Watanasiri, "Acid gas cleaning using DEPG physical solvents: validation with experimental and plant data," *The USA: Aspen Technology Inc,* 2015.

[18] A. J. Kidnay, W. R. Parrish, and D. G. McCartney, *Fundamentals of natural gas processing*. CRC press, 2011.

[19] O. M. Basha, "Personal Communication, Postcombustion CO_2 Capture," May 6, 2018.

[20] E. J. Granite and H. W. Pennline, "Photochemical removal of mercury from flue gas," *Energy & Industrial Engineering Chemistry Research,* vol. 41, no. 22, pp. 5470-5476, 2002.

[21] S. Wang *et al.*, "Mercury emission and speciation of coal-fired power plants in China," vol. 10, no. 3, pp. 1183-1192, 2010.

[22] E. Oko, M. Wang, and A. S. Joel, "Current status and future development of solvent-based carbon capture," *International Journal of Coal Science & Technology,* vol. 4, no. 1, pp. 5-14, 2017.

[23] F. Li, J. Zhang, C. Shang, D. Huang, E. Oko, and M. Wang, "Modelling of a post-combustion CO_2 capture process using deep belief network," *Applied Thermal Engineering,* vol. 130, pp. 997-1003, 2018.

[24] H. Rangwala, B. Morrell, A. Mather, and F. Otto, "Absorption of CO_2 into aqueous tertiary amine/MEA solutions," *The Canadian Journal of Chemical Engineering,* vol. 70, no. 3, pp. 482-490, 1992.

[25] Y. Peng, B. Zhao, and L. Li, "Advance in post-combustion CO_2 capture with alkaline solution: a brief review," *Energy Procedia,* vol. 14, pp. 1515-1522, 2012.

[26] Y. E. Kim, J. A. Lim, S. K. Jeong, Y. I. Yoon, S. T. Bae, and S. C. Nam, "Comparison of carbon dioxide absorption in aqueous MEA, DEA, TEA, and AMP solutions," *Bulletin of the Korean Chemical Society,* vol. 34, no. 3, pp. 783-787, 2013.

[27] H. R. Godini and D. Mowla, "Selectivity study of H_2S and CO_2 absorption from gaseous mixtures by MEA in packed beds," *Chemical Engineering Research and Design,* vol. 86, no. 4, pp. 401-409, 2008.

[28] A. Chakma, A. Mehrotra, B. Nielsen, and CHP, "Comparison of chemical solvents for mitigating CO_2 emissions from coal-fired power plants," *Heat Recovery Systems,* vol. 15, no. 2, pp. 231-240, 1995.

[29] W. M. Budzianowski, "Mitigating NH_3 vaporization from an aqueous ammonia process for CO_2 capture," *International journal of chemical reactor engineering,* vol. 9, no. 1, 2011.

[30] G. Versteeg, L. Van Dijck, Van Swaaij, and W. P. Maria, "An overview on the kinetics between CO_2 and alkanolamines both in aqueous and non-aqueous solutions. ," *Chemical Engineering Communications,* vol. 144, no. 1, pp. 113-158, 1996.

[31] P. Danckwerts, "The reaction of CO_2 with ethanolamines," *Chemical Engineering Science,* vol. 34, no. 4, pp. 443-446, 1979.

[32] G. F. Versteeg and W. P. M. Van Swaaij, "Solubility and diffusivity of acid gases (carbon dioxide, nitrous oxide) in aqueous alkanolamine solutions," *Journal of Chemical & Engineering Data,* vol. 33, pp. 29-34, 1988.

[33] S. Xu, F. D. Otto, and A. E. Mather, "Physical properties of aqueous AMP solutions," *Journal of Chemical and Engineering Data,* vol. 36, pp. 71-75, 1991.

[34] A. K. Saha, S. S. Bandyopadhyay, and A. K. Biswas, "Solubility and diffusivity of nitrous oxide and carbon dioxide in aqueous solutions of 2-amino-2-methyl-1-propanol," *Journal of Chemical and Engineering Data,* vol. 38, pp. 78-82, 1993.

[35] A. K. Saha, S. S. Bandyopadhyay, and A. K. Biswas, "Kinetics of absorption of CO2 into aqueous solutions of 2-amino-2-methyl-1-propanol," *Chemical Engineering Science,* vol. 50, pp. 3587-3598, 1995.

[36] A. Aroonwilas and P. Tontiwachwuthikul, "High-efficiency structured packing for CO2 separation using 2-amino-2-methyl-1-propanol (AMP)," *Separation and purification technology,* vol. 12, pp. 67-79, 1997.

[37] G. Vázquez, E. Alvarez, J. M. Navaza, R. Rendo, and E. Romero, "Surface tension of binary mixtures of water+ monoethanolamine and water+ 2-amino-2-methyl-1-propanol and tertiary mixtures of these amines with water from 25 C to 50 C," *Journal of Chemical & Engineering Data*, vol. 42, pp. 57-59, 1997.

[38] Y.-J. Chen and M.-H. Li, "Heat Capacity of Aqueous Mixtures of Monoethanolamine with 2-Amino-2-methyl-l-propanol," *Journal of Chemical & Engineering Data,* vol. 46, pp. 102-106, 2001.

[39] J.-J. Ko, T.-C. Tsai, C.-Y. Lin, H.-M. Wang, and M.-H. Li, "Diffusivity of nitrous oxide in aqueous alkanolamine solutions," *Journal of Chemical & Engineering Data,* vol. 46, pp. 160-165, 2001.

[40] E. Álvarez, Á. Cancela, R. Maceiras, J. M. Navaza, and R. Táboas, "Surface tension of aqueous binary mixtures of 1-amino-2-propanol and 3-amino-1-propanol, and aqueous ternary mixtures of these amines with diethanolamine, triethanolamine, and 2-amino-2-methyl-1-propanol from (298.15 to 323.15) K," *Journal of Chemical & Engineering Data*, vol. 48, pp. 32-35, 2003.

[41] A. Henni, J. J. Hromek, P. Tontiwachwuthikul, and A. Chakma, "Volumetric properties and viscosities for aqueous AMP solutions from 25 C to 70 C," *Journal of Chemical & Engineering Data,* vol. 48, pp. 551-556, 2003.

[42] B. P. Mandal, M. Kundu, and S. S. Bandyopadhyay, "Physical solubility and diffusivity of N2O and CO2 into aqueous solutions of (2-amino-2-methyl-1-propanol+ monoethanolamine) and (N-methyldiethanolamine+ monoethanolamine)," *Journal of Chemical & Engineering Data,* vol. 50, pp. 352-358, 2005.

[43] H. Arcis, L. Rodier, and J.-Y. Coxam, "Enthalpy of solution of CO2 in aqueous solutions of 2-amino-2-methyl-1-propanol," *The Journal of Chemical Thermodynamics,* vol. 39, pp. 878-887, 2007.

[44] A. Chakraborty, G. Astarita, and K. J. C. E. S. Bischoff, "CO2 absorption in aqueous solutions of hindered amines," vol. 41, no. 4, pp. 997-1003, 1986.

[45] S. Lee, H.-J. Song, S. Maken, H.-C. Shin, H.-C. Song, and J.-W. Park, "Physical solubility and diffusivity of N_2O and CO_2 in aqueous sodium glycinate solutions," *Journal of Chemical Engineering Data,* vol. 51, no. 2, pp. 504-509, 2006.

[46] H.-J. Song, S. Lee, S. Maken, J.-J. Park, and J.-W. Park, "Solubilities of carbon dioxide in aqueous solutions of sodium glycinate," *Fluid Phase Equilibria,* vol. 246, no. 1-2, pp. 1-5, 2006.

[47] S. Lee, H.-J. Song, S. Maken, J.-W. J. I. Park, and e. c. research, "Kinetics of CO2 absorption in aqueous sodium glycinate solutions," vol. 46, no. 5, pp. 1578-1583, 2007.

[48] F. Harris, K. A. Kurnia, M. I. A. Mutalib, M. J. J. o. C. Thanapalan, and E. Data, "Solubilities of carbon dioxide and densities of aqueous sodium glycinate solutions before and after CO2 absorption," vol. 54, no. 1, pp. 144-147, 2008.

[49] S.-W. Park, Y.-S. Son, D.-W. Park, and K.-J. Oh, "Absorption of carbon dioxide into aqueous solution of sodium glycinate," *Separation Science Technology,* vol. 43, no. 11-12, pp. 3003-3019, 2008.

[50] H.-J. Song *et al.,* "Simplified estimation of regeneration energy of 30 wt% sodium glycinate solution for carbon dioxide absorption," vol. 47, no. 24, pp. 9925-9930, 2008.

[51] W. Zhao, Y. SHI, J.-w. WEI, and Q. J. J. o. C. E. o. C. U. YE, "Experimental study on CO2 absorption and regeneration of aqueous sodium glycinate solutions," vol. 22, pp. 690-695, 2008.

[52] V. n. Salazar, Y. Sánchez-Vicente, C. Pando, J. A. Renuncio, A. J. J. o. C. Cabañas, and E. Data, "Enthalpies of absorption of carbon dioxide in aqueous sodium glycinate solutions at temperatures of (313.15 and 323.15) K," vol. 55, no. 3, pp. 1215-1218, 2009.

[53] S. Mazinani, A. Samsami, A. Jahanmiri, A. J. J. o. C. Sardarian, and E. Data, "Solubility (at low partial pressures), density, viscosity, and corrosion rate of carbon dioxide in blend solutions of monoethanolamine (MEA) and sodium glycinate (SG)," vol. 56, no. 7, pp. 3163-3168, 2011.

[54] K. P. Resnik, J. T. Yeh, and H. W. Pennline, "Aqua ammonia process for simultaneous removal of CO_2, SO_2 and NO_x," *International journal of environmental technology management,* vol. 4, no. 1-2, pp. 89-104, 2004.

[55] V. Darde, K. Thomsen, W. J. Van Well, and E. H. J. E. P. Stenby, "Chilled ammonia process for CO2 capture," vol. 1, no. 1, pp. 1035-1042, 2009.

[56] F. Kozak, A. Petig, E. Morris, R. Rhudy, and D. J. E. P. Thimsen, "Chilled ammonia process for CO2 capture," vol. 1, no. 1, pp. 1419-1426, 2009.

[57] H. Benson, J. Field, and Jimeson, "CO/sub 2/absorption: employing hot potassium carbonate solutions," *Chemical Engincering Program,* vol. 50, no. 7, 1954.

[58] D. W. Savage, G. Astarita, and S. Joshi, "Chemical absorption and desorption of carbon dioxide from hot carbonate solutions," *Chemical Engineering Science,* vol. 35, no. 7, pp. 1513-1522, 1980/01/01/ 1980.

[59] A. H. G. Cents, D. W. F. Brilman, and G. F. Versteeg, "CO_2 absorption in carbonate/bicarbonate solutions: The Danckwerts-criterion revisited," *Chemical Engineering Science,* vol. 60, no. 21, pp. 5830-5835, 2005/11/01/ 2005.

[60] M. Ahmadi, V. G. Gomes, and K. Ngian, "Advanced modelling in performance optimization for reactive separation in industrial CO2 removal," *Separation and Purification Technology,* vol. 63, no. 1, pp. 107-115, 2008/10/01/ 2008.

[61] A. Aboudheir, P. Tontiwachwuthikul, R. J. I. Idem, and e. c. research, "Rigorous model for predicting the behavior of CO2 absorption into AMP in packed-bed absorption columns," vol. 45, no. 8, pp. 2553-2557, 2006.

[62] F. Yi, H.-K. Zou, G.-W. Chu, L. Shao, and J.-F. Chen, "Modeling and experimental studies on absorption of CO2 by Benfield solution in rotating packed bed," *Chemical Engineering Journal,* vol. 145, no. 3, pp. 377-384, 2009/01/01/ 2009.

[63] K. A. Mumford *et al.*, "Post-combustion capture of CO_2: results from the solvent absorption capture plant at Hazelwood power station using potassium carbonate solvent," *Energy fuels,* vol. 26, no. 1, pp. 138-146, 2011.

[64] A. M. a. C. J. L. Paitoon Tontiwachwuthikul, "Novel Pilot Plant Technique for Sizing Gas Absorbers with Chemical Reactions," *The Canadian Journal of Chemical Engineering,* vol. 67, August, 1989 1989.

[65] T. Pintola, P. Tontiwachwuthikul, and A. Meisen, "Simulation of pilot plant and industrial CO_2-MEA absorbers," *Gas Separation and Purification,* vol. 7, pp. 47-52, 1993.

[66] F. M. Khan, V. Krishnamoorthi, and T. Mahmud, "Modelling reactive absorption of CO_2 in packed columns for post-combustion carbon capture applications," *Chemical Engineering Research and Design,* vol. 89, pp. 1600-1608, 2011.

[67] Anand B. Rao, Edward S. Rubin, and M. B. Berkenpas, "An integrated modeling framework for carbon management technologies. United states," 03.01.2004 2004.

[68] I. P. Prevention, "Control Reference Document on Best Available Techniques for the Manufacture of Large Volume Inorganic Chemicals-Ammonia," *Acids and Fertilisers dated on August,* 2007.

[69] P. Luis, "Use of monoethanolamine (MEA) for CO_2 capture in a global scenario: Consequences and alternatives," *Desalination,* vol. 380, pp. 93-99, 2016.

[70] L. Dubois and D. Thomas, "Screening of aqueous amine ‐ based solvents for postcombustion CO2 capture by chemical absorption," *Chemical engineering & technology,* vol. 35, no. 3, pp. 513-524, 2012.

[71] L. Raynal *et al.*, "The DMX™ process: an original solution for lowering the cost of post-combustion carbon capture," *Energy Procedia,* vol. 4, pp. 779-786, 2011.

[72] J. Zhang, Y. Qiao, W. Wang, R. Misch, K. Hussain, and D. W. Agar, "Development of an energy-efficient CO2 capture process using thermomorphic biphasic solvents," *Energy Procedia,* vol. 37, pp. 1254-1261, 2013.

[73] D. Shaw, "Cansolv CO2 capture: The value of integration," *Energy Procedia,* vol. 1, no. 1, pp. 237-246, 2009.

[74] Siemens. (2015). *Innovative Power Plant Solutions*. Available: https://new.siemens.com/global/en/products/energy/power-generation/power-plants.html

[75] F. Chopin *et al.*, "Advanced amine process technology operations and results from demonstration facility at EDF Le Havre," *Energy Procedia,* vol. 63, pp. 6173-6187, 2014.

[76] MIT. (2016). *E.ON Karlshamn Fact Sheet: carbon dioxide capture and storage project.* Available: http://sequestration.mit.edu/tools/projects/eon_karlshamn.html

[77] BBC-News. (2015). *Carbon trading*. Available: https://www.bbc.com/news/science-environment-34356604

[78] F. Gozalpour, S. R. Ren, B. J. O. Tohidi, G. Science, and T.-R. IFP, "CO2 Eor and Storage in Oil Reservoir," vol. 60, no. 3, pp. 537-546, 2005.

[79] S. Bachu, J. C. Shaw, and R. M. Pearson, "Estimation of Oil Recovery and CO2 Storage Capacity in CO2 EOR Incorporating the Effect of Underlying Aquifers," presented at the SPE/DOE Symposium on Improved Oil Recovery, Tulsa, Oklahoma, 2004/1/1/, 2004. Available: https://doi.org/10.2118/89340-MS

[80] D. Damiani, J. T. Litynski, H. G. McIlvried, D. M. Vikara, and R. D. Srivastava, "The US department of Energy's R&D program to reduce greenhouse gas emissions through beneficial uses of carbon dioxide," *Greenhouse Gases: Science and Technology*, vol. 2, no. 1, pp. 9-16, 2012.

[81] G. Astarita, D. W. Savage, and A. Bisio, *Gas treating with chemical solvents*. J. Wiley and Sons ,New York (NY), 1983, p. 493.

[82] J. W. Morse, "Carbonic Acid," pp. Pages 509-583, 2013.

[83] M. Caplow, "Kinetics of carbamate formation and breakdown," *Journal of the American Chemical Society*, vol. 90, no. 24, pp. 6795-6803, 1968.

[84] B. Lv, B. Guo, Z. Zhou, and G. Jing, "Mechanisms of CO_2 Capture into Monoethanolamine Solution with Different CO_2 Loading during the Absorption/Desorption Processes," *Environmental Science and Technology*, vol. 49, pp. 10728-10735, 2015.

[85] R. Segura Silva, E. J. Pérez Sánchez, and A. Pérez Sánchez, "Design of a Packed-Bed Absorption Column Considering Four Packing Types and Applying Matlab," *Nexo Revista Científica*, vol. 29, no. 2, pp. 83-104, 2016.

[86] M. Beychok. (2008). *Diagram of a packed bed absorption column*. Available: http://en.citizendium.org/wiki/File:Packed_Bed_Absorption_Column.png

[87] C. J. Geankoplis, *Transport process and separation process principles*. 2003.

[88] T. Sherwood, G. Shipley, F. J. I. Holloway, and E. Chemistry, "Flooding velocities in packed columns," vol. 30, no. 7, pp. 765-769, 1938.

[89] S. Piché, F. Larachi, and B. P. A. Grandjean, "Flooding Capacity in Packed Towers: Database, Correlations, and Analysis," *Industrial & Engineering Chemistry Research*, vol. 40, no. 1, pp. 476-487, 2001/01/01 2001.

[90] M. J. C. e. p. Leva, "Reconsider packed-tower pressure-drop correlations," vol. 88, no. 1, pp. 65-72, 1992.

[91] R. Billet and M. Schultes, "Fluid dynamics and mass transfer in the total capacity range of packed columns up to the flood point," *Chemical Engineering Technology: Industrial Chemistry ‐ Plant Equipment ‐ Process Engineering ‐ Biotechnology*, vol. 18, no. 6, pp. 371-379, 1995.

[92] T. K. Sherwood, G. H. Shipley, and F. A. L. Holloway, "Flooding Velocities in Packed Columns," Industrial and Engineering Chemistry vol. 30, no. 7, July 1938.

[93] M. Leva, "Reconsider packed-tower pressure-drop correlations," *Chemical engineering progress,* vol. 88, no. 1, pp. 65-72, 1992.

[94] G. Towler and R. Sinnott, "Separation Columns (Distillation, Absorption, and Extraction)," 2013, pp. 807-935.

[95] R. Billet and M. Schultes, "A physical model for the prediction of liquid hold‐up in two‐phase countercurrent columns," *Chemical Engineering & Technology: Industrial Chemistry‐Plant Equipment‐Process Engineering‐Biotechnology,* vol. 16, pp. 370-375, 1993.

[96] R. Billet and M. Schultes, "Prediction of mass transfer columns with dumped and arranged packings: updated summary of the calculation method of Billet and Schultes," *Chemical Engineering Research & Design,* vol. 77, no. 6, pp. 498-504, 1999.

[97] R. Billet and M. Schultes, "Predicting mass transfer in packed columns," *Chemical Engineering Technology: Industrial Chemistry‐Plant Equipment‐Process Engineering‐Biotechnology,* vol. 16, no. 1, pp. 1-9, 1993.

[98] F. Heymes, P. Manno Demoustier, F. Charbit, J. Louis Fanlo, and P. Moulin, "Hydrodynamics and mass transfer in a packed column: Case of toluene absorption with a viscous absorbent," *Chemical Engineering Science,* vol. 61, no. 15, pp. 5094-5106, 2006/08/01/ 2006.

[99] J. Stichlmair, J. Bravo, J. J. G. S. Fair, and Purification, "General model for prediction of pressure drop and capacity of countercurrent gas/liquid packed columns," vol. 3, no. 1, pp. 19-28, 1989.

[100] S. McCabe, Harriot, *Unit Operations of Chemical Engineering* 5th ed. (McGraw-Hill Chemical Engineering Series).

[101] R. Wellek, R. Brunson, and F. Law, "Enhancement factors for gas‐absorption with second‐order irreversible chemical reaction," *The Canadian Journal of Chemical Engineering,* vol. 56, no. 2, pp. 181-186, 1978.

[102] R. E. Treybal, "Adiabatic Gas Absorption and Stripping in Packed Towers " *Industrial and Engineering Chemistry,* vol. 61, no. 7, July,1969 1969.

[103] P. V. Danckwerts, G. E. H., and Joostent, "Chemical reaction and effective interfacial areas in gas absorption " *Chemical Engincering Science,* vol. 28, pp. pp. 453-46 1. , June,1972 1972.

[104] Robert M. Kelly, T Ronald W. Rousseau, and J. K. Ferrell, "Design of Packed, Adiabatic Absorbers: Physical Absorption of Acid Gases in Methanol," *Ind. Eng. Chem. Process Des. Dev,* vol. 23, no. 1, pp. 102-109 1984.

[105] L.Deleyeg.F.Fromen, "Rigorous simulation and design of columns for gas absorption and chemical reaction-1," *Compurers & Chemical Engineerin,* vol. 10, no. 5, pp. pp. 493-504, 1986.

[106] V. N. V. Dipayan Sanyal, and Deoki N. Saraf, "Modeling of Carbon Dioxide Absorber Using Hot Carbonate Process," *Ind. Eng. Chem. Res,* vol. 27, no. 11, pp. 2149-2156, 1988.

[107] R. E. Treybal, "Adiabatic gas absorption and stripping in packed towers," *Industrial Engineering Chemistry*

vol. 61, no. 7, pp. 36-41, 1969.

[108] J. D. Pandya, "Adiabatic gas absorption and stripping with chemical reaction in packed towers," *Chemical Engineering Communications,* vol. 19, no. 4-6, pp. 343-361, 1983.

[109] D.-Y. Peng and D. B. Robinson, "A new two-constant equation of state," *Industrial Engineering Chemistry Fundamentals,* vol. 15, no. 1, pp. 59-64, 1976.

[110] R. C. Reid, J. M. Prausnitz, and B. E. Poling, "The properties of gases and liquids," 1987.

[111] D. C. Rennels and H. M. Hudson, "Pipe Flow: A Practical and Comprehensive Guide," *Pipe Flow: A Practical and Comprehensive Guide,* pp. 263-267, 2012.

[112] S. K. Shibata and S. I. Sandler, "Critical Evaluation of Equation of State Mixing Rules for the Prediction of High-Pressure Phase Equilibria," *Industrial and Engineering Chemistry Research,* vol. 28, pp. 1893-1898, 1989.

[113] A. I. M. Zografos, William A and J. E. Sunderland, "Fluid properties as a function of temperature," *Computer Methods in Applied Mechanics and Enginering,* vol. 61, 1987.

[114] W. Sutherland, "The viscosity of gases and molecular force," *The London, Edinburgh, and Dublin Philosophical Magazine and Journal of Science,* vol. 36, no. 223, pp. 507-531, 1893/12/01 1893.

[115] R. LMNO Engineering, and Software, Ltd. Gas Viscosity Calculator [Online].

[116] T. A. Davidson, "A Slmple and Accurate Method for Calculatlng Viscosity of Gaseous Mixtures," p. Report of Investigations 9456, 1993.

[117] F. Herning and L. J. G. u. W. Zipperer, "Calculation of the viscosity of technical gas mixtures from the viscosity of the individual gases," vol. 79, p. 69, 1936.

[118] J. W. Buddenberg and C. R. Wilke, "Calculation of Gas Mixture Viscosities," *Industrial & Engineering Chemistry,* vol. 41, no. 7, pp. 1345-1347, 1949/07/01 1949.

[119] H. A. Al-Ghawas, D. P. Hagewlesche, G. Ruiz-Ibanez, and O. C. Sandall*, "Physicochemical Properties Important for Carbon Dioxide Absorption in Aqueous Methyldiethanolamine," *J. Chem. Eng,* vol. 34, pp. 385-391 1989.

[120] Engineering ToolBox. (2018, 01.03.2019). *Water - Thermal Conductivity.* . Available: https://www.engineeringtoolbox.com/water-liquid-gas-thermal-conductivity-temperature-pressure-d_2012.html

[121] A. L. Lindsay and L. A. Bromley, "Thermal Conductivity of Gas Mixtures," *Industrial & Engineering Chemistry,* vol. 42, no. 8, pp. 1508-1511, 1950/08/01 1950.

[122] A. J. P. Z. Eucken, "Über das Wärmeleitvermögen, die spezifische Wärme und die innere Reibung der Gase," vol. 14, no. 8, pp. 324-332, 1913.

[123] E. N. Fuller, P. D. Schettler, J. C. J. I. Giddings, and E. Chemistry, "New method for prediction of binary gas-phase diffusion coefficients," vol. 58, no. 5, pp. 18-27, 1966.

[124] D. F. Fairbanks and C. R. Wilke, "Diffusion Coefficients in Multicomponent Gas Mixtures," *Industrial & Engineering Chemistry,* vol. 42, no. 3, pp. 471-475, 1950/03/01 1950.

[125] F. A. Aly and L. L. Lee, "Self-consistent equations for calculating the ideal gas heat capacity, enthalpy, and entropy," *Fluid Phase Equilibria,* vol. 6, no. 3-4, pp. 169-179, 1981.

[126] Thermopedia. (2020). *Thermopedia Data Engine for Thermodynamics, Heat & Mass Transfer, and Fluids Engineering*.

[127] G. F. Versteeg and W. P. M. van Swaaij, "Solubility and Diffusivity of Acid Gases (CO2, N2O) in Aqueous Alkanolamine Solutions," *Journal of Chemical and Engineering Data,* vol. 33, pp. 29-34, 1988.

[128] S. Laddha, L. SS, D. JM, and D. PV, "The N2O analogy: the solubilities of CO2 and N2O in aqueous solutions of organic compounds," 1981.

[129] T. C. Tsai, J. J. Ko, H. M. Wang, C. Y. Lin, and M. H. Li, "Solubility of nitrous oxide in alkanolamine aqueous solutions," *Journal of Chemical and Engineering Data,* vol. 45, pp. 341-347, 2000.

[130] B. P. Mandal, M. Kundu, and S. S. Bandyopadhyay, "Physical Solubility and Diffusivity of N2O and CO2 into Aqueous Solutions of (2-Amino-2-methyl-1-propanol + Monoethanolamine) and (N -Methyldiethanolamine + Monoethanolamine)," *Journal of Chemical & Engineering Data,* vol. 50, pp. 352-358, 2005.

[131] C. Y. Lin, H. M. Wang, M. H. Li, J. J. Ko, and T. C. Tsai, "Diffusivity of nitrous oxide in aqueous alkanolamine solutions," *Journal of Chemical and Engineering Data,* vol. 46, pp. 160-165, 2001.

[132] C. Wilke and P. Chang, "Correlation of diffusion coefficients in dilute solutions," *AIChE Journal,* vol. 1, no. 2, pp. 264-270, 1955.

[133] J. L. Monteith, and Unsworth, M.H. (2008). *Principles of Environmental Physics (3rd ed.)*.

[134] Y. J. Heintz, "Carbon dioxide capture from fuel gas streams under elevated pressures and temperatures using novel physical solvents," University of Pittsburgh, 2012.

[135] J. Gabrielsen, M. L. Michelsen, E. H. Stenby, and G. M. Kontogeorgis, "A model for estimating CO_2 solubility in aqueous alkanolamines," *Industrial engineering chemistry research,* vol. 44, no. 9, pp. 3348-3354, 2005.

[136] R. Hiwale, S. Hwang, and R. Smith, "Model Building Methodology for Multiphase Reaction Systems · Modeling of CO_2 Absorption in Monoethanolamine for Laminar Jet Absorbers and Packing Beds," *Industrial Engineering Chemistry Research,* vol. 51, no. 11, pp. 4328-4346, 2012.

[137] P. M. Mathias and J. P. O'Connell, "The Gibbs–Helmholtz equation and the thermodynamic consistency of chemical absorption data," *Industrial Engineering Chemistry Research,* vol. 51, no. 13, pp. 5090-5097, 2012.

[138] D. Hopkinson, D. Luebke, Z. Li, and S. Chen, "Solvent optimization of conventional absorption processes for CO_2 capture from postcombustion flue gases," *Industrial Engineering Chemistry Research,* vol. 53, no. 17, pp. 7149-7156, 2014.

[139] N. McCann, M. Maeder, and H. Hasse, "Prediction of the overall enthalpy of CO2 absorption in aqueous amine systems from experimentally determined reaction enthalpies," *Energy Procedia,* vol. 4, pp. 1542-1549, 2011.

[140] I. Kim, K. A. Hoff, and T. Mejdell, "Heat of absorption of CO2with aqueous solutions of mea: New experimental data," *Energy Procedia,* vol. 63, pp. 1446-1455, 2014.

[141] I. Kim and H. F. Svendsen, "Heat of absorption of carbon dioxide (CO2) in monoethanolamine (MEA) and 2-(aminoethyl)ethanolamine (AEEA) solutions," *Industrial and Engineering Chemistry Research,* vol. 46, pp. 5803-5809, 2007.

[142] A. Abdulkadir *et al.*, "Heat of absorption and specific heat of carbon dioxide in aqueous solutions of monoethanolamine,3-piperidinemethanol and their blends," *Energy Procedia,* vol. 63, pp. 2070-2081, 2014.

[143] Y. M. Christophe Mathonat, Alan E. Mather, and Loren G. Hepler, "Excess Molar Enthalpies of (Water + Monoalkanolamine) Mixtures at 298.15 K and 308.15 K," *Journal of Chemical and Engineering Data,* vol. 42, no. 5, pp. 993-995, 1997.

[144] A. E. M. Yadollah Maham, and Loren G. Hepler, "Excess Molar Enthalpies of (Water + Alkanolamine) Systems and Some Thermodynamic Calculations," *American Chemical Society,* 1997.

[145] M. Ballard, M. Bown, S. James, and Q. Yang, "NMR studies of mixed amines," *Energy Procedia,* vol. 4, pp. 291-298, 2011.

[146] D. Barth, P. Rubini, and J. Delpuech, "Determination of Thermodynamic Parameters for the Formation of Amino-Alcohol Carbamates in Aqueous-Solutions by C-13 Nuclear Magnetic-Resonance Spectroscopy," *Bulletin De La Societe Chimique De France Partie I-Physicochimie Des Systemes Liquides Electrochimie Catalyse Genie Chimique,* no. 7-8, pp. 227-230, 1984.

[147] S. H. Park, K. B. Lee, J. C. Hyun, and S. H. Kim, "Correlation and prediction of the solubility of carbon dioxide in aqueous alkanolamine and mixed alkanolamine solutions," *Industrial & engineering chemistry research,* vol. 41, no. 6, pp. 1658-1665, 2002.

[148] F. Y. Jou, A. E. Mather, and F. D. Otto, "The solubility of CO2 in a 30 mass percent monoethanolamine solution," *The Canadian Journal of Chemical Engineering,* vol. 73, no. 1, pp. 140-147, 1995.

[149] V. Swaij, *On the Kinetics between CO2 and Alkanolamines*.

[150] P. M. M. Blauwhoff, G. F. Versteeg, and W. P. M. V. Swaaij, "A study on the reaction between co, and alkanolamines in aqueous solutions," *Chemical Engineering Science,* vol. 39, pp. pp-207-225, 28 November 1982(Received) 1984.

[151] R. H. Weiland, J. C. Dingman, D. B. Cronin, and G. J. Browning, "Density and viscosity of some partially carbonated aqueous alkanolamine solutions and their blends," *Journal of Chemical and Engineering Data,* vol. 43, pp. 378-382, 1998.

[152] R. M. DiGuilio, R.-J. Lee, S. T. Schaeffer, L. L. Brasher, and A. S. Teja*, "Densities and Viscosities of the Ethanolamines," *J. Chem. Eng,* vol. 37, pp. 239-242, 1992.

[153] E. D. Snijder, M. J. M. te Riele, G. F. Versteeg, and W. P. M. van Swaaij, "Diffusion coefficients of several aqueous alkanolamine solutions," *Journal of Chemical & Engineering Data,* vol. 38, no. 3, pp. 475-480, 1993/07/01 1993.

[154] Dortmund. Viscosity of Liquid Water [Online]. Available: http://ddbonline.ddbst.de/VogelCalculation/VogelCalculationCGI.exe?component=Water

[155] D. Fu, Y. F. Xu, L. F. Wang, and L. H. Chen, "Experiments and model for the surface tension of carbonated monoethanolamine aqueous solutions," *Science China Chemistry,* vol. 55, pp. 1467-1473, 2012.

[156] J. Han, J. Jin, D. A. Eimer, and M. C. Melaaen, "Density of water (1) + monoethanolamine (2) + CO 2 (3) from (298.15 to 413.15) K and surface tension of water (1) + monoethanolamine (2) from (303.15 to 333.15) K," *Journal of Chemical and Engineering Data,* vol. 57, pp. 1095-1103, 2012.

[157] D. B. Dortmund. Surface Tension of Pure Water [Online].

[158] D. R. Linde and H. V. Kehiaian, *CRC Handbook of Thermophysical and Thermochemical Data*. Boca Raton, FL: CRC Press, 1994.

[159] Y. J. Chen and M. H. Li, "Heat capacity of aqueous mixtures of monoethanolamine with 2-amino-2-methyl-l-propanol," *Journal of Chemical and Engineering Data,* vol. 46, pp. 102-106, 2001.

[160] L. F. Chiu and M. H. Li, "Heat capacity of alkanolamine aqueous solutions," *Journal of Chemical and Engineering Data,* vol. 44, pp. 1396-1401, 1999.

[161] NIST. *NIST Chemistry Webbook.*

[162] L. Faramarzi, G. M. Kontogeorgis, M. L. Michelsen, K. Thomsen, and E. H. Stenby, "Absorber Model for CO 2 Capture by Monoethanolamine," pp. 3751-3759, 2010.

[163] C. J. Geankoplis, *Transport Processes and Unit Operations*, 3rd ed.

[164] C. Colburn. Chliton-colburn Methodology [Online].

[165] W. Ambrosini, N. Forgione, A. Manfredini, and F. Oriolo, "On various forms of the heat and mass transfer analogy: Discussion and application to condensation experiments," *Nuclear Engineering and Design,* vol. 236, no. 9, pp. 1013-1027, 2006.

[166] Y. W. Wang, S. Xu, F. D. Otto, and A. E. Mather, "Solubility of N_2O in alkanolamines and in mixed solvents," vol. 48, pp. 31-40, 1992.

[167] T. Aspen, "Rate Based MEA Model with Aspen Plus."